Developments in Magnetic Resonance Spectroscopic Imaging Acquisition and Analysis

By Rebecca Joanne Sawbridge

A thesis submitted to the

University of Birmingham

For the degree of

DOCTOR OF PHILOSOPHY

Physical Sciences of Imaging in the Biomedical Sciences

School of Chemistry

College of Engineering and Physical Sciences

University of Birmingham

September 2017

Abstract

Magnetic Resonance Spectroscopic Imaging (MRSI), a functional MR imaging technique, has proven via the identification of metabolite biomarkers to be useful in the diagnosis and prognosis of numerous diseases, for example brain tumours. However, a number of factors impede its routine clinical use: i) long acquisition times mean its use is limited to low resolution 2-dimensional slabs, ii) large quantity of data produced means its interpretation can be time consuming and iii) data quality can be variable and therefore interpretation can be difficult for a non-expert. Further developments in MRSI are designed to reduce the impact of these issues. The focus of this work is to address some of the above issues; developing acquisition protocols and optimising analysis methods in order to increase the clinical feasibility of MRSI. Within this study a fast-MRSI protocol has been developed for absolute metabolite quantitation and has demonstrated its feasibility for clinical use, accurately reproducing data in a shorter clinically feasible acquisition time. An experimentally derived fitting model has been developed which increases metabolite measurement accuracy. Finally, a 3D MRSI protocol has been successfully optimized allowing robust metabolite information to be mapped throughout the brain.

Dedication

I would like to dedicate this work to my family for their continuous support throughout my studies. I would especially like to thank my husband Gareth, who has been there through the late nights writing and has truly been my rock. I would also like to extend my thanks to my supervisors Martin Wilson, Andrew Peet and Hamid Dehghani who have provided so much help and knowledge throughout the years. Special thanks to Martin and Andrew who gave me the amazing opportunity to work as a part of the Children's Brain Tumour Research Team.

Declaration

I declare that the work presented within this thesis is entirely my own. The following aspects of this study were performed in collaboration:

(1) Clinical data presented in Chapter 5 were acquired by the radiographers at Birmingham Children's Hospital Radiology Department.

(2) Totally Automated Robust Quantitation in NMR (TARQUIN) software used for spectral analysis was developed by Dr Martin Wilson and Dr Greg Reynolds.

Acknowledgements

I would like to gratefully acknowledge the funding provided from the EPSRC conjunction with the Physical Sciences of Imaging within the Biomedical Sciences (PSIBS) Doctoral Training Centre at the University of Birmingham EP/F50053X. Imaging was performed at Birmingham Children's Hospital NHS Foundation Trust at the NIHR 3T MR Research Centre and at the Birmingham University Imaging Centre (BUIC). Funding was also received from NIHR Professorship (1/1/13-31/3/18), PI A Peet, Ref: 13-0053.

Contents

List of Figures

List of Tables

Abbreviations

NMR	**Nuclear Magnetic Resonance**
MRI	**Magnetic Resonance Imaging**
MRSI	**Magnetic Resonance Spectroscopic Imaging**
VOI	**Volume of Interest**
MM	**Macromolecule**
COV's	**Coefficients of Variance**
SENSE	**Sensitivity Encoding**
SNR	**Signal-to-Noise Ratio**
FWHM	**Full Width Half Maximum**
SE	**Spin Echo**
PRESS	**Point Resolved Spectroscopy**
TE	**Echo Time**
SPAIR	**Spectral Attenuation Inversion Recovery**
QC	**Quality Control**
RF	**Radiofrequency**
FID	**Free Induction Decay**
TR	**MRI/MRSI Repeat Time**
PPM	**Parts Per Million**
SVS	**Single Voxel Spectroscopy**
CHESS	**Chemical Shift Selective Pulses**
FOV	**Field of View**
EPSI	**Echo Planar Spectroscopic Imaging**
TARQUIN	**Totally Automated Robust Quantitation in NMR**

Si.BL	**MRSI Simulated Baseline Model**
Ex.BL	**MRSI Experimental Baseline Model**

Glossary of Terms

Voxel	**A 3-dimensional cubic volume from which spectra can be acquired.**
MRSI	**NMR spectra are obtained for multiple adjacent voxels within a grid.**
SVS	**NMR spectra is acquired from a single voxel**
VOI	**A 3D volume-of-interest from which in MRSI multiple voxels can acquired.**
Phantom	**Test object which can be used to model structures/features contained within living subjects.**
K-Space	**A spatial frequency domain which maps the spatial frequencies contained within an image.**
FID	**The exponential decay of transverse magnetization induced by an RF pulse over time.**
Shimming	**The application of small currents to ensure the main magnetic field is uniform across the volume of interest.**
TARQUIN	**A metabolite quantitation software which models spectral data within the time domain using parameterised basis sets.**
EX.BL	**Basis set comprised of an experimentally derived MM spectra signal contribution with the inclusion of metabolite signals.**
Si.BL	**Simulated basis set derived from the parameterisation of metabolite and MM signals.**
SENSE	**A fast-MRSI technique which reduces scan time by reducing the k-space sampling density and applying algorithms to reconstruct the fully sampled data.**

ANOVA	**A statistical test "Analysis of Variance" where the variation in a set of observations is divided into distinct components to determine if a significant difference between multiple populations is observed.**
T-test	**Statistical test to establish if a significant difference is observed between the means of two populations.**

Presentations and Publications

First Author Poster Presentations

1. ISMRM 23rd Annual Meeting & Exhibition 2015, poster presentation

R.Birch et al.; 'The influence of Macromolecule Baseline on 1H Magnetic Resonance Spectroscopic Imaging Reproducibility', abstract 1965

2. Joint Annual Meeting ISMRM-ESMRMB 2014, poster presentation

R Birch et al.; 'Sensitivity encoding for fast (1) H MR spectroscopic imaging water reference acquisition', abstract 2916

First Author Publications

1. R.Birch et al.; 2017 'The influence of Macromolecule Baseline on 1H Magnetic Resonance Spectroscopic Imaging Reproducibility'. Magnetic resonance in medicine, 77(1), 34-43.doi:10.1002/mrm.26103
2. R. Birch et al.; 2015 'Sensitivity encoding for fast (1) H MR spectroscopic imaging water reference acquisition'. Magnetic resonance in medicine, 73(6), 2081-2086.doi:10.1002/mrm.25355

1. Introduction

1.1 Developments in Magnetic Resonance Spectroscopic Imaging (MRSI.

^{1}H Magnetic Resonance Spectroscopic Imaging (MRSI) allows metabolite quantities to be mapped over a volume of interest (VOI). Spectra are acquired over multiple voxels and spectral features can be identified to map metabolism within the body for example the brain. Metabolism can be altered within the body, if there is a change in tissue composition for example the presence of a brain tumour. MRSI can be used to monitor this and therefore discern between healthy and diseased tissue. This thesis will focus on developments in acquisition and analysis of MRSI in the brain.

1.2 MRSI in Clinic: It's Advantages and Limitations.

MRSI is a non-invasive functional MR imaging technique. It has proven, via the identification of metabolite biomarkers, to be useful in the diagnosis and prognosis of numerous diseases such as; brain tumours (1–3), neurodegenerative diseases (4) and neuro-metabolic disorders (5,6). Although widely used in research its routine clinical adoption has been slow due to a number of limiting factors: i) long acquisition times mean its use is largely limited to low resolution 2-dimensional slabs, ii) the large quantity of data produced means its interpretation can be time consuming and iii) data quality can be variable and therefore interpretation can be difficult for a non-expert.

1.3 Research Motivation

Developments in MRSI are needed in order to make its use in the clinic more feasible. Improvements in acquisition time, analysis and protocol optimisation would aid in its routine clinical implementation.

1.4 Aims and Objectives

1. Investigate the effect of both acquisition parameters and fitting methods on ^{1}H MRSI reproducibility.
2. Investigate the effect of fast-MRSI techniques on accuracy for absolute metabolite quantitation.
3. Evaluate the use of fast-MRSI techniques in clinical practice.
4. Develop and optimise a 3D-MRSI protocol and evaluate its effectiveness with respect to data quality and clinical feasibility.

1.5 Thesis Organisation

The principles and applications of magnetic resonance imaging and spectroscopy, along with a literature review of fast MRSI in the brain has been summarised in Chapter 2.

Chapter 3 investigates the influence of the macromolecule baseline on ^{1}H MRSI Reproducibility. As previously stated in Section 1.2 one of the issues with MRSI is that data quality can be variable. Robust protocol designs are important in order to minimise error within spectral data. Due to the strong overlap of Macromolecular signals (MM) with metabolites of interest found within the brain; error can be introduced to the spectral fitting if the MM content is not fully characterised. A number of methods have been proposed, which either act to reduce the MM contribution with acquisition methodology or by accounting for it within the analysis using a specialised fitting model. This chapter addressed this issue by comparing the use of a simulated and experimental MM analysis schemes and different acquisition methods. Their effect on the reproducibility of ^{1}H MRSI spectra were evaluated using coefficients of variance (COV's %) and the mean metabolite concentrations were also determined for each method. This work has been presented as a poster presentation at the ISMRM 23rd Annual Meeting & Exhibition 2015 and has also

been peer reviewed and published within the Magnetic Resonance in Medicine Journal (7). Although reproducibility studies exist within the literature and previous comparisons have been made between simulated and experimental baseline models; this was the first study to investigate the effect of both echo time and macromolecular analysis schemes on the reproducibility of 2D ^{1}H MRSI data at 3Tesla. This study was designed to help aid in the protocol design for clinical studies.

As stated previously in section 1.2, long acquisition times have often precluded the routine clinical use of MRSI. Chapter 4 addresses this issue by testing the fast-MRSI technique sensitivity encoding (SENSE) and the “gold standard” reduced resolution technique in their ability to reconstruct the fully sampled water reference data. Their ability to do so was established through the construction of Bland Altman plots, the calculation of mean differences and metabolite concentration comparisons. The work detailed in chapter 4 has been presented as a poster presentation at the Joint Annual Meeting ISMRM-ESMRMB 2014 and has also been peer reviewed and published in Magnetic Resonance in Medicine Journal Volume 73, Issue 6 June 2015. To our knowledge this was the first study to use SENSE for the purpose of water reference data collection.

The clinical implementation of the protocol developed in chapter 4 is investigated in Chapter 5. Spectroscopy data was acquired for 15 patients to test and validate the protocols use in the clinic and establish its clinical value for the determination of neurocognitive deficit. Quality control parameters such as signal-to-noise ratio (SNR) and water line width (FWHM) were calculated for each dataset in order to establish the protocols accuracy. Individual patient metabolite concentrations were also determined and structural images used to assess any post tumour/treatment effects in the parietal white matter region of the brain. The translations of protocols to the clinic are not always successful, therefore studies of this kind are needed to assess their efficacy.

Long acquisition times have largely limited the use of MRS to low resolution 2D slabs. Chapter 6 shows the development of a 3D MRSI protocol on volunteers for use clinically and in research. The extension to 3D would prove useful for clinical studies to allow more information on metabolism to be provided throughout the brain. It would be particularly useful for studies of brain tumours where heterogeneity may not necessarily lie within the axial plane. The move towards more whole brain spectroscopic imaging (via Spin-Echo sequencing) would be particularly desired to provide better sampling (increased number of voxels) across the brain. Accuracy of this method was assessed using QC thresholds, highlighted previously, in order to establish any data loss (via number of voxels) due to poor quality data. Outer volume lipid levels were also used to test the efficacy of outer volume lipid removal using lipid suppression techniques. The reproducibility of the Spin-Echo protocol was also calculated in order to establish its robustness. To the best of our knowledge this is the first study to look at the combination of a spin echo with SENSE and lipid nulling to establish its reproducibility and the clinical feasibility of this methodology.

The final chapter 7 includes the conclusions and discusses potential future work in the developments of MRSI acquisition and analysis methods.

2 MRSI Principles and Applications

2.1 How the MR signal is acquired

2.1.1 Basic Principles

Nuclear spin is a fundamental quantum mechanical property of matter. An odd number of protons and/or neutrons within the nuclei will produce a net spin and magnetic moment. The human body is made up of ~75% water; the proton nuclei ^{1}H within the water have a net spin and magnetic moment. Therefore, due to the proton nuclei's high abundance in tissue and Nuclear Magnetic Resonance (NMR) sensitivity (high gyromagnetic ratio) the hydrogen nucleus is most commonly used for both magnetic resonance imaging and spectroscopy. The hydrogen nuclei interact with the main field of the MR Scanner and the protons experience a torque due to this external field. The proton in turn tries to align itself to the field causing it to precess around the direction of the field. The frequency ω_0 of this precession is proportional to the external magnetic field B_0 as defined by the Larmor Equation:

Equation 2-1 Larmor Equation

$$\omega_0 = \gamma B_0$$

Where:

γ is the proton gyromagnetic ratio=2.7×10^{8} rad s^{-1} T^{-1}

The proton can precess in two possible stable states (Figure 2-1): parallel (almost aligned with B0) and anti-parallel (aligned almost opposite to B0). The magnetic moment is at an angle to the external field B0 and therefore independent of orientation will trace a circle around the direction of the field (represented by the dashed line). The ratio of protons spinning in these two states is dependent on its energy, the strength of B0 and inversely

on temperature. Both states are stable but statistically the distribution of protons favours the lower energy parallel state. The protons can change state by either gaining or losing energy in the form of a photon i.e. electromagnetic radiation.

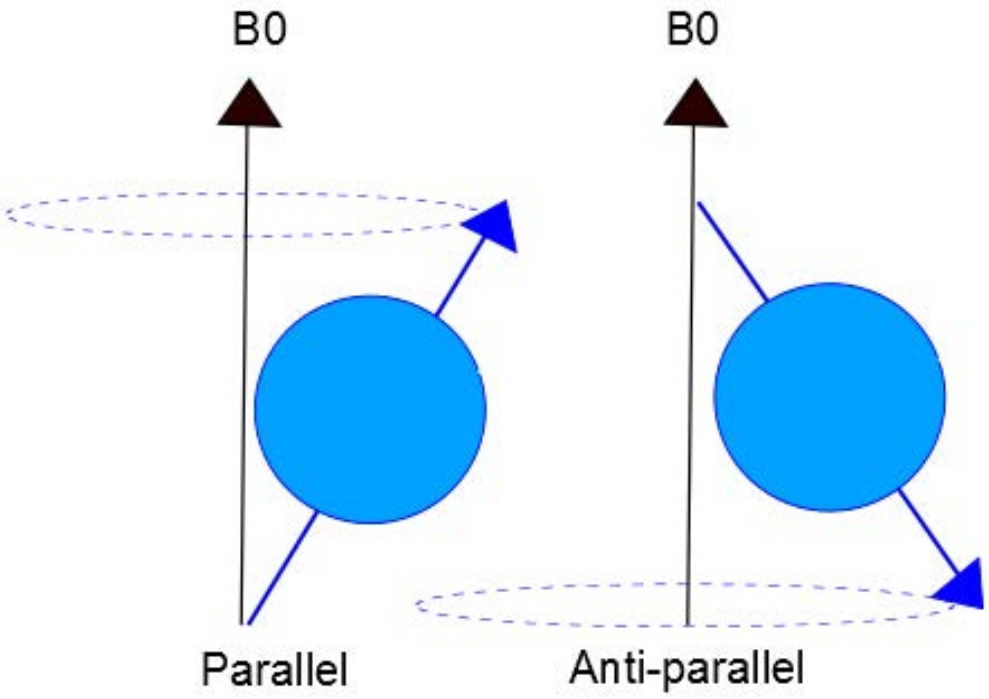

Figure 2-1 Parallel and Anti-parallel proton states in an external magnetic field B0 highlighting the magnetic moment precession

The energy difference between the parallel and anti-parallel state is directly proportional to B0 and the frequency of the electromagnetic radiation is equal to the Larmor frequency ω_0 therefore also equates to equation 2-1. Therefore, it can be shown that the precessional frequency is equal to the frequency of radiation required to cause a transition between the two states.

At equilibrium, a collection of proton nuclei are out of phase with each other, and the direction of magnetic moment vectors will be spread out evenly in the plane perpendicular to B_0. Due to the high number of protons groups of vectors can be simplified to an average magnetic moment or “Spin” which precesses at the same frequency ω_0. The net

magnetization M_0 can therefore be defined as the vector sum of the spins. M_0 is aligned exactly with B_0 and is defined as the z direction.

2.1.2 How the MR signal is measured

The magnetization within the body M_0 is of a much smaller order (microtesla) compared to the external field B_0, most common clinical scanners being an order of 1.5 or 3 Tesla. Thus, it cannot be measured reliably at equilibrium. However, if the magnetization is tipped 90 degrees from the z axis, using a resonant radiofrequency (RF) pulse, into the transverse x-y plane the magnetization can be detected and measured easier as the measurement can be made in a separate axis to the external field B_0. The RF pulse defines the flip angle (α) applied to the magnetization and will cause the spins to align. For a simple RF pulse which is turned on and then off the flip angle is defined as:

Equation 2-2 Flip Angle

$$\alpha = \gamma B_1 t_p$$

Where:

B_1 is the strength of the RF magnetic field

γ is the gyromagnetic ratio

t_p is the duration of the pulse

A 90-degree RF pulse will cause the magnetization to tip fully into the transverse plane. A 180-degree pulse is applied by doubling the length/amplitude of a RF pulse. The strength of the pulse can also be altered to produce different flip angles. M_0 precesses clockwise into the transverse x-y plane inducing a voltage into the receiver coil.

Once the RF pulse has flipped the protons into the transverse plane, they will relax back to the equilibrium i.e. longitudinal position M_0 once the pulse is removed. At this point M_0 is comprised of two magnetization components transverse magnetization M_{xy} and longitudinal magnetization M_z. The first decays along the transverse axis due to spin-spin relaxation with a characteristic time T2. This parameter also contains a T2* component which takes into account the dephasing of spins due to susceptibility field inhomogeneity effects. M_z is the restoration of the longitudinal magnetization at a tissue dependent time T1 (spin-lattice relaxation).

T2 relaxation is modelled as an exponential decay where the transverse components of M_{xy} decay or dephase with respect to time constant T2. As defined below:

Equation 2-3 T2 Relaxation

$$M_{xy} = M_0 e^{-\frac{t}{T2}}$$

T2 is defined as the time it takes for the transverse magnetization to fall to approximately 37% of the original value of M_{xy}.

T1 relaxation is modelled as an exponential growth process defined by the following equation:

Equation 2-4 T1 Relaxation

$$M_z = \mathrm{M}_0 \left(1 - \mathrm{e}^{\frac{-\mathrm{t}}{\mathrm{T1}}}\right)$$

Where M_z is the longitudinal magnetization

M_0 is the maximum magnetization

t is time

T1 is relaxation time

T1 is modelled as a first order time constant and therefore is defined as the value at which M_z recovers up to 63% of its maximum value M_0 for a particular tissue signal. Different tissue types have different T1 relaxation times. If a 180-degree inversion pulse is applied, reversing the longitudinal magnetization M_z, the M_z will then begin to recover via T1 relaxation going from negative to positive. A signal can be generated at time TI which is based on the individual T1 of each tissue type. Because of this a null point can be found for different tissue signals. The null point TI_{null} for a particular tissue type is defined as:

Equation 2-5 Tissue null point equation

$$TI_{null} = T1\left(\ln(2) - ln\left(1 + e^{-TR/T1}\right)\right)$$

If TR>>1 then the equation simplifies to:

Equation 2-6 Simplified tissue null point equation

$$TI_{null} = \ln(2) \times T1$$

See figure 2-9 for a demonstration of this process in the nulling of lipid signals.

The receiver coil is designed to only be sensitive to magnetization in the transverse plane M_{xy}. The coil sees an oscillating field inducing a voltage which varies at the Larmor frequency creating the readout signal. The signals amplitude decays exponentially to zero as the protons dephase rapidly from each other. This can typically take up to a few seconds. For example, water T2 relaxation times for white matter and gray matter within the brain at 3T of 110ms and 80ms have been found (8). This is signal is known as a Free Induction Decay (FID) (Figure 2-2).

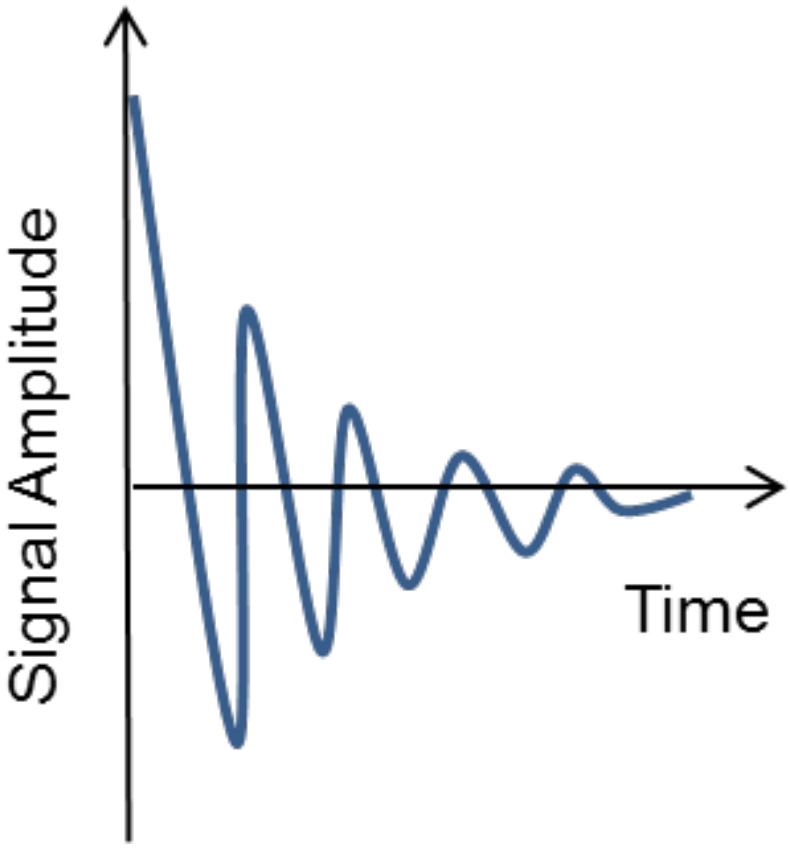

Figure 2-2 Free Induction Decay (FID)

For slice selection and spatial localization of MR signals echoes are created using different pulse sequences.

2.1.3 MR Image Formation, Localisation and Pulse Sequences

Magnetic field gradients are applied to form the pulse sequence required to localize the signal. Pulse sequence diagrams are used to illustrate the steps required to acquire the MR signal. As a simple example to demonstrate the steps required: Figure 2-3 illustrates this for a gradient echo sequence. For example, in the gradient echo sequence a slice selective gradient G_{ss} is applied simultaneously to the RF pulse. This restricts the excitation to the desired slice within the body.

A phase encoding gradient G_{PE} is applied for spatial localisation. Phase encoding works by applying a magnetic field gradient which in turn dephases spins along the direction of

the applied gradient. Once the gradient is turned off, the signal from each pixel will have a different phase shift dependent on its position along the gradient. The individual signal amplitudes can be extracted out because of this difference using a Fourier transform.

In MRI, a frequency encoding gradient G_{FE} is also applied, as the data is acquired to encode the data as spatial frequencies. This sequence gets repeated for every line of data/each phase-encode gradient value until the k-space matrix is filled. K- space is a spatial frequency domain which maps the spatial frequencies contained within an image. Each point in k-space corresponds to a spatial frequency component with an associated amplitude. A Fourier transform can be applied to the k-space map to produce the MRI image using these components.

Two pulse sequence parameters are echo time TE and Repetition Time TR. TE is the time between the RF pulse to the center of the gradient echo where the signal is refocused. Signal-to-noise decreases with increasing TE. This is due to the dephasing of the MR signal and therefore lower signal measured during the readout. The parameter TR is defined as the time period between each repeated excitation RF pulse. The total scan time can be defined as:

Equation 2-7 Scan Time Calculation

$$Scan\ time = NSA \times N_{PE} \times TR$$

Where:

NSA is the number of signal averages

N_{PE} is the phase encoding matrix size

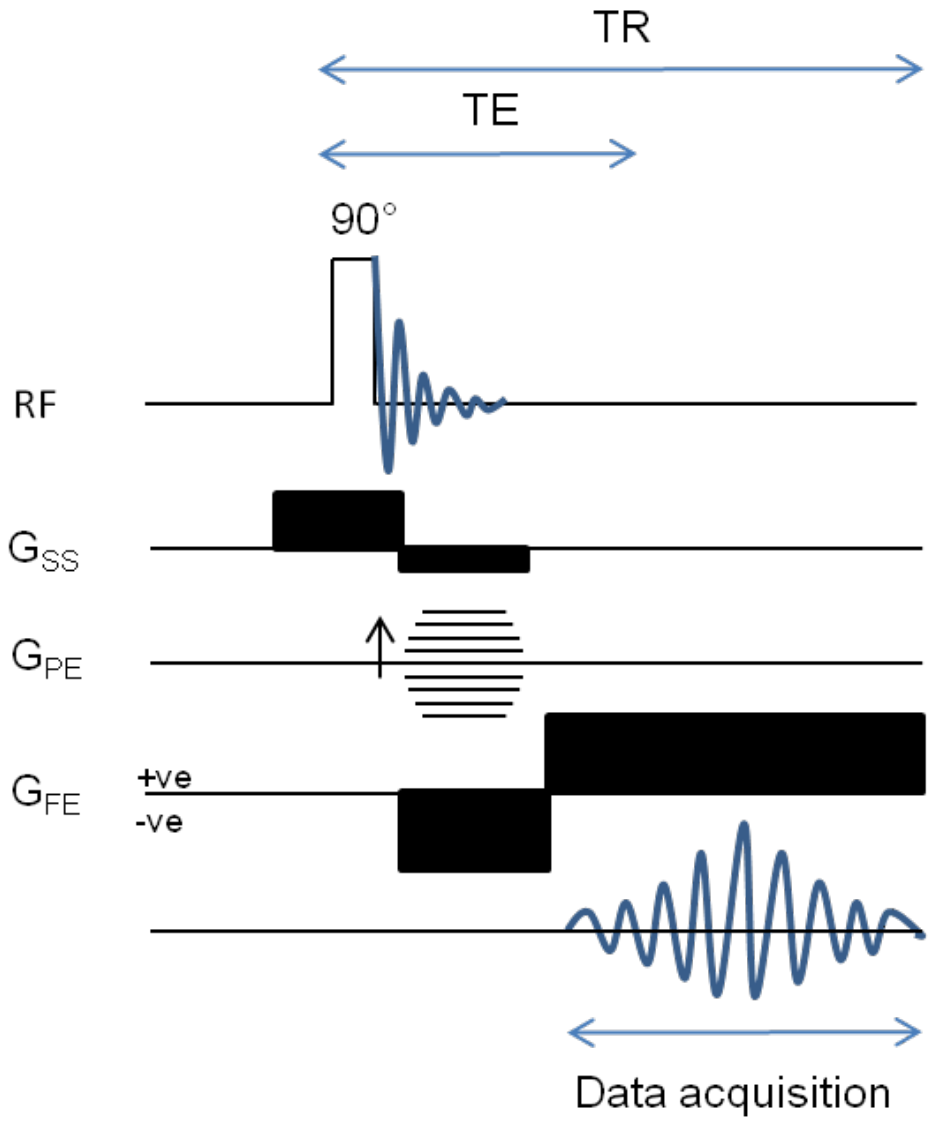

Figure 2-3 Gradient Echo Sequence

2.2 Magnetic Resonance Spectroscopy (MRS) Acquisition

2.2.1 MRS Basics

The protons imaged in ^{1}H MRS are subject to slightly different magnetic environments. The local magnetic fields of different chemical compounds will vary, resulting in a chemical shift in the local Larmor frequency. The compounds are shifted to a different frequency ω_0 (j) according to their molecular environment type j, pH is also known to

have an impact on $\omega_0(j)$. This frequency measurement is in rads^{-1} but is often presented as parts per million (ppm) as defined below:

Equation 2-8 Larmor Frequency

$$\delta = \frac{\omega_0(j) - \omega_0(ref)}{2\pi B_0} \times 10^6$$

Where:

$\omega_0(j)$ is the frequency of the metabolite in rads^{-1}

$\omega_0(ref)$ is the frequency of the reference metabolite in rads^{-1}

B_0 is the strength of the external magnetic field in Tesla

The chemical shift of a nuclei is dependent on the effect of the surrounding electrons within the molecules. These electrons partially shield the nucleus from the external magnetic field B_0. Therefore, differences in chemical composition will cause the molecule to resonate at a unique frequency. As shown in Equation 2-4 this will result in frequency shifts between different molecules allowing the separation and identification of different metabolites as they will appear at different positions within the spectrum. J coupling is the process where metabolite peaks can split due to the effect of nuclear spins from neighboring nuclei within the same molecule. In ^{1}H MRS this can result due to a single neighboring proton, resulting in a doublet peak, or more than one, resulting in a multiplet pattern.

In MRS these different compounds can be measured spectrally providing information on the chemical/metabolic processes that are occurring within that volume. A typical brain spectrum is comprised of a number of metabolite, lipid and macromolecular signals (see section 2.4). The spatial localisation of these signals can be split into two categories

Single Voxel Spectroscopy (SVS) and multi voxel techniques known as MR Spectroscopic Imaging (MRSI).

2.2.2 Single Voxel Spectroscopy (SVS)

Single voxel spectroscopy (SVS) acquires a single spectrum from a voxel placed within a specific location (e.g. the brain). Three slice selective mutually orthogonal pulses are applied in order to collect the echo signal from that single intersecting volume in space i.e. the voxel (Figure 2-4). SVS is most commonly acquired using a Point RESolved Spectroscopy (PRESS) sequence which uses a single slice selective 90-degree pulse and two 180-degree slice selective refocusing pulses in order to acquire spectra from a single volume.

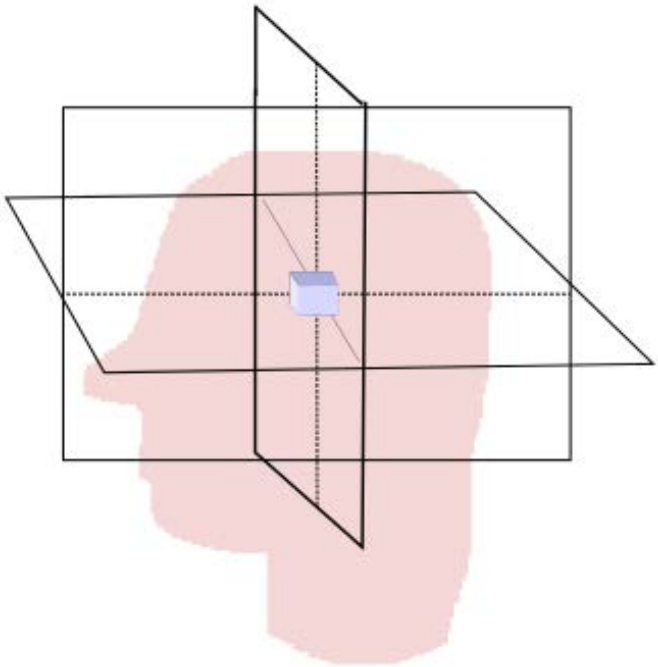

Figure 2-4 Voxel selection using three mutually orthogonal pulses

Any outer volume signals are either crushed using dephasing gradients and/or through phase cycling of the RF pulses (9).

SVS has been widely adopted clinically due its robustness, short scan times, good field homogeneity, and ease of implementation, processing and interpretation. However, because of its restriction to data collection from one single location, the number of appropriate clinical applications are restricted. For example, it provides limited information in disease cases where heterogeneity may exist e.g. in tumours or in cases where the area of interest is not known.

2.2.3 Multi-voxel: Magnetic Resonance Spectroscopic Imaging (MRSI)

Two-dimensional MRSI acquisitions are acquired by applying phase encoding in two directions for spatial localisation. Unlike MRI it does not have a frequency encoded gradient as we are interested in the individual chemically shifted frequencies. The acquisition is stepped through the voxels after every complete sequence defined by repetition time TR. MRSI is a multi-voxel technique which allows you to map metabolites across a predefined VOI (2D PRESS MRSI shown in Figure 2-5) (8). MRSI is a promising technique for the study of diseases such as brain tumours since heterogeneity (9) and diffuse margins (10) are common features and can be observed more easily with MRSI. It can also be used to monitor neurodegenerative diseases such as Alzheimer's (11) and neuro-metabolic disorders (12,13). MRSI is particularly useful in cases where the clinically relevant area may not be known in advance. Both SVS and MRSI are widely available clinically and can be used in conjunction easily with standard MRI examinations.

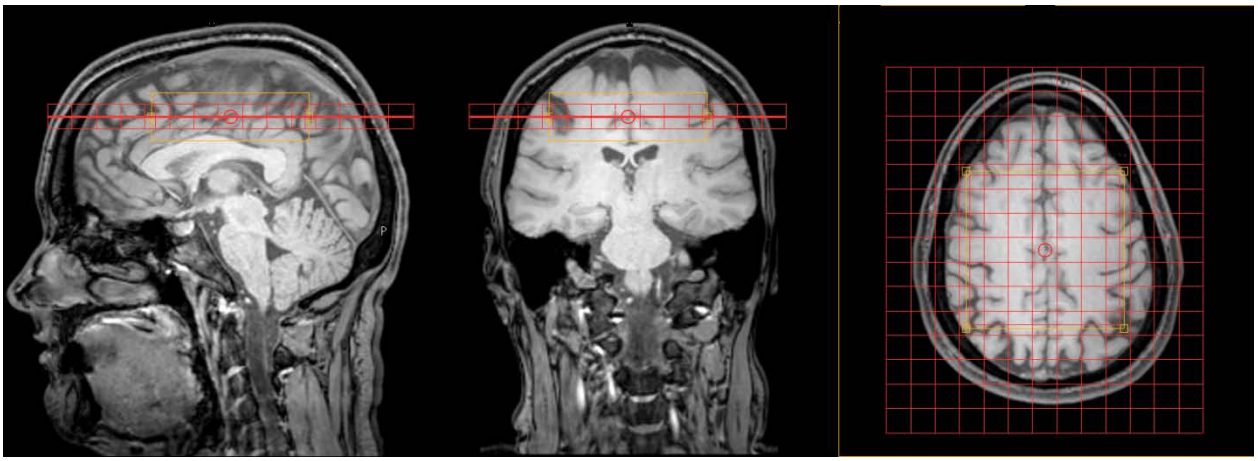

Figure 2-5 2D MRSI Plan

2.2.4 3D MRSI

Two-dimensional MRSI can be extended into 3 dimensions through the addition of an extra phase encoding direction, so the frequencies are spatially encoded in three directions. Metabolism can be mapped through multiple slices, useful in cases where heterogeneity may not necessarily lie in the axial plane and once again for diseases where the area of interest may not be known. 3D acquisitions can be categorized into two sections: Multi-slice 2D (Figure 2-6) and 3D MRSI. For 3D MRSI signal collection and SNR is considered to be more efficient as signal from the whole region is collected at all times (10). However, maintaining a homogenous field across a large VOI can prove difficult. Long acquisition times due to phase encoding in three directions may also hinder its use. Multi-slice 2D provides sharper slice profiles as it is not defined by the excitation pulse point spread function (10). Both techniques have long acquisition times and therefore require fast-MRSI techniques (section 2.2.7) in order to be deemed clinically feasible.

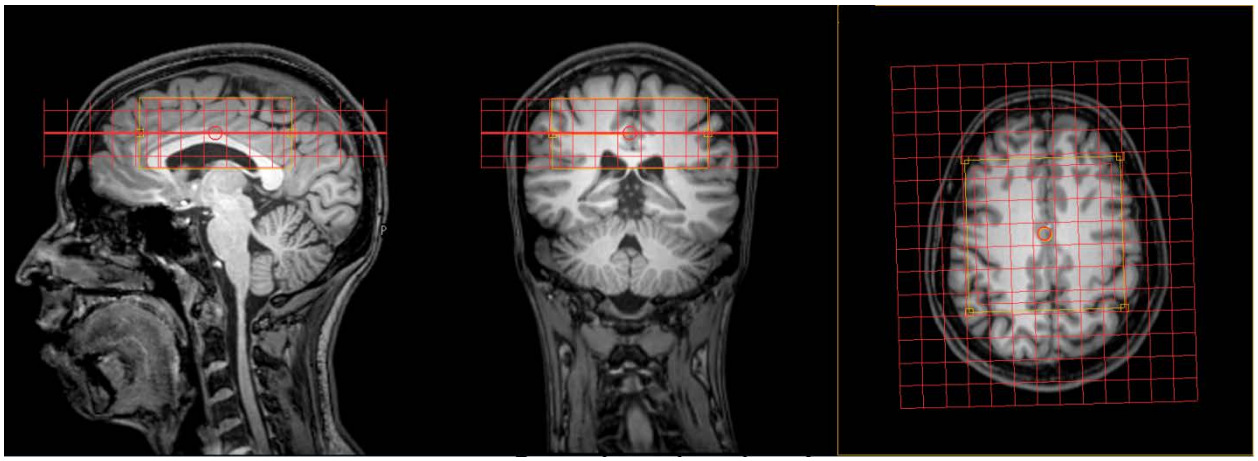

Figure 2-6 Example 3D-MRSI Plan

2.2.5 MRS Pulse Sequences

The Spin Echo sequence (Figure 2-7) allows the spins to dephase after the initial 90-degree pulse after some time a 180-degree pulse is applied on the +y' axis which flips the spins through 180 degrees about this axis. This reverses the spin phase angles, if the spin was located within lower magnetic field strength it will have been dephasing anti-clockwise. The 180-degree pulse flips these spins so they appear to have been in a high field thus dephasing clockwise and vice versa for the initial high field spins. After the 90-180 degree delay the spins will now continue to dephase and a spin echo will be formed as the spins come back into phase along the +y' axis. Spin-echo relies on phase-reversal the signal decay will only depend on T2 (see section 2.1.5) and diffusion and not on the field inhomogeneity or tissue susceptibility.

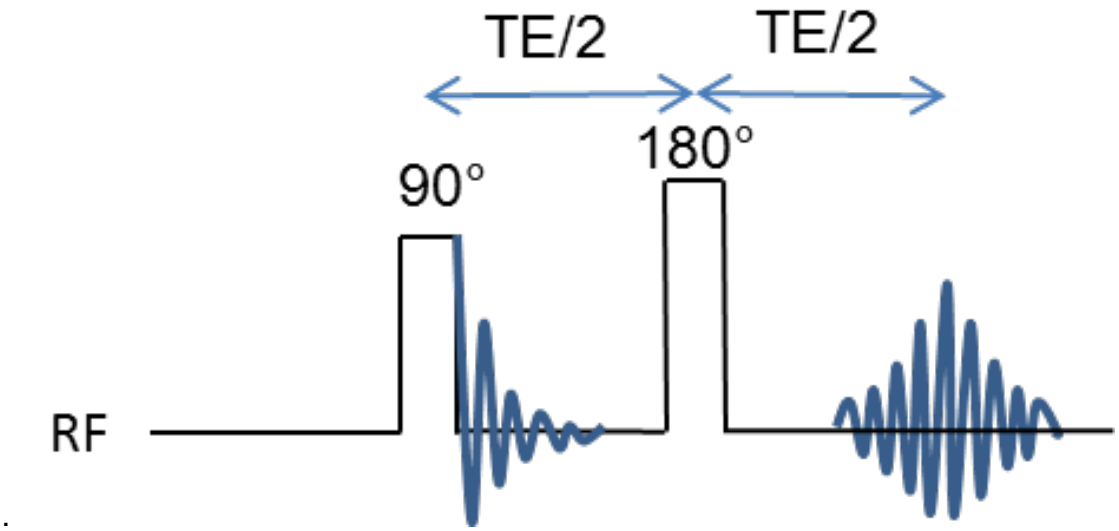

Figure 2-7 Spin Echo Sequence

Point RESolved Spectroscopy (PRESS) is based on the Spin Echo sequence and comprises of a single slice selective 90-degree pulse and two 180-degree slice selective refocusing pulses (Figure 2-8). Each pulse has a slice selective gradient on each of the principle axes in order to ensure only protons within the voxel/volume are excited.

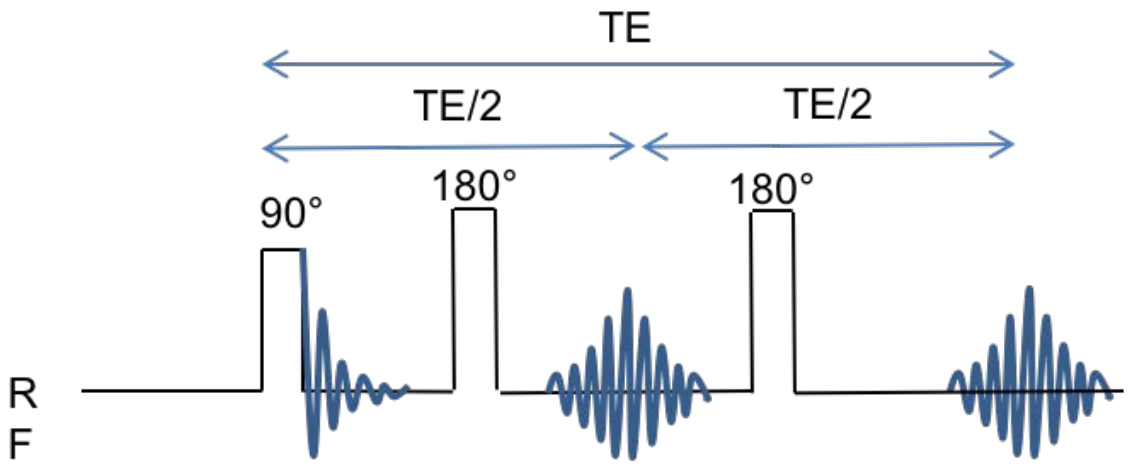

Figure 2-8 PRESS Sequence

2.2.5 Water Suppression

Due to the high abundance of water within the body, there is a large signal contribution from these protons within the acquired spectra. The brain water signal has a much higher

magnitude compared to the metabolites of interest. Therefore, as metabolite contributions are so much smaller, it is necessary to suppress the water signal to allow reliable and accurate measurement of the smaller metabolite signals. Water resonances have shorter T2 relaxation times compared to the metabolites and therefore suppression can be more effective at longer echo time TE. However, this method is insufficient and pre-saturation of the water signal prior to the localization pulse sequence is preferred. Water suppression techniques e.g. CHEmical Shift Selective pulses (CHESS) (11) uses frequency selective pulses in combination with well-defined flip angles in order to effectively suppress the water signal.

2.2.6 Lipid Suppression

Large signal contributions originating from peri-cranial fat can be observed at high levels within the brain. These signals can contaminate the spectra once again reducing the reliability and accuracy of the metabolite measurement. A number of methods have been proposed to either suppress (using outer volume suppression pulses i.e. Saturation Bands) or avoid exciting the outer volume lipid signals (pulse sequences such as STEAM and PRESS). Saturation bands can also be applied over the peri-cranial region which crush the lipid signal so it does not appear within the in-volume spectra. Inversion pulses can also be used to suppress the lipid signal. Lipids have a shorter T1 time comparison to metabolites and therefore can be nulled at an inversion time TI where the metabolite signal is non-zero and can be measured. Figure 2-9 illustrates how a SPectral Attenuated Inversion Recovery (SPAIR) sequence nulls the lipid signal so only metabolite signal is acquired.

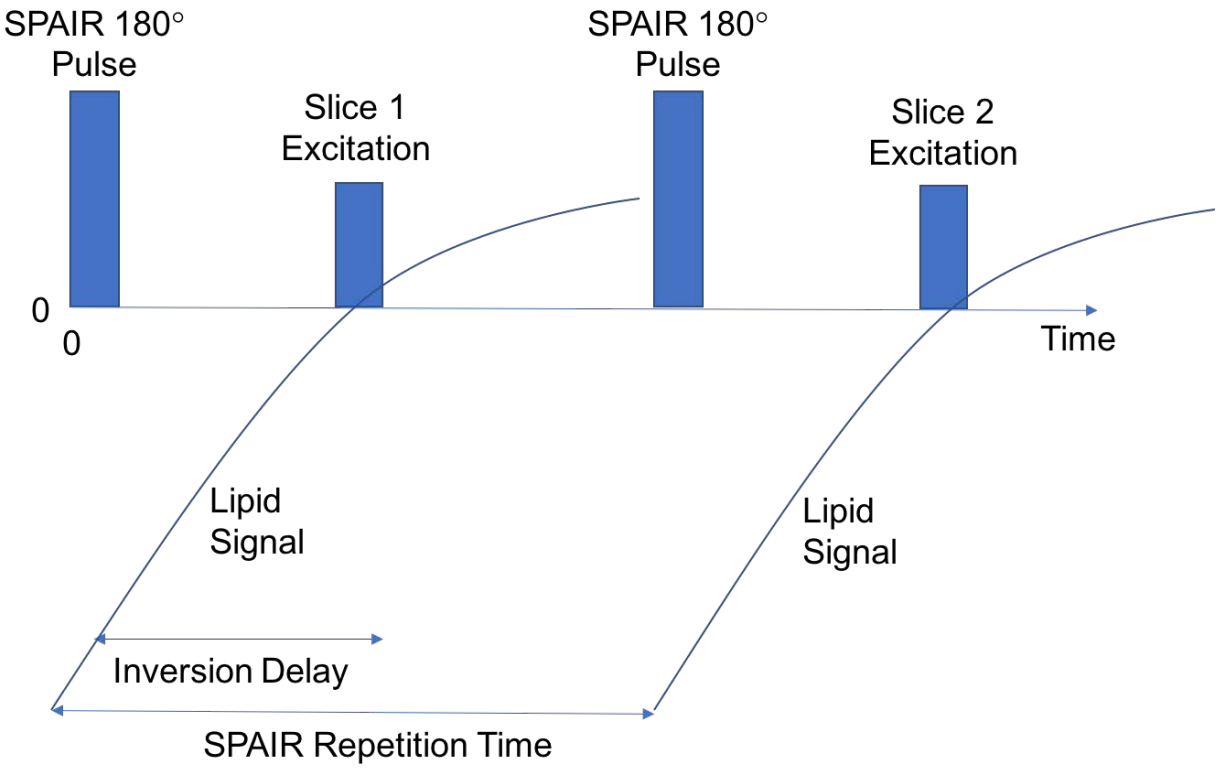

Figure 2-9 SPectral Attenuated Inversion Recovery (SPAIR) Sequence to null lipid signals

A 180-degree inversion pulse is applied. The lipid signals are nulled after an inversion delay with inversion time TI. At this point the metabolite peaks are inverted but non-zero. Therefore, the metabolite signals alone can be detected if an excitation pulse is applied at inversion time TI.

2.2.7 Fast-MRSI Techniques

2.2.7.1 Reduced Resolution

Reduced k-space acquisition (reduced resolution) is a simpler MRSI technique, currently used as the "gold standard" technique at Birmingham Children's Hospital. This technique reduces scan time by sampling fewer points in k-space, resulting in a lower resolution scan. In order to obtain absolute concentrations, the outer rim of k- space is zero filled in order to increase the matrix to the correct fully sampled size. It can then be used as a

quantitation reference for higher resolution water suppressed scans. This effectively performs an interpolation of the missing data in spatial domain (12).

2.2.7.2 Compressed Sensing

Compressed sensing, first derived from mathematics in the literature of information and approximation theories, is a method which reconstructs signals from sparse data comprised of “random” linear combinations of signal values, much smaller than the original full data set (13). In MR, a small subset of k-space is acquired instead of full k-space. MRI data is well suited to compressed sensing as it fulfills the following criteria: the resultant image is compressible and therefore is a sparse representation in a known transform domain. Any aliasing artefacts due to k-space under sampling are incoherent/noise like and non-linear reconstruction can be applied. Thus, compressed sensing can accurately reconstruct the fully sampled k-space data. By under sampling k-space the acquisition time can be reduced. Compressed sensing can also be used in conjunction with sensitivity encoding (see section 2.2.7.3) allowing an even greater speed up of scan time.

2.2.7.3 Sensitivity Encoding (SENSE)

Fast-MRSI methods have been developed which act to reduce the number of phase encoding steps and therefore scan time. Sensitivity encoding (SENSE) is a parallel imaging technique which reduces the k-space sampling density by exploiting the known spatial sensitivity profiles of multiple receiver coils. Allowing more rapid spatial encoding (10,14). A reduction factor R defines the amount of k space sampling density (15), for example R=3 represents a three times reduction in the number of phase encoding steps. The fully sampled data information is then algorithmically reconstructed from the under sampled data from each coil and the corresponding sensitivity and noise profiles (10,14).

SENSE can be easily incorporated within any existing MRSI pulse sequence which is an advantage over other fast techniques as any pulse sequence related SNR losses can be avoided (10). There are associated SNR losses for SENSE with increasing reduction factors, but spatial resolution is theoretically preserved (15).

2.2.7.4 Echo Planar Spectroscopic Imaging (EPSI)

EPSI was first proposed by Mansfield et al in 1984 (16) with its use in the brain first adapted by Posse et al (17). An oscillating read gradient is applied during the readout (Figure 2-10). One-dimensional spatial encoding can therefore be acquired in a single shot, as each time domain data point corresponds to one lobe of read gradient. To extend into 2-dimensions an additional phase encoding loop is applied. This ultimately reduces the phase encoding steps by one dimension and therefore the acquisition time is drastically reduced.

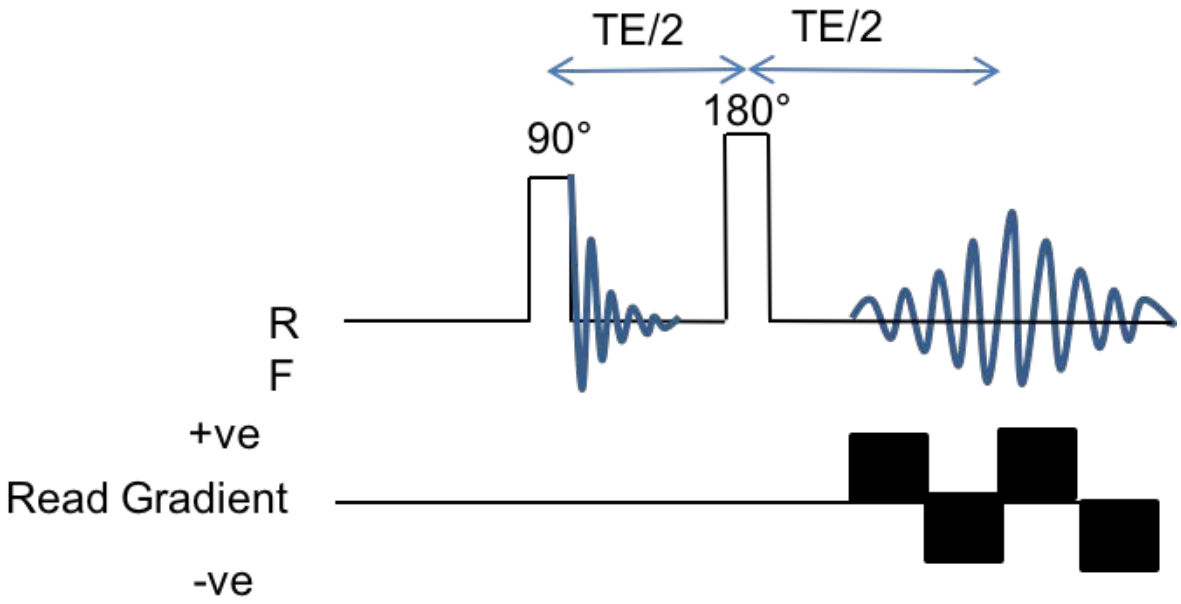

Figure 2-10 EPSI Sequence

A few disadvantages of this technique are: technical problems can arise due to the stress the rapidly oscillating read gradient puts on the gradient system. Ghosting (spurious echoes) can also be observed due to imbalances in the positive and negative lobes within

the read gradient/ due any off-resonance effects. The latter can be compensated through the separate processing of the positive and negative lobes. However, this creates a reduction in spectral bandwidth (18).

2.3 Magnetic Resonance Spectroscopy Analysis

2.3.1 Fitting Methods: Modelling of MRS data

MRS fitting methods can be categorized into three sections: black box, peak fitting and basis sets. Black box methods use either Linear Predictive Singular Value Decomposition (LPSVD) (19) or Hankel Singular Value Decomposition (HSVD) (20) which do not require any additional spectral information. However, because of this these methods struggle to fit complex data, where additional knowledge of spectral features is needed. This model also assumes a lorentzian lineshape which is rarely valid.

Peak fitting methods such as AMARES (21), which model metabolite peaks individually, allow more prior knowledge to be introduced into the fitting model. Therefore, peak fitting models are more successful at fitting data with a higher complexity compared to black box methods.

The spectral information acquired for short echo is more complex containing more metabolite peaks compared to longer echo times, as lower metabolite signals will have decayed at longer TE. To model these individually would be too labour intensive. The introduction of metabolite basis sets to the fitting model, as utilised by LCmodel (22) and Totally Automatic Robust Quantitation in NMR (TARQUIN) (23), is much more sufficient for the modelling of complex short TE spectra. LC model models the data within the frequency domain modelling the data as a linear combination of metabolite, lipids and macromolecule; accounting for the baseline signals through the use of smoothing splines.

TARQUIN was chosen to fit the spectral data within this thesis due to its ability to model complex short TE spectra. TARQUIN is a fully automatic software which models the data using a parameterized basis set of metabolites, lipids and macromolecules within the time domain. Time domain truncation removes baseline interference and uses constraints, such as non-negative metabolite quantities. These are enforced to improve reliability. In order to estimate signal amplitudes a non-negative least squares projection is used. Lipids and macromolecules are included in the basis set in order to impose soft constraints on the least squares projection, with the aim to reduce overfitting errors. In order to model spectral features the TARQUIN algorithm consists of three main stages: preprocessing, basis set simulation and finally the solution of the non-linear least squares problem. In pre-processing, residual water is removed by modelling the signal and its subsequent removal via subtraction from the FID. A zero-order phase correction is also applied in this stage in order to make visual inspection of spectra easier. Finally, automatic referencing is applied to make sure the water signal resonates at the center of the spectrum (24). For basis set simulation, metabolite components are simulated in TARQUIN using chemical shift and J coupling values from Govinderaju et al (25). A solution is then generated using the non-linear least squares projection. More details of these stages can be found in the following paper by Martin Wilson et al (24).

2.3.2 Macromolecular Analysis Schemes: Modelling Macromolecular Contributions

Macromolecular (MM) signals (their origin explained in section 2.4.9) have a significant contribution in short TE spectra which overlap the metabolite resonances. At longer TE the MM signal is reduced, due to shorter T2 relaxation times compared to the metabolite signals. If its contribution is not accounted for effectively error can be introduced into the fitting of short TE spectra. A number of methods have been proposed which either

decrease the MM contribution or to characterize it and include it within the fitting model. Increasing the echo time (TE) of the MRS acquisition will decrease these background signals. This method takes advantage of shorter MM T2 relaxation times found for compared to metabolites (26) due to their smaller molecular weight (27,28). However, at longer TE's there is an inherent reduction in metabolite signal to noise ratio (SNR) due to T2 relaxation. Complex dephasing of multiplets can also reduce quantitation accuracy. The measurement of multiplets and lower SNR metabolites may therefore be more effective for short-TE acquisitions.

MM analysis schemes have been developed to help characterize the MM signals and account for them in the fitting model. (28), with the view to improve the reliability of metabolite estimates. The inclusion of individually simulated macromolecule and lipid components within the analysis basis set is currently the most common method used to account for the MM contribution (29). These features can be obtained through the parameterization of metabolite nulled spectra. Seeger et al (29) parameterized the macromolecules by fitting an average MM spectrum to four broad lines which included the main MM resonances 1-7. Subsequently they can be introduced as prior knowledge into the spectral fitting. The MM signal can also be experimentally acquired using an inversion recovery (IR) sequence (27) since metabolite signals can be nulled at inversion time (TI) due to shorter MM T1 relaxation. Any residual metabolite peaks can be removed in post processing.

2.3.3 Absolute Concentrations

A number of methods have been proposed for the calculation of absolute metabolite concentrations. The most common being: (i) reference to water which acts as an internal standard (ii) reference signal to an external standard (iii) principle of reciprocity signal calibration (30).

The most common method (i) obtains absolute concentrations by referencing the metabolite signal to the signal obtained from water which acts as an internal standard (31–33). This assumes the water content within the tissue which can be inaccurate for unknown diseases and within focal lesions. Water content also differs between Cerebral Spinal Fluid (CSF), grey and white matter but this can be accounted via segmentation. An unsuppressed water spectrum is acquired as well as the metabolite suppressed spectra within the same session. Its use for SVS has been effective as there is a minimal increase in scan time (<20s) and therefore can be applied in routine clinical practice. However, for MRSI the acquisition time becomes significantly longer due to the increased number of phase encoding steps, vital for spatial localisation, that are needed for both the metabolite and water reference data. This may preclude absolute quantitation of MRSI data for routine clinical use.

2.4 Metabolites, Lipids and Macromolecules

As seen in Figure 2-11, the spectral signal obtained from the brain is comprised of multiple metabolites, Macromolecule and Lipid resonances. A number of these have been proven to be useful in the diagnosis and prognosis of disease. The following section details the function, frequency and their use as biomarkers for disease for a range of spectral components.

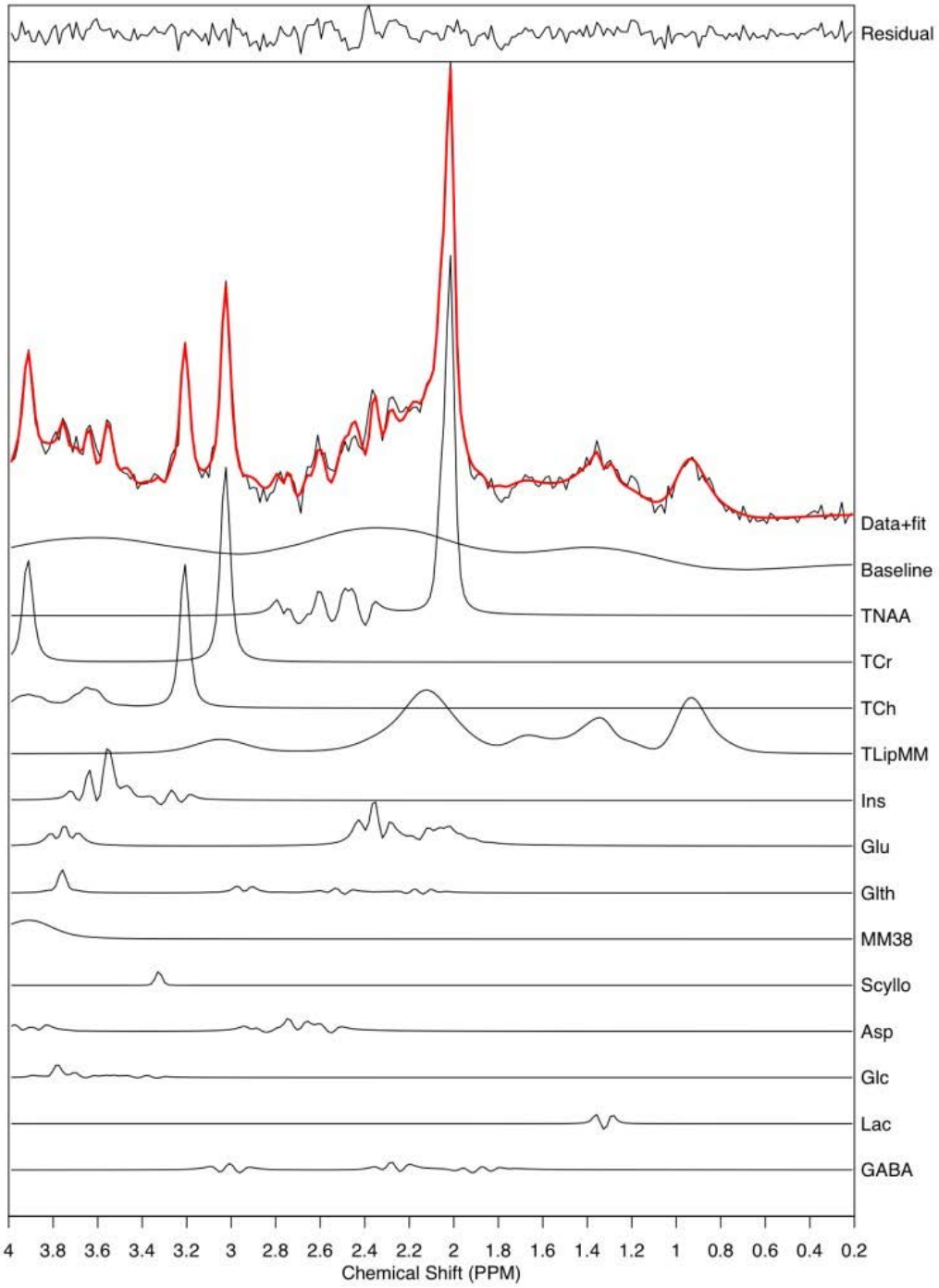

Figure 2-11 Example healthy brain fitted spectra shown in red, with separation of individual metabolite peaks, macromolecules (MM) and lipids (Lip) from the fit.

2.4.1 NAA

The most prominent N-acetyl aspartate (NAA) signal resonates at 2.01ppm and is the largest metabolite signal found within a healthy brain spectrum. N-acetyl aspartyl glutamate (NAAG), an unresolved contribution, can also be found at 2.04ppm. These are often combined to form total NAA (tNAA). Additionally, the aspartyl group also has a strongly coupled pH sensitive resonance ~2.6ppm. NAA is considered to be a neuronal "marker" and is exclusively located within the neurons, axons and dendrites of the central and peripheral nervous system. Its levels have been found to be reduced in pathologies associated with neuronal loss, for example brain tumours. Although observations of dynamic changes in neuronal concentrations indicate changes in NAA levels may also reflect neuronal dysfunction (34). In MRS it has been found to be a useful biomarker of neuronal integrity/density (10). NAA concentrations can vary between regions with higher concentrations observed in grey matter (~8-11mM) when compared to white matter (~6-9mM) (35).

2.4.2 Creatine

Creatine is a methyl resonance at 3.03ppm that is involved in energy metabolism as ATP is generated through the creatine kinase reaction. This peak consists of both creatine and phospho-creatine contributions to form total Creatine (tCr). A second resonance at 3.91ppm can also be observed originating from the CH_2 component of creatine, provided it has not been saturated due to the water suppression pulses. Creatine levels within normal brain have been shown to vary between regions with lower concentrations found for white matter (5.3-5.7mM) when compared to grey matter (6.4-9.7mM).

2.4.3 Choline

The choline peak can be found at 3.20ppm and is comprised of glycerophosphocholine (GPC) and phosphocholine (PC) and free choline. The combination of these is often referred to as total Choline (tCho). Choline plays a role in the synthesis of membranes and also their degradation. In disease states such as brain tumours elevated levels have been found to be a marker of membrane turnover. Within normal brain higher levels have been observed in white matter than in grey, with increased concentrations also found within specific regions of the brain such as the thalamus. The concentration of tCho in normal brain has been found to be approximately 1-2mM (36).

2.4.4 Glutamate, Glutamine and Glx

Glutamate (Glu) is a neurotransmitter and the most abundant amino acid within the brain. When neuronal excitation occurs, glutamate is released and diffuses across the neuronal synapse. It is then taken up by astrocytes and converted to glutamine (Gln). For studies at 1.5Tesla, Glu and Gln are often combined to create a Glx peak due to their strong overlap at this field strength. Their main resonance is at 3.7ppm however multiplet peaks do occur between 2.1 and 2.4ppm. Glx is typically assigned from the latter due to strong overlap of signals at 3.7ppm. At 3 Tesla and higher fields Glu and Gln can be separated more effectively and measured more accurately. Average Glu concentrations ranges from 6 to 12.5mM and 2 to 4mM for Gln (26).

2.4.5 Myo-inositol

Myo-inositol (Ins) resonates between 3.5 and 3.6ppm and is one of the higher signals observed in short echo time spectra. It is a pentose sugar which is involved in cell messenger systems. Elevated levels have been observed in diseases such as Alzheimer's (37–39) and altered levels observed in brain injury (40–42).

2.4.6 Taurine

Taurine comprises of two triplet peaks centred at 3.25ppm and 3.42ppm. Its exact function is poorly understood but it has been proposed that it acts as an osmoregulator and modulator for neurotransmission. In healthy human brain its concentration is found to be approximately 1.5mM (34).

2.4.7 Glutathione

Glutathione, in its reduced form (GSH) is formed of a tripeptide consisting of glycine (3.77ppm singlet), cysteine (three doublets of doublets 2.93, 2.98 and 4.56ppm) and glutamate (3.77ppm doublet of doublets and multiplets at 2.15 and 2.55ppm) (26). It can be found within the brain with concentrations between 1-3mM in healthy tissue (43–45). GSH is an antioxidant which maintains normal red blood cell structure and maintains haemoglobins ferrous state. It also acts as an amino acid transport system and is a storage form of cysteine (45). Interest in GSH has been found for studies of Parkinson's disease and neurodegenerative diseases within the basal ganglia (46,47).

2.4.8 Lactate

The doublet Lactate peak can be found at 1.3ppm and is a marker of cell death and necrosis. It is the end product of anaerobic glycolysis and is present at low concentrations within the brain (48). Increased levels are observed in conditions where blood flow is restricted for example in ischemic stroke (49–51) and tumours (5,52). Its spectral appearance varies between echo times; at longer echo time (TE=144ms) the lactate peaks are inverted and therefore can be effectively separated from overlapping lipid signals which also will have decayed away due to its shorter T2 (52,53).

2.4.9 Lipids and Macromolecules

Mobile lipid resonances can occur around 1.3ppm. Their observation in brain tumours is well known and can be indicative of malignancy and used for predicting survival (1,54,55). Lipids have also been observed in stroke (56) and multiple sclerosis (57–59) patients.

MM signals are broad signals and have been attributed to the methyl and methylene resonances in cytosolic proteins (60). Approximately 10 main MM resonances can be observed (Figure 2-12): M1 (0.93 ppm), M2 (1.24 ppm), M3 (1.43ppm), M4 (1.72ppm), M5 (2.05 ppm), M6 (2.29ppm), M7 (3.00 ppm), M8 (3.20 ppm), M9 (3.8-4.0ppm) and M10 (4.3ppm).

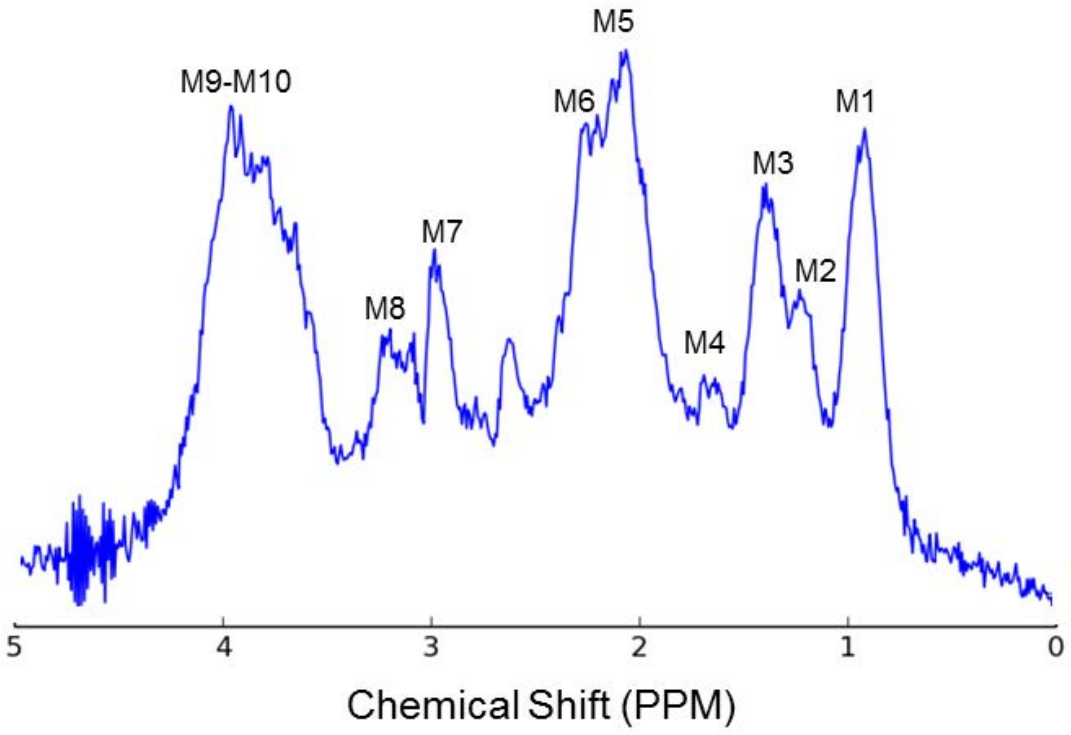

Figure 2-12 Example healthy volunteer MM spectra with main 10 MM components highlighted

The MM signal can be extracted as shown in Figure 2-12 using the inversion recovery (IR) technique (61). The metabolite signal can be nulled at a particular inversion time (TI)

due to differing T1 relaxation times. Due to their short T1, lipid contributions can also be found within the metabolite nulled spectra.

The MM content itself can provide useful clinical information for various diseases. For example, altered MM levels have been observed in both stroke (62,63) and brain tumours (52).

2.5 Data Quality, Issues and Artefacts

As stated previously the data quality of MRS can be variable this can arise for various reasons and quality control measures have to be defined. A number of which are discussed within this section.

2.5.1 Signal to Noise Ratio

Signal to Noise Ratio (SNR) can be defined in frequency domain (FD) as the height of the largest peak/root mean square (rms) amplitude of the noise in signal free part of the spectrum. Low SNR can become a problem particularly in determining low concentration metabolites as their peaks can become indistinguishable from the noise introducing error into metabolite estimations. A number of things can be done to prevent low signal to noise; SNR is proportional to the VOI size, therefore a larger VOI or voxel size will achieve a better SNR. However increased voxel sizes will also reduce the sampling resolution as fewer spectra can be acquired within the VOI. The optimisation of hardware can also help improve SNR. For example, the use of phased-array head coils. Acquiring more signal averages will also provide better SNR due to its proportionality to the square root of the number of acquisitions. However more signal averages will result in the extension of scan time which may prove disadvantageous in clinic. Therefore, careful consideration is needed for SNR optimisation.

2.5.2 Line width

Line width is determined as the full width at half maximum (FWHM) of the peak height in FD (Figure 2-13). The line width represents the attainable resolution available to discern between spectral peaks. Metabolite peaks will start to overlap with increasing FWHM resulting in poorly defined spectra, line width therefore is a useful tool for the rejection of poor MRSI data. As fitting models can rely heavily on line width an increase in FWHM can introduce error into the fitting estimates.

Shimming is a method that adjusts the field gradients in order to improve the magnetic field homogeneity across a voxel. Spectral resolution can be improved by using higher order shims in order to obtain better shimming across the VOI, by using a smaller VOI or by moving the VOI away from tissue interfaces.

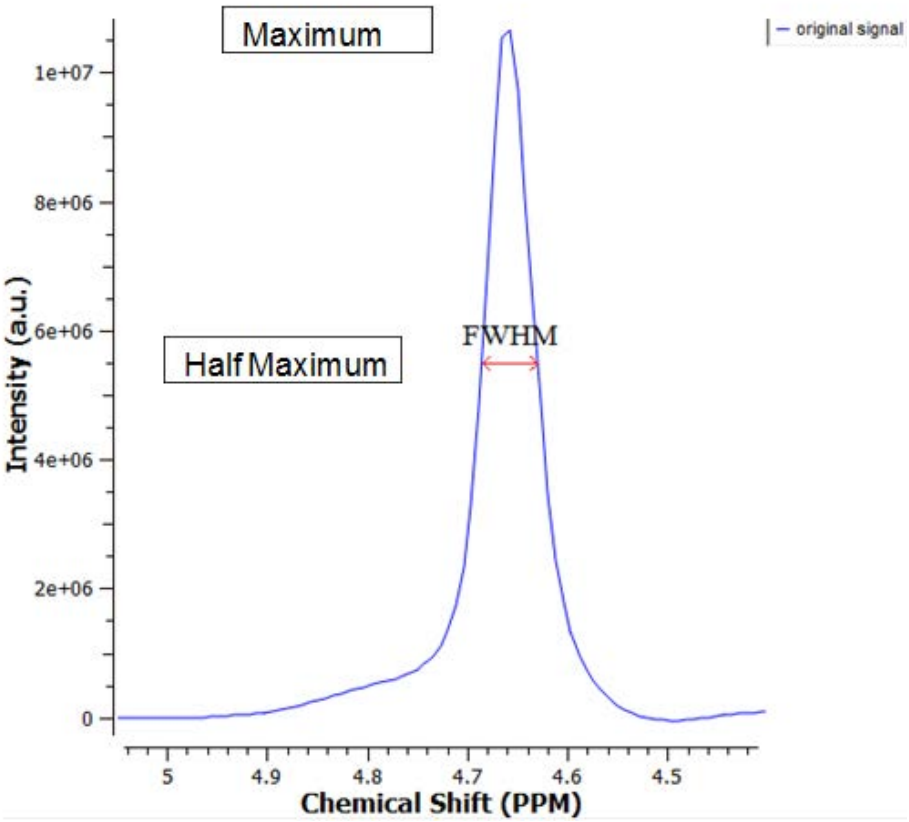

Figure 2-13 Illustration demonstrating how the Line width (FWHM) is determined from a spectral peak (water line width in this instance)

2.5.3 Statistical Methods

2.5.3.1 Precision and Accuracy

The precision of a measurement system is the degree to which repeated measurements undertaken in identical conditions can reproduce the same result. Closely related to precision is the parameter reproducibility. A measure of reproducibility is needed in order to define normal ranges; it can be used to highlight systematic and random error in order establish how robust a technique is. Overall reproducibility can be determined using Coefficients of Variance (COV's) defined as the ratio of the standard deviation and mean across the samples. This particular measure can be useful in indicating how reliable a particular method is, allowing normal ranges to be established and new protocols to be validated. Accuracy relates to how well a method can produce the true value. The ability of a method to extract the correct values for example, expected metabolite concentrations, must be investigated to ensure that the correct information is extracted as any error may lead to false interpretation. Therefore, comparisons to normal values are needed in combination with a test for robustness in order to assess a techniques performance.

2.5.3.2 Bland Altman Statistics

The introduction of new protocols for a particular measurement often requires a validation to be carried out against the already established "old" method. Assessment is required to establish whether the new technique can offer improvement whilst minimizing the measurements variation from the "old" method. The variation between them needs to be low enough in order to replace the current technique with the new one. Correlation coefficients (r) measure the strength of a relationship between two measurements but do not test how well they agree. The use of Bland-Altman statistics allows the agreement

between two methods to be measured using graphical techniques and simple equations (64).

A plot of difference versus the mean of the two methods allows you to determine the relationship between measurement error and establish any bias from the true value. As the true value cannot be easily established, the mean provides a good estimate. The mean difference is calculated in order to estimate bias and the spread of the data (standard deviation of the differences). Figure 2-14 shows an example of a Bland-Altman plot taken from chapter 4 which compares the water amplitude measurement with the new proposed method SENSE R=3 and the full acquisition data SENSE R=1 (old method) in this case.

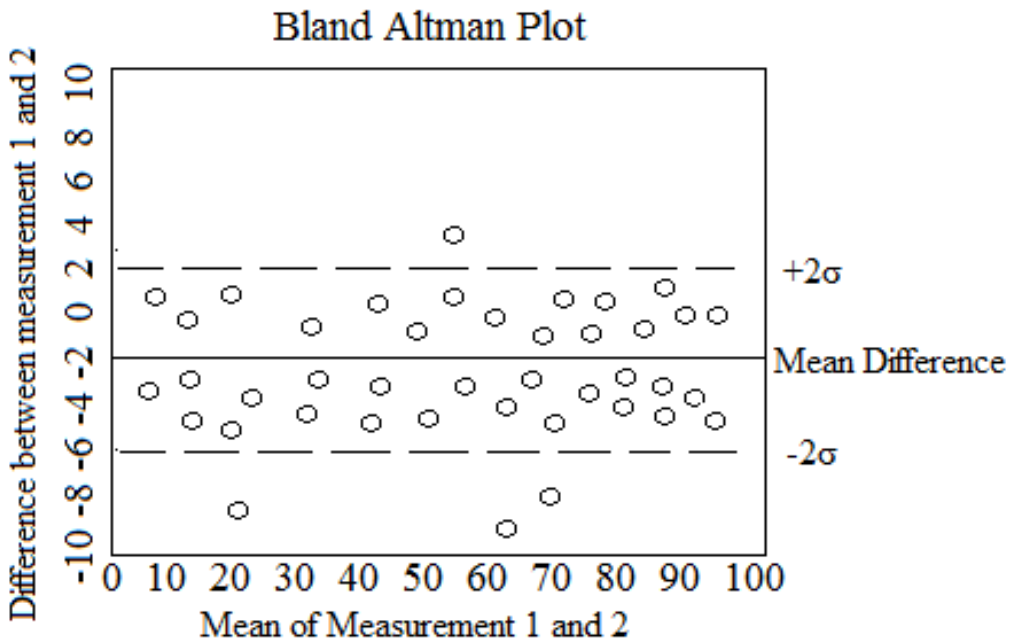

Figure 2-14 Example Bland Altman Plot used to estimate bias and assess the agreement between two methods (σ is defined the standard deviation)

The mean difference line indicates the bias caused by systematic differences between the two methods. For Figure 2-14 the points show a randomly distributed error. The majority of points also lie within the 2σ cut-off; therefore, it can be concluded that there is

good agreement is shown between these two methods, provided the standard deviation is low enough to be deemed acceptable.

2.5.5 Chemical Shift Artefact

Volume selection methods, e.g. PRESS, rely on frequency encoding to selectively excite spins resonating at the Larmor frequency located within the VOI only. However, metabolite signals with different chemical shifts i.e. resonances will experience different slice selections. Thus, the VOI experiences a shift in location between differing metabolites. Slice selection is defined by the RF pulse bandwidth, the chemical shift ω_0 of the metabolite of interest and the selective gradient strength. Therefore, the amount the VOI is displaced is dependent on these parameters. The effect of this shift increases with field strength (30,65). To minimise the voxel shift it has been suggested that the transmit frequency be set to the middle of the spectral region of interest (found to be 2.5ppm for water suppressed data and on the water resonance for unsuppressed) (30).

2.5.6 Point Spread Function and Outer Volume Signal Bleed Through

Ideally RF excitation pulses would have a rectangular profile. However, in reality the RF slice selection is imperfect as a very long pulse duration is needed in order to obtain sharp slice profile. In order to achieve this the minimum TE would need to be increased, a compromise is needed. This signal therefore does not necessarily reflect the original desired rectangular shape of the voxel of interest. As these volume selection pulses are not completely optimal, unwanted spin contributions will be excited outside the VOI. Therefore, when the Fourier transform is applied to allow the original signal to be reconstructed the voxel will be contaminated with signals from adjacent regions/voxels. This is known as “Signal Bleed Through”. This becomes a particular issue for outer volume lipids originating from the scalp which causes contamination within the spectra.

Therefore, effective lipid suppression techniques must be applied as detailed in section 2.2.6. It is also worth noting that PSF also improves with higher resolution scans.

Mathematically signal bleed through can be modelled using a point spread function (PSF) (12). Figure 2-15 shows an example PSF in 3-dimensions. Where position (X, Y, Z) = (0, 0, Z) mm is the centre of the desired voxel and at increasing distance away from this point describes the influence of outer volume signals contributing to the overall voxel signal.

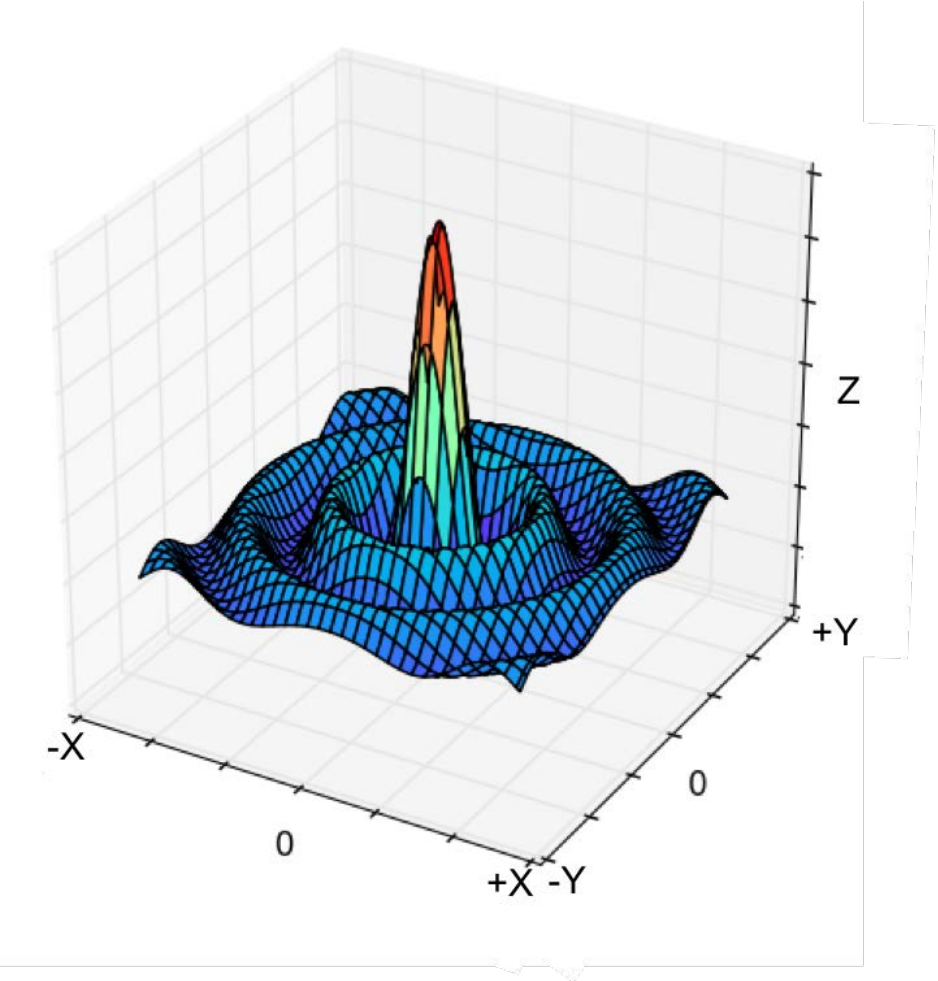

Figure 2-15 Example PSF Function

2.5.7 Water Suppression

Due to the high level of water within tissue, if it is not suppressed effectively this can prove problematic in the determination of more downstream metabolite peaks such as myo-

inositol. It can be accounted for in the data fitting/ post processing software, provided that the residual water is smooth and not large in comparison to the metabolite signal. However, dominating residual water peaks lead to sidebands and offsets being introduced to the spectra causing error in metabolite determination. Post processing methods can help minimize its impact but may result in the suppression/loss of metabolite information around this region.

2.5.8 Movement

Subject movement can cause a number of issues; repeated small motions e.g. respiration can cause an increase in line width, frequency shifts and reduced metabolite measurements due to phase cancellation maybe observed (66). If subject movement occurs during the spectroscopy sequence, it will result in the data being collected from the wrong location. This can be observed as a doubling of all peaks i.e. single peaks will appear as double peaks (30). In MRSI movement also causes spatial blurring where metabolite signals will be observed outside the head (67). For the spatial localisation of metabolite signals it is important that the subject remains still throughout the scan session, this can prove difficult in long acquisitions.

2.6 Conclusion

^{1}H MRSI has proven to be a useful technique in the diagnosis and prognosis of disease within the brain. However, developments in both the acquisition and analysis of this technique are needed in order to ease its implementation into routine clinical use. Long acquisition times and variable data quality all preclude its use. Developments in new protocols that act to speed up scan time, expand the sampling volume e.g. 2D to 3D and improve data quality need to be fully validated before their clinical use in order to assess their efficacy.

3. Influence of Macromolecule Baseline on 1H MRSI Reproducibility

3.1 Introduction

Macromolecular (MM) signals are broad resonances which overlap with metabolites of interest. Error can be introduced into the spectral fitting model if their contributions are either (i) removed or (ii) characterised incorrectly. An increase in echo time will decrease the MM contribution during the acquisition due to shorter T2 relaxation times compared to their metabolite counterparts. The use of macromolecular analysis schemes (simulated and experimentally acquired) in the fitting model have also been proposed to account for the MM signals in the fitting (28). A recent study by Karim Snoussi et al (68) found no significant differences between MM signals in white and grey matter regions of the brain, implying the use of a single MM baseline spectra could be sufficient to include in a basis set for the fitting of spectra from multiple brain regions.

MRS reproducibility studies are vital in order to assess the reliability of imaging protocols for their optimization. A number of reproducibility studies in MRS exist within the literature; covering a large range of echo times, field strengths and techniques (69–75). A recent study by Danesh K.Deelchand et al combined an experimental baseline with single voxel ^{1}H MRS (SVS) for two sites within the brain and found highly reproducible neurochemical profiles could be achieved between scanners and regions, providing optimized protocols were kept consistent (74). Previously comparisons have been made between the use of simulated baselines and experimental baselines in the fitting of spectra (76–78); however their effect on the reproducibility of 2D ^{1}H MRSI data has not previously been evaluated. In this study two types of MM schemes: simulated Si.BL and experimentally acquired Ex.BL and three echo times (35, 80 and

144ms) and their effect on the short term 1H MRSI data reproducibility at 3Tesla have been investigated to aid in protocol design for future clinical studies. The following work has been peer reviewed and published as a full paper in the Magnetic Resonance in Medicine Journal (7).

3.2 Methods

All MR scanning was performed on a 3 Tesla Philips Achieva TX MR system with a 32-channel head coil at Birmingham Children's Hospital, UK. All volunteers who participated in the study gave their informed consent under full ethical approval.

3.2.1 MRSI data collection

2D MRSI data was collected from 8 healthy volunteers (aged 23-30). An initial 3D T1 weighted anatomical MRI reference scan was obtained for MRSI grid positioning. All MRSI grids were manually placed for two regions A) above the Corpus Callosum (3 volunteers), see figure 3-1A and 3-1B and B) level with the Basal Ganglia (5 volunteers), see Figure 3-1C and 3-1D, with the following acquisition parameters: Field of View (FOV) matrix size 15x13 voxels; voxel size 13mm x 13mm x 13mm; TR=2s. Pencil beam shimming was applied. Data was collected at three different echo times on separate volunteers: TE=35ms (region: A=1 and B=2 volunteers), TE=80ms (region: A=1 and B=1 volunteer) and TE=144ms (region: A=1 and B=2 volunteers). PRESS localization was used to excite a 6x6 voxel volume of interest (VOI) (78 mm x 78 mm x 13 mm) fixed centrally to the FOV; corresponding to a fully excited 5x5 voxel region with a ½ voxel margin around the PRESS excitation region, edge voxels were discarded in post processing and the VOI extracted via a water signal threshold. In order to assess short term reproducibility all scans were acquired in triplicate without

grid repositioning; reshimming and water suppression frequency optimization in between scans was performed if deemed necessary. Due to lengthy scanning times, different volunteers were scanned for each echo time and region. Absolute concentrations were obtained by collecting water unsuppressed data during the first scan for each volunteer using the same scanning parameters as the suppressed (metabolite) data collection.

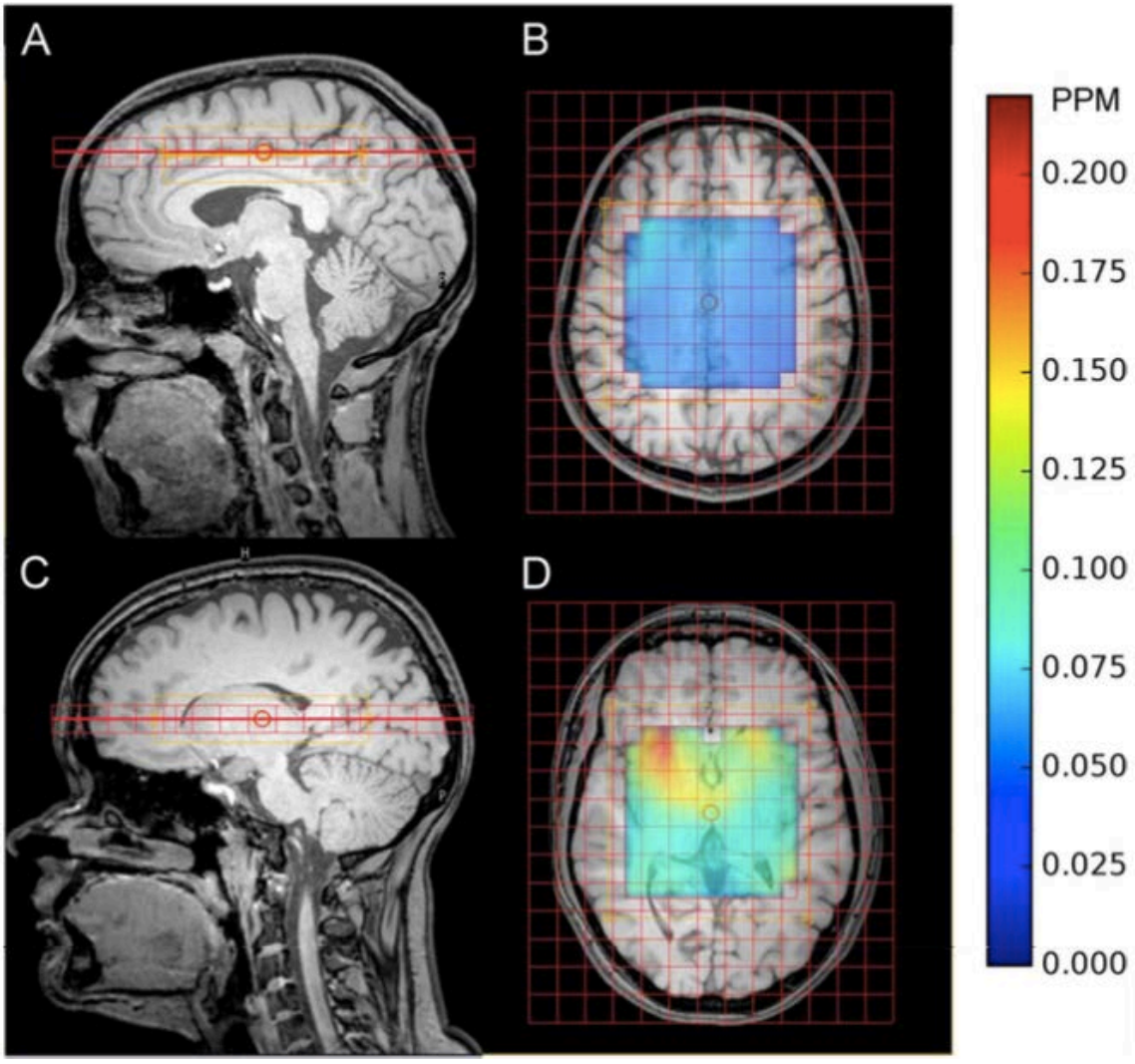

Figure 3-1 Example healthy volunteer MRSI grid placement for: above the Corpus Callosum (A) sagittal view and (B) axial view and the Basal Ganglia (C) sagittal and (D) axial view. Water line width (FWHM) maps overlaid for (B) Corpus Callosum and (D) Basal Ganglia for the PRESS box

3.2.2 Spectral Fitting

All spectral analysis was performed using the TARQUIN software package (23). The simulated macromolecular analysis scheme (Si.BL) used the following basis set to fit the MRSI data comprised of 16 individually simulated components: Alanine (Ala), Aspartate (Asp), Creatine (Cr), -CrCH2, Gamma-aminobutyric acid (GABA), Glucose (Glc), Glutamine (Gln), Glutathione (Glth), Glycerophosphorylcholine (GPC), Myo-inositol (Ins), Lactate (Lac), Lipid peaks at 0.9, 1.3a, 1.3b and 2.0ppm, Macromolecules at 0.9, 1.2, 1.4 and 2.0ppm, N-Acetyl-Aspartate (NAA), N-Acetyl-Aspartateglutamate (NAAG), Phosphorylcholine (PC), Phospho-creatine (PCr), Scyllo-inositol (s-Ins), and Taurine (Tau). All metabolite components were simulated in TARQUIN using chemical shift and J coupling values from Govinderaju et al (34). The simulated macromolecular signal is taken to be the combination of the individual macromolecular and lipid component as listed in Table 1 of the paper describing the TARQUIN algorithm (24).

3.2.3 Experimental Baseline Model Derivation (Ex.BL)

A Single Voxel Spectroscopy (SVS) inversion recovery sequence was used to acquire metabolite nulled data for improved macromolecular determination (TE/TR=35/2500ms PRESS excitation). An initial experiment was performed (data presented in section 3.3.1) to establish the optimal inversion time for metabolite signal nulling. Spectra were acquired for TI=500,650 to 850ms in 50ms steps and an optimal TI=750ms was determined. SVS inversion recovery data was collected from 7 healthy volunteers (aged 23-30) from left and right parietal white matter regions. Ten voxels were chosen across the 7 volunteers due to their high spectral quality i.e. free from artefacts caused by spurious echoes and inefficient water suppression. These data

were then compiled to create an average MM spectrum. The average spectrum was subsequently fitted using TARQUIN to obtain a noise free model of the macromolecular baseline. A macromolecule basis set composed of Gaussian peaks was initially constructed based on known peak positions and visual inspection. This basis set was fit to the average spectrum allowing peak amplitudes, widths and frequencies to be optimized. The basis set was then updated with the newly determined frequencies and peak widths and this process of basis set refinement was repeated until fitting resulted in negligible adjustment to the basis set (Table 3-1). In addition to macromolecular signals, narrow metabolite signals for NAA, NAAG, TCho, TCr and TCrCH2 were also included in the basis set to account for metabolite signals that were partially nulled (Figure 3-2). The fitted residual metabolite signals contributions were removed (via subtraction) in post processing to obtain the MM contribution only. Finally, the optimized macromolecule peaks (excluding residual metabolite signals) were summed and added to a basis set of metabolite signals (described above) – replacing the individual macromolecular and lipid components. Analysis using this experimentally derived baseline model will be referred to as Ex.BL.

3.2.4 Data analysis

MRSI spectra exported from the scanner workstation in DICOM format were imported into TARQUIN. Spectra were fitted with two different basis sets: one including the Ex.BL and another that models the MM baseline using a set of individually simulated macromolecular resonances (Si.BL). Subsequent data analysis was performed using Python programming language. Metabolite coefficients of variance (COV) were calculated as the voxel wise ratio of the standard deviation and mean for each volunteer and TE over the three MRSI acquisitions. COV's were then grouped

according to echo time, irrespective of region, and a mean COV for each metabolite calculated. This was performed to avoid regional bias with respect to data quality. A zero fill with a k space factor of 2 was used to improve the spatial resolution and number of voxels available for analysis. The VOI was extracted via a water amplitude threshold of >50% of the maximum water amplitude, and only voxels with a water line width <0.1 ppm (12.8Hz) were analyzed. A total number of voxels of 200/324, 198/230 and 246/246 were extracted for TEs = 35, 80 and 144ms respectively with this line width threshold. For analyses in section 3.3.4 the total number of voxels for line width criterion 0-0.06ppm were 94, 54 and 158 for TE=35, 80 and 144ms respectively. For line width criterion 0.06-0.1ppm the total number of voxels were 106 for TE=35ms, 144 for TE=80ms and 88 for TE=144ms. For a water line width criterion of 0.1-0.15ppm 70 voxels were found for a TE=35 and 32 for a TE = 80ms. Water line width was defined as the full width half maximum FWHM of the unsuppressed water peak in frequency domain. The unsuppressed water peak was taken to be our measure of data quality due to its robustness in comparison with metabolite line width - which can become unstable with noise and artifacts. We also assume that the water line width is directly correlated with metabolite FWHM, and therefore can be used as a proxy for data quality. Metabolite COV's were calculated to assess technical reproducibility for TE=35, 80 and 144ms comparing the two macromolecular analysis schemes: 1) Ex.BL and 2) Si.BL. COV's for the following metabolites were evaluated: total N-Acetyl Aspartate (tNAA), total Creatine (tCr), total Choline (tCho), Glutamate (Glu), Glutamine (Gln), Glutamate + Glutamine (Glx), Taurine (Tau), Glutathione (Glth) and myo-inositol (Ins). A One-Way Analysis of variance (ANOVA) test was performed for the metabolite COV's to test if a difference between the three data sets from TE=35, 80 and 144ms

were significant (degrees of freedom between groups = 2). For each volunteer, the voxel wise mean was calculated across the three scans. The mean voxel COV values were then grouped according to echo time and an overall mean COV calculated for each echo time. All statistical tests were performed on these resultant COV's for each metabolite. For this study, each mean voxel COV was considered to be independent from each other. Subsequent unpaired t-tests were carried out to assess the statistical significance of any differences in reproducibility in comparison with TE=80ms, those with $p<0.05$ were deemed significant. For this chapter, in consistence with the current literature the P-value was chosen to show any statistically significant differences. The degrees of freedom have been calculated for each test in order to express by how much the values can vary. These values have been chosen to highlight any significance in results, as due to the large quantity of data expressed within this study and to be consistent with studies of this nature, they have been chosen for ease of interpretation.

Average white matter metabolite concentrations were also calculated to validate quantitation methodology. Metabolite concentrations were measured from white matter voxels selected using the axial T1 anatomical image registered to the MRSI grid. Average metabolite concentrations for 36 white matter voxels were taken from the slice going through the Corpus Callosum (12 from each scan) for TE=35, 80 and 144ms (3 volunteers total). This was done for both Si.Bl and Ex.Bl MM analysis schemes and a percentage difference in concentration was calculated between these two fitting methods. T2 relaxation correction was applied assuming a T2 of water of 60ms and metabolite T2 of 200ms.

This analysis focused on the average across voxels in order to ease the ability to make direct comparisons between subjects and literature values. Although an advantage of MRSI is the increase in spatial specificity for individual cases, when comparing multiple subjects' due to the large amount of data acquired an average comparison is more suitable.

3.3 Results

3.3.1 Experimental Baseline Acquisition

In order to determine the optimum inversion time (TI) for nulling the metabolite signals a SVS inversion recovery sequence was used. Spectra were acquired for TI=500 and 650 to 850ms in 50ms intervals (Figure 3-2).

Figure 3-2 shows the inversion recovery spectra for the above TI's. For this TI range the metabolite signal can be seen to go from positive to negative in magnitude. An optimal inversion time of 750ms was determined as it was most efficient at nulling the metabolite signal containing the lowest metabolite signal contributions and no negative signal contributions. Subsequently SVS inversion recovery data (TI=750ms) was collected from 7 healthy volunteers (aged 23-30) from left and right parietal white matter regions. Ten out of fourteen volunteer voxels were chosen for further analysis due to their high spectral quality, voxels were excluded which contained artefacts or distortions that overlapped with the MM spectral contributions. Consistent MM content was found i.e. good overlap of spectral features between all voxels across the volunteers was observed (Figure 3-3).

The resultant mean MM spectrum was determined across the ten voxels and fitted using a MM basis set (see section 3.2.3) in TARQUIN to obtain a noise free model of

the MM baseline and is shown in Figure 3-4, the basis set and its properties split into its 13 components can be viewed in Table 3-1. Within the literature, 10 main resonances have been identified and therefore contributions are grouped and named as M1 to M10 (Figure 2-12). As we identified 13 contributions within our acquired MM model we have therefore named these contributions according to their chemical shift e.g. MM 40 is positioned at 4.0PPM.

The optimised MM peaks with the exclusion of the residual metabolite peaks (removed in post processing) were then summed and added to a basis set of metabolite signals to form the experimentally acquired baseline model Ex.BL.

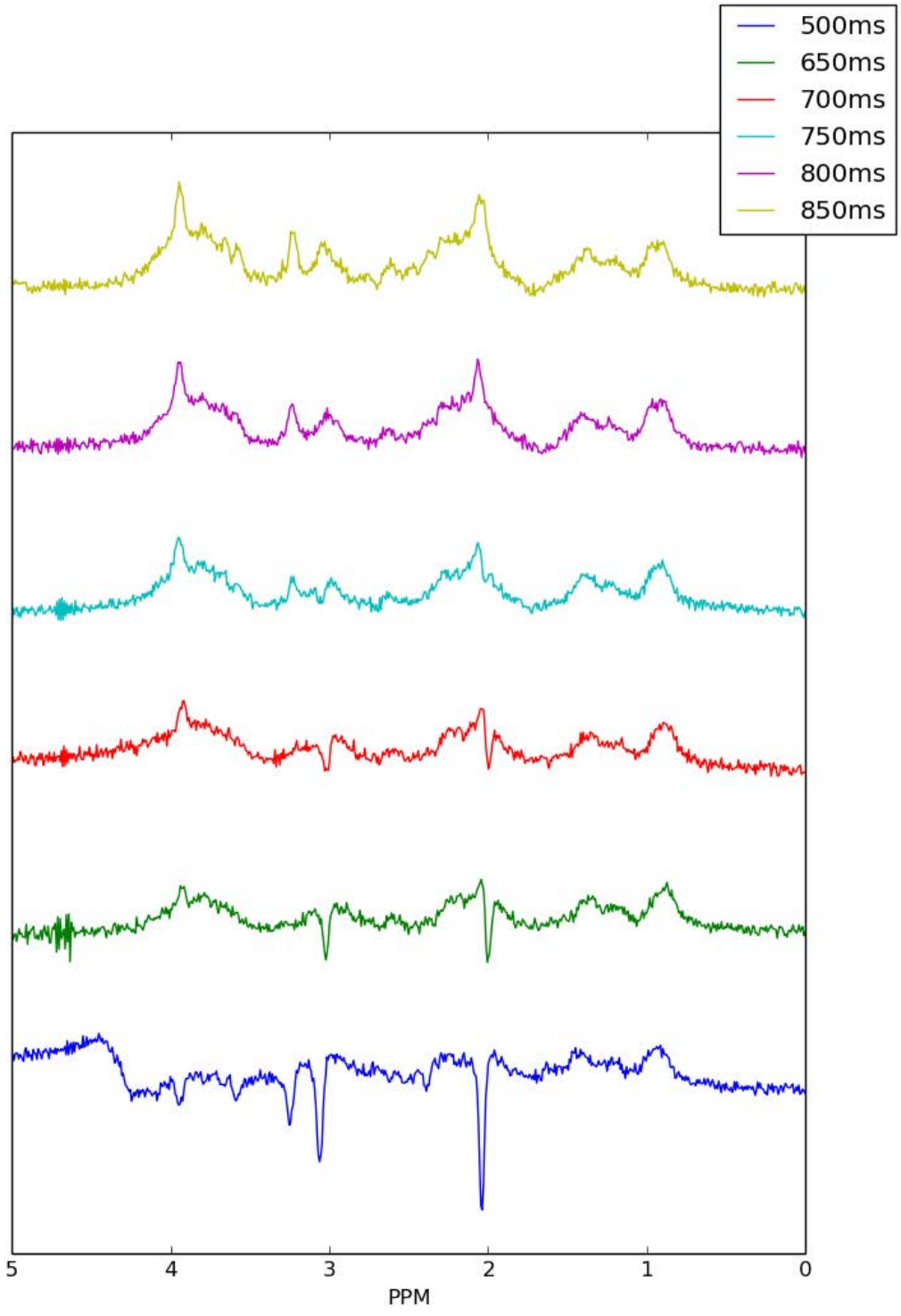

Figure 3-2 Inversion Recovery Spectra for inversion time (TI) for a range 500-850ms

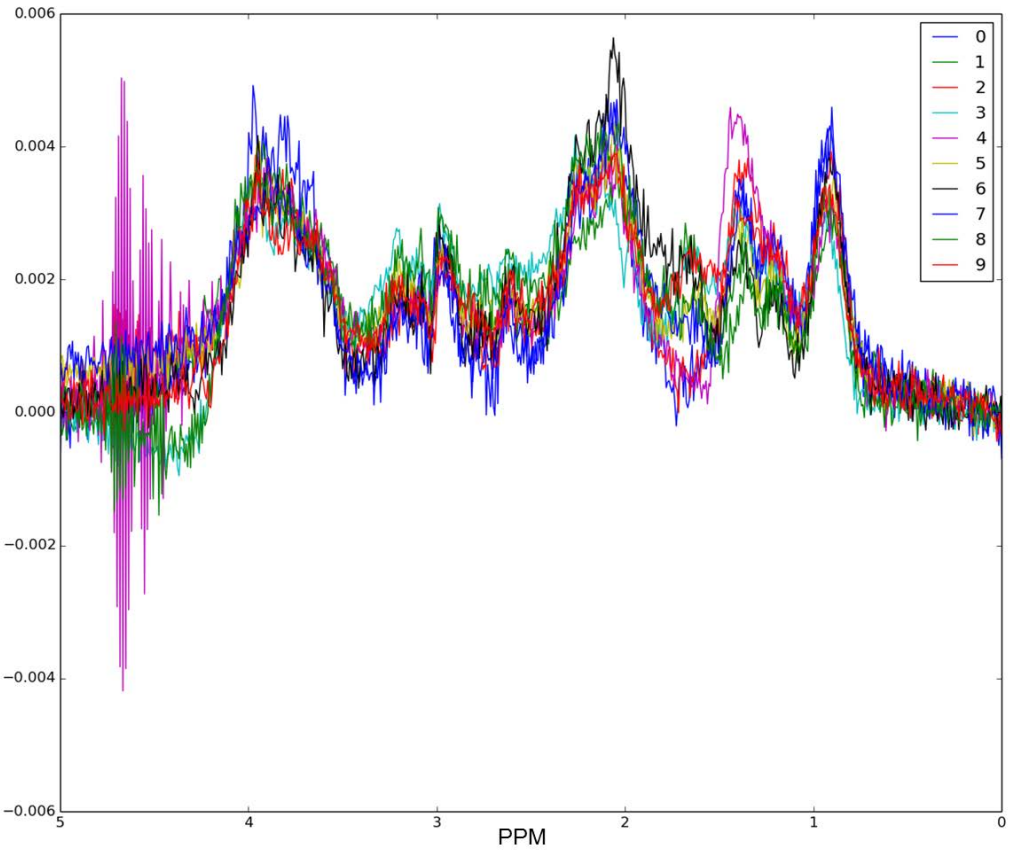

Figure 3-3 Spectral Overlap of Inversion Recovery Metabolite Nulled Spectra TI=750ms for 10 volunteer voxels

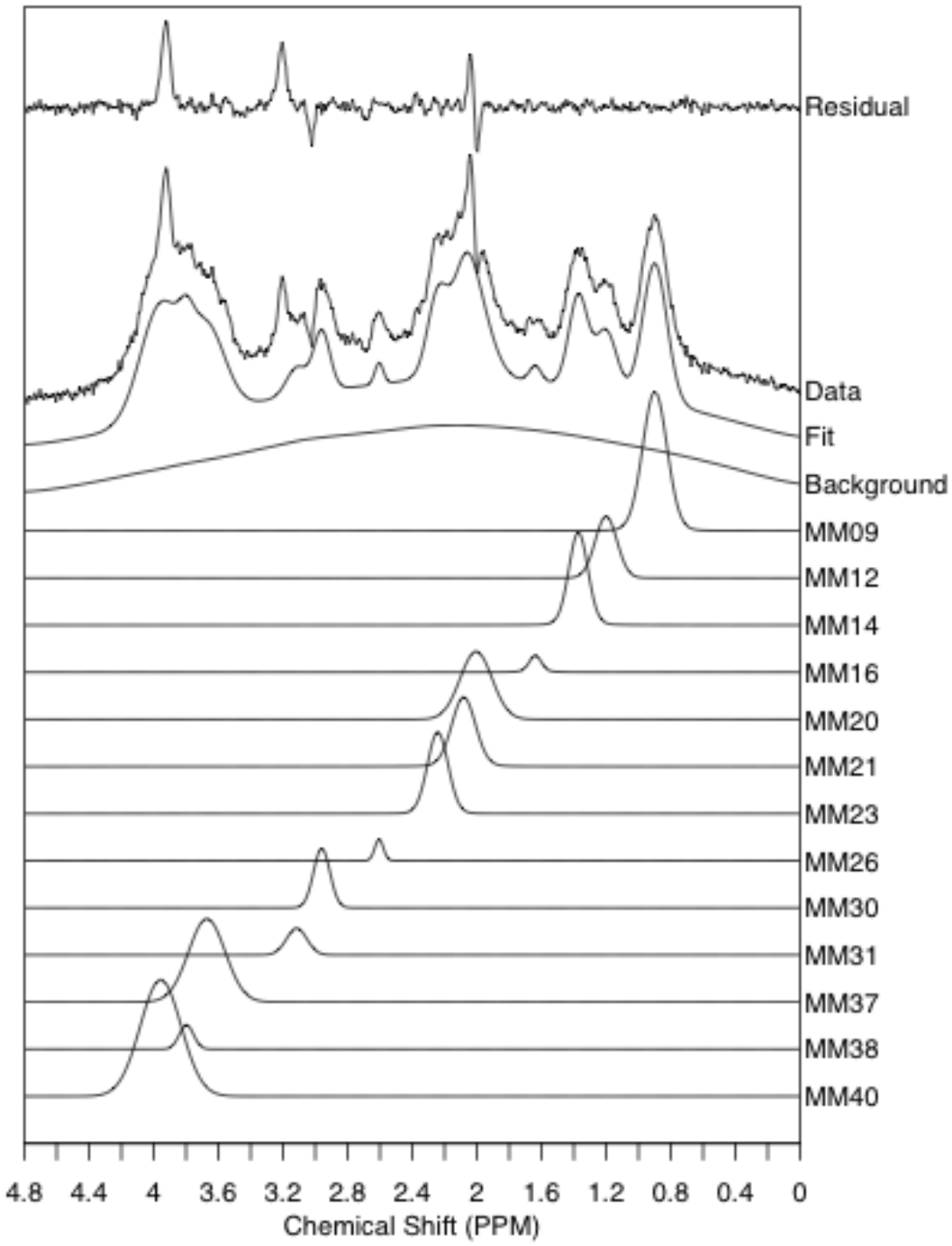

Figure 3-4 Mean Ex.BL MM Spectra taken from 7 healthy volunteers split into its MM and residual metabolite components. MM contributions within our Ex.BL MM model are labelled according to their Chemical shift e.g. MM40 is at 4.0PPM.

Table 3-1 The Ex.BL broken down into its thirteen MM components detailed according to Amplitude (AU), PPM and FWHM (Hz).

Name	Amplitude (AU)	Freq (PPM)	FWHM (Hz)
MM09	0.72	0.90	21.20
MM12	0.28	1.21	19.16
MM14	0.38	1.38	15.90
MM16	0.05	1.63	7.50
MM20	0.45	2.01	29.03
MM21	0.36	2.09	20.53
MM23	0.36	2.25	17.89
MM26	0.04	2.61	5.30
MM30	0.20	2.96	14.02
MM31	0.11	3.11	17.89
MM37	0.64	3.67	33.52
MM38	0.07	3.80	11.85
MM40	1.00	3.96	37.48

3.3.2 Impact of Echo Time on and Ex.Bl on spectral fitting

It can be seen from Figure 3-5A and 3-5B that the inclusion of a better-defined MM model Ex.BL, reduces the level of the broad background signals (obtained from a 50-point moving average filter of the fit residual) compared to Si.BL for the fitting of short TE spectra. A reduction in MM content relative to the metabolite signals was also observed via an increase in echo time to 80 and 144ms (Figure 3-5C and 3-5D) due to shorter T2 relaxation times. A reduction in SNR is also observed within increasing echo time due to T2 relaxation effects and the dephasing of metabolite multiplets.

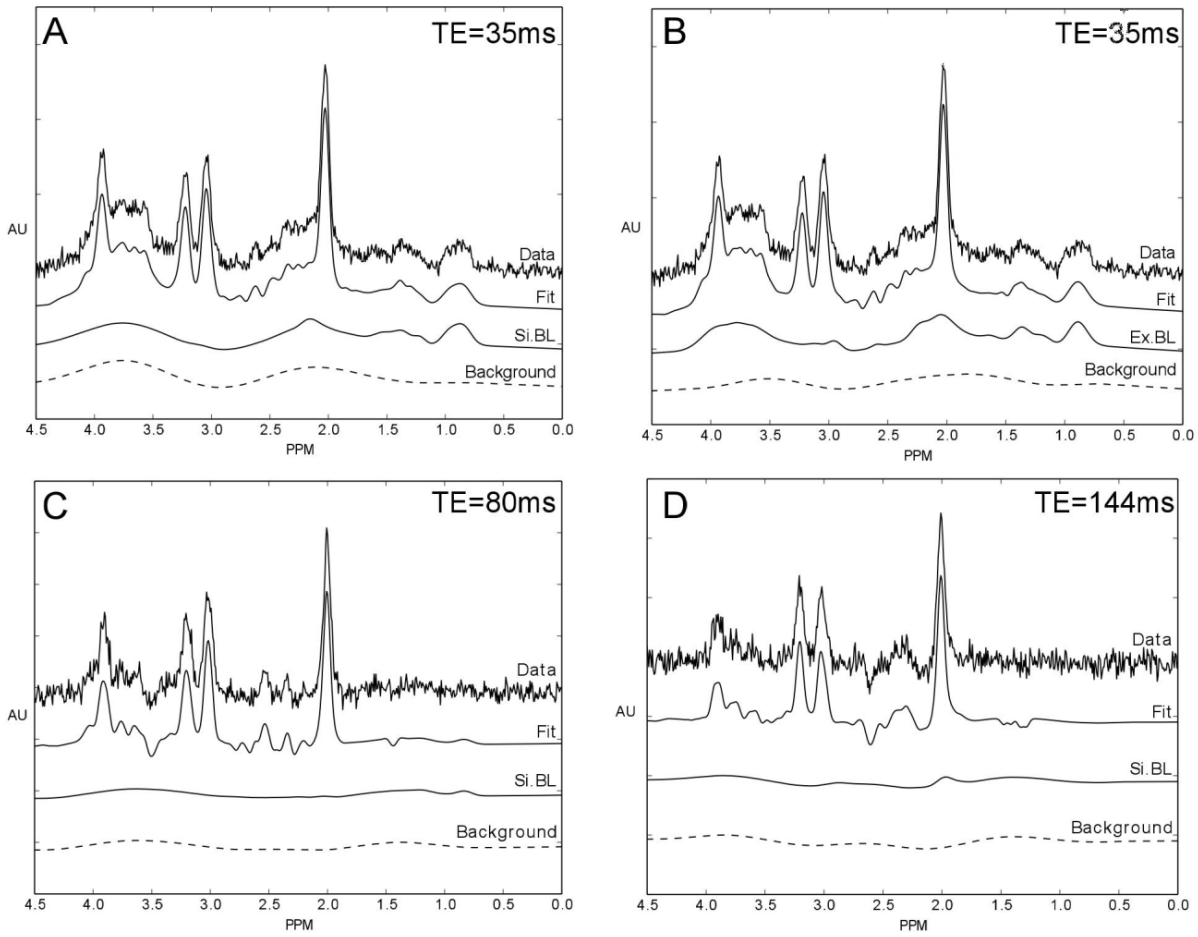

Figure 3-5 Example healthy volunteer spectra split into four components: Data, Fit, MM analysis scheme (Si.BL or Ex.BL) and residual background signal for TE's: A) TE=35ms (Si.BL); B) TE=35ms (Ex.BL); C) TE=80ms (Si.BL) and D) TE=144ms (Si.BL)

3.3.3 The Effect of Echo Time and Macromolecular Analysis Schemes on Reproducibility

Coefficients of Variance (COV's) were calculated for voxels containing spectra that meet the line width value criteria <0.1ppm (Table 3-2). Overall, for both Si.BL and Ex.BL MM analysis schemes, COV's across the three echo times 35, 80 and 144ms were found to be statistically different via an ANOVA test for the following metabolites: tNAA, tCr, Glu, Gln, Ins, Glth and Tau ($p<0.00001$). An echo time of 80ms was found to provide the most reproducible metabolite estimates for tNAA, tCho and tCr with

COV's<9%. Additionally, a TE of 80ms showed improved reproducibility, for both MM analysis schemes, compared to TE=35ms ($p<0.01$) for the following five metabolites: tNAA, tCr, Gln, Glth and Tau (Table 3-2).

Table 3-2 Metabolite Coefficients of Variance (COV's) for TE=35, 80 and 144ms for voxels containing spectra that meet the overall water line width criteria of between 0 and 0.1ppm showing significant ($p<0.05$) differences from an unpaired t-test between Si.BL and Ex.BL for TE=35ms (†), TE=80ms (‡) and TE=144ms (¥). Significances of $p<0.01$ are denoted as: TE=35ms (††), TE=80ms (‡‡) and TE=144ms (¥¥). ANOVA degrees of freedom within groups= 641.

Line width	**0-0.1ppm**							
	TE=35ms		**TE=80ms**		**TE=144ms**		**Echo time comparison**	
Metabolite	**Coefficient of Variance %**		**Coefficient of Variance %**		**Coefficient of Variance %**		**ANOVA**	
	Si.BL	Ex.BL	Si.BL	Ex.BL	Si.BL	Ex.BL	Si.BL	Ex.BL
tNAA††¥¥	9.99	7.56	6.03	5.35	12.31	7.81	<0.00001	<0.00001
tCr	10.13	9.25	7.18	7.22	11.56	10.91	<0.00001	<0.00001
tCho	9.00	9.40	8.16	8.10	9.78	9.61	0.1209	0.1027
Glu††	20.35	16.33	22.36	22.82	45.96	47.57	<0.00001	<0.00001
Gln¥	83.80	88.85	56.22	60.19	47.37	53.22	<0.00001	<0.00001
Glx††¥	24.85	19.95	22.81	23.25	22.49	25.39	0.1525	0.0001
Ins	15.36	15.36	16.97	17.87	34.46	33.84	<0.00001	<0.00001
Glth†	48.43	68.14	28.33	27.67	69.06	68.39	<0.00001	<0.00001
Tau††	127.97	89.93	70.56	70.56	70.71	66.25	<0.00001	<0.00001

Note: Significant differences shown from an unpaired t-test between Si.BL and Ex.BL for TE=35ms (†), TE=80ms (‡) and TE=144ms (¥) †, ‡ and ¥ <0.05 and ††, ‡‡ and ¥¥<0.01.

The most reproducible metabolites across with CoV's< 13% for all echo times were found to be tNAA, tCr and tCho. Lower variation using the Ex.BL model at TE=35ms compared to TE=80ms was observed for Glu ($p<0.01$) and Glx ($p<0.05$), it is likely that this is the result of signal dephasing, therefore a short echo acquisition maybe preferred depending on metabolite of interest. The highest variation was found for long echo TE=144ms spectra with Ex.BL COV's tNAA=7.81%, tCr=10.91% and tCho=9.61%; compared to 7.56%, 9.25% and 9.4%for TE=35ms and 5.35%, 7.22% and 8.1% for TE=80ms respectively (Table 3-2). Variation is significantly reduced with the use of an Ex.BL for TE=35ms compared to Si.BL for tNAA, Glu, Glx and Tau ($p<0.01$). However, a Si.BL provided significantly better reproducibility for the measurement of Glth ($p<0.05$).

3.3.4 The Effect of Line Width and Macromolecular Analysis Schemes on Reproducibility

Data quality, along with echo-time and analysis methods, can have a significant impact on MRS reproducibility. Therefore, voxels were stratified according to their line width: "good" 0-0.06ppm (Table 3-3); "acceptable" 0.06-0.1ppm (Table 3-4) and "poor" 0.1-0.15ppm (Table 3-5) groups were identified to investigate the impact of line width on reproducibility. An improvement in COV of ~35% and ~22% for tNAA was observed between "good" and "acceptable" data for Si.BL and Ex.BL respectively.

The use of an Ex.BL macromolecular analysis scheme found improved reproducibility for poorer line widths compared to the Si.BL analysis. Ex.BL analysis resulted in a large reduction in tNAA COV of 38% for "poor" line widths between 0.1 and 0.15ppm (Table 3-5). Smaller reductions of ~30% and ~15% were observed for acceptable

(0.06-0.1ppm) and “good” (0-0.06ppm) line widths respectively. For increasing echo time, improved reproducibility between Si.BL and Ex.BL was found for tNAA, tCr, tCho, Glx and Tau (Tables 3-3 and 3-4) – most likely due to a reduction in MM signal contribution at longer TE’s.

Table 3-3 Metabolite Coefficients of Variance (COV’s) for TE=35, 80 and 144ms for voxels containing spectra that meet the “good” water line width criteria of between 0 and 0.06ppm showing significant (p<0.05) differences from an unpaired t-test between Si.BL and Ex.BL for TE=35ms (†), TE=80ms (‡) and TE=144ms (¥). Significances of p<0.01 are denoted as: TE=35ms (††), TE=80ms (‡‡) and TE=144ms (¥¥). ANOVA degrees of freedom within groups = 303.

Line width	**0-0.06ppm**							
	TE=35ms		**TE=80ms**		**TE=144ms**		**Echo time comparison**	
Metabolite	**Coefficient of Variance %**		**Coefficient of Variance %**		**Coefficient of Variance %**		**ANOVA**	
	Si.BL	Ex.BL	Si.BL	Ex.BL	Si.BL	Ex.BL	Si.BL	Ex.BL
tNAA¥¥	7.79	6.59	4.07	3.81	10.96	7.55	<0.00001	<0.00001
tCr†	10.52	8.69	4.70	4.25	10.19	9.90	<0.00001	<0.00001
tCho	8.16	8.19	5.91	5.75	9.16	8.81	<0.05	<0.05
Glu††	17.30	13.73	16.80	17.87	37.08	41.52	<0.00001	<0.00001
Gln	83.98	93.24	41.61	46.79	46.91	52.31	<0.00001	<0.00001
Glx††	19.54	15.39	18.55	19.80	22.01	24.50	<0.05	<0.00001
Ins	15.94	15.69	10.24	10.94	27.00	27.22	<0.00001	<0.00001
Glth	33.08	38.41	27.34	25.37	62.60	61.22	<0.00001	<0.00001
Tau††	127.87	89.93	62.30	60.61	60.63	56.44	<0.00001	<0.00001

Note: Significant differences shown from an unpaired t-test between Si.BL and Ex.BL for TE=35ms(†), TE=80ms(‡) and TE=144ms(¥) †, ‡ and ¥ <0.05 and ††, ‡‡ and ¥¥<0.01.

Table 3-4 Metabolite Coefficients of Variance (COV's) for TE=35, 80 and 144ms for voxels containing spectra that meet the "acceptable" water line width criteria of between 0.06 and 0.1ppm showing significant (p<0.05) differences from an unpaired t-test between Si.BL and Ex.BL for TE=35ms (†), TE=80ms (‡) and TE=144ms (¥). Significances of p<0.01 are denoted as: TE=35ms (††), TE=80ms (‡‡) and TE=144ms (¥¥). ANOVA test degrees of freedom within groups = 335.

Line width	0.06-0.1ppm							
	TE=35ms		TE=80ms		TE=144ms		Echo time comparison	
Metabolite	Coefficient of Variance %		Coefficient of Variance %		Coefficient of Variance %		ANOVA	
	Si.BL	Ex.BL	Si.BL	Ex.BL	Si.BL	Ex.BL	Si.BL	Ex.BL
tNAA††¥¥	11.94	8.41	6.77	5.92	14.73	8.27	<0.00001	<0.0001
tCr	9.78	9.74	8.12	8.33	14.02	12.73	<0.00001	<0.001
tCho	9.75	10.47	9.00	8.98	10.89	11.03	0.2815	0.1056
Glu†	23.06	18.63	24.45	24.68	62.45	59.21	<0.00001	<0.00001
Gln	83.65	85.64	61.78	65.36	48.18	54.81	<0.00001	<0.00001
Glx†	29.56	23.99	24.41	24.54	23.34	26.99	0.01	0.3328
Ins	14.85	15.06	19.49	20.47	47.85	45.72	<0.00001	<0.00001
Glth†	63.00	102.50	28.71	28.53	92.26	88.03	<0.00001	<0.00001
Tau††	128.16	96.08	73.74	74.43	91.93	86.37	<0.00001	<0.01

Note: Significant differences shown from an unpaired t-test between Si.BL and Ex.BL for TE=35ms (†), TE=80ms (‡) and TE=144ms (¥) †, ‡ and ¥ <0.05 and ††, ‡‡ and ¥¥<0.01.

Table 3-5 Metabolite Coefficients of Variance (COV's) for TE=35 and 80ms for voxels containing spectra that meet the "poor" water line width criteria of between 0.1 and 0.15ppm showing significant (p<0.05) differences from an unpaired t-test between Si.BL and Ex.BL for TE=35ms (†) and TE=80ms (‡). Significances of p<0.01 are denoted as: TE=35ms (††) and TE=80ms (‡‡). Degrees of freedom = 101

Line width	0.1-0.15ppm			
	TE=35ms		TE=80ms	
Metabolite	Coefficient of Variance %		Coefficient of Variance %	
	Si.BL	Ex.BL	Si.BL	Ex.BL
tNAA††‡‡	23.09	14.39	12.96	6.53
tCr	15.53	14.92	10.21	10.22
tCho	15.15	14.17	18.44	17.44
Glu	30.62	27.46	44.72	40.21
Gln	56.13	56.46	92.37	101.36
Glx	23.99	23.75	42.56	38.28
Ins	27.85	27.22	34.79	38.10
Glth†	103.15	121.31	44.15	46.19
Tau	141.42	131.06	73.90	77.15

Note: Significant differences shown from an unpaired t-test between Si.BL and Ex.BL for TE=35ms (†) and TE=80ms (‡) † and ‡ <0.05 and †† and ‡‡ <0.01.

Figure 3-1B and 3-1D show the effect imaging region can have on water line width. Line widths approximately three times higher were observed for the Basal Ganglia imaging slice compared to a higher placed slice above the corpus callosum. A mean water line width of 0.07, 0.07 and 0.06ppm were observed across both regions for TE=35, 80 and 144ms respectively for voxels analyzed with the water line width criteria <0.1ppm. Poorer line widths were particularly observed in the frontal region of the basal ganglia slice through the brain. Magnetic field inhomogeneity effects, which result in

spectral line broadening, are most commonly observed in MRSI data where there is a close proximity to air-tissue interfaces e.g. the sinuses (79). Poor line width increased fitting error resulting in a reduction in overall reproducibility. Short echo (TE=35ms) spectra had the greatest voxel loss of 38% of the total voxels across all scans and volunteers' due to poor line width >0.01ppm; compared to 14% and 3% for TE=80ms and 144ms respectively. Analysis showed these voxels were localised predominantly in the basal ganglia region.

3.3.5 The Effect of Echo Time and Macromolecular Analysis Schemes on Metabolite Quantitation

Average white matter metabolite concentrations were calculated to assess the ability of the techniques to reproduce the expected metabolite concentrations and validate the overall quantitation methodology. The absolute metabolite concentrations taken from white matter voxels for each echo time and a comparison between Si.BL and Ex.Bl MM analysis schemes are shown in Table 3-6. Absolute concentrations for TE=35ms and 80ms were found to be consistent with those in the literature for healthy parietal white matter (70,80). For a TE=144ms a slight underestimation was observed suggesting accuracy maybe reduced at longer TE due to increased T2 relaxation. Additionally, it is also worth noting that differences in metabolite concentrations could be attributed to natural variation across volunteers. A percentage difference of below 23% was found between Si.BL and Ex.BL across all echo times for tNAA, tCr and tCho. Larger differences especially for an echo time of 35ms were observed for poorly determined metabolites such as Gln, Glth and Tau.

Table 3-6 Average healthy volunteer metabolite concentrations for left and right white matter for TE=35, 80 and 144ms for both Ex.BL and Si.BL MM analysis schemes. A percentage difference Δ between Si.BL and Ex.BL is also shown.

	TE=35ms			TE=80ms			TE=144ms		
	Mean Concentration (mmol)		Δ (%)	Mean Concentration (mmol)		Δ (%)	Mean Concentration (mmol)		Δ (%)
Metabolite	Si.BL	Ex.BL		Si.BL	Ex.BL		Si.BL	Ex.BL	
tNAA	7.0	6.5	7.2	7.6	7.8	-1.3	5.7	6.6	-14.7
tCr	4.9	4.5	9.3	3.6	3.5	1.4	2.3	2.3	-0.1
tCho	1.4	1.3	9.1	1.1	1.1	1.6	1.0	1.0	3.6
Glu	5.2	5.3	-2.9	4.0	4.0	0.0	1.0	0.9	17.2
Gln	0.8	0.5	45.3	0.5	0.5	10.2	1.2	1.0	17.5
Glx	6.0	5.8	3.9	4.5	4.5	1.2	2.2	1.8	17.4
Ins	2.8	2.9	-3.5	3.6	3.5	1.8	1.3	1.3	-0.3
Glth	1.0	0.3	66.1	0.7	0.8	-1.1	0.2	0.2	-34.5
Tau	0.1	0.5	-543.6	0.4	0.4	-1.8	0.4	0.4	-2.9

3.4 Discussion

The effect of echo time and macromolecular analysis schemes on ^{1}H MRSI reproducibility has been investigated for three different echo times 35, 80 and 144ms and a comparison made between two different MM analysis schemes Si.Bl and Ex.Bl. An Ex.BL model was developed and optimised to extract a metabolite nulled MM signal for inclusion in the Ex.BL basis set. Overall, it was found that a TE=80ms was significantly more reproducible for the following five metabolites: tNAA, tCr, Gln, Glth and Tau. However, the short echo acquisition TE=35ms combined with Ex.BL performed significantly better for Glu and Glx.

The experimentally acquired healthy volunteer baseline signal was found to be consistent between volunteers with respect to MM content. This is found to further compliment the study by Snoussi et al (68), that suggested the use of a single MM baseline spectra could be sufficient to include in a basis set for the fitting of spectra. Residual metabolite peaks present in the metabolite nulled spectra due to their differing T1 relaxation properties, can be easily removed in post processing. Therefore, the resultant MM signal could be successfully introduced into the Ex.BL basis set.

Metabolites tNAA, tCr and tCho within healthy brain spectra, are known to have higher SNR in comparison with other lower level metabolites. Therefore, as expected they were found to be the most reproducible. This can be attributed to an inherent increase in fitting precision compared to lower level metabolite signals. The use of an Ex.BL significantly improved the reproducibility compared to Si.BL for short TE spectra for four metabolites: tNAA, Glu, Glx and Tau. The Ex.BL model also found increased

performance for spectra with poor line widths – this method could therefore be used to improve the reliability of poor quality spectra.

Several reproducibility studies exist within the literature. However, they are varied and cover a wide range of techniques, echo times and field strength. This means direct comparisons between studies can prove difficult. A recent study by Veenith et al (81), which used a simulated baseline model at TE=70ms, found within session reproducibility COVs of 9.9% for tNAA, 10.6% tCr and 14.3% for tCho compared to our studies values at TE=80ms of 6.03%, 7.18% and 8.16% for tNAA, tCr and tCho respectively using the Si.BL MM analysis scheme. Further improvement in our study at TE=80ms was observed with the use of an Ex.BL for the above metabolites with COVs of 5.35% for tNAA and 8.1% for tCho. Use of different methodologies between these two studies could attribute to the observed differences in results, some of which include: Spin-Echo versus PRESS acquisition, differing analysis software and a slightly different line width quality control criterion of <12Hz. Our protocol also had a slightly increased echo time of 80ms, which would allow MM signals to decay further, decreasing their contribution and potentially reducing their impact on the overall reproducibility. A combination of all these factors could have contributed to the improved reproducibility observed within our study.

For some studies, protocols have been developed and tested for the optimized measurement of specific metabolites. A short echo time (TE=40ms) study by Gasparovic et al (82) at 3Tesla found comparable COV's to our study of 5% for tNAA, 6% Cr, 7% Cho, 11% Ins, 10% Glu and 13% for Glx. Their TE=40ms was chosen for optimized detection of Glu. Additionally, a study by Jang et al (83) at a lower field strength of 1.5Tesla also found an optimal short TE of 40ms using PRESS for the

measurement of Glutamate. Comparable COV's of 11 and 13.1% for anterior cingulate cortex and insula respectively were also found. In our study at TE=35ms a slightly increased COV of 16.33% was for Glu may have been found as our sequence had not been specifically optimized for this metabolite.

There is a growing clinical interest in the use of MRS in the measurement of glutamate for the study of schizophrenia (84); brain tumor metabolism (85) and cognition (86). In this study, the combination of Ex.BL and an echo time of 35ms yielded the most reproducible measure of glutamate (COV=14%). This finding is in agreement with a previous study by Hancu et al, where simulations and in-vivo data were used to demonstrate that shorter TE acquisitions showed better reproducibility for glutamate measurements (87). Additionally, work by Mullins et al also found a shorter echo time to be optimal for Glu with CoV's of 2.6% for TE=40ms and 7.6% for TE=80ms (88). Contrary to this, a study by Schubert et al (89), assessed the determination of glutamate using SVS at 3Tesla, proposed an intermediate TE of 80ms to be optimal. However, Schubert et al only focused on TE's between 50ms and 330ms and did not evaluate short-echo spectra <50ms. In addition, macromolecular signals were not included in the analysis basis set, therefore analysis of echo times shorter than 50ms would have resulted in greater interference from macromolecular signals. In this study, for TE=80ms a COV of 17% for glutamate was achieved compared with 10% from Schubert et al, this difference may be attributed to the generally higher data quality available from SVS. Whilst this study was focused on MRSI, it is worth noting that the findings here broadly agree with similar SVS studies measuring glutamate, this indicates our results may also be applicable to the design of SVS studies. Hancu and Port et al (90) suggest a TE=80ms is optimal for Glutamine with in vivo COVs of 12.7%

compared to 122% for a TE=35ms. Due to dephasing, a shorter TE was better for Glutamate with simulation COV's of 4.2% for TE=35ms and 5.1% for TE=80ms. This finding is in agreement with our study. Our study however shows increased variation for Glutamate as expected in vivo when compared to simulation. J-modulation effects for Glutamate at longer TE could explain why glutamate is dephased at longer TE, whereas glutamine can still be reliably measured. It is also worth noting that as glutamine is present in low levels in healthy subjects its reproducibility can be difficult to determine accurately.

Another metabolite of interest within MRS studies is Lactate. Increased levels of lactate are thought to be associated with hypoxia or ischemia. Therefore this signal is widely measured in clinical MRS studies in order to investigate pathologies such as brain tumors and mitochondrial disease (10). A characteristic signal inversion at TE=144ms means this long echo time is often used for the measurement of lactate, due to an improved separation from lipid signals at 1.3ppm (10,91). As low levels of lactate exist in normal brain, this metabolite was not considered in this study, however this example highlights that a single echo time may not be optimal for all metabolites. Therefore, protocol optimization is important and will always benefit from prior knowledge of the important metabolites for a particular clinical question. However, in the absence of a prior hypothesis, a shorter TE with appropriate macromolecular and lipid analysis will give good results for most metabolites due to reduced multiplet dephasing and T2 weighting.

It is worth noting that in addition to metabolites, the MM spectral content itself is also of clinical interest, since it has been shown to provide additional information for a number of diseases, such as brain tumors where MM content was found to be useful

in assigning tumor grade (52). A recent mouse model study by Craveiro et al has shown that human glioma has exhibited several alterations in the macromolecule spectrum when compared to healthy controls corresponding to mobile lipids and also a broad MM component between 3.6 and 3.7ppm. This introduced significant errors into the quantification of Lac and Asp (92). Therefore, any difference in MM content due to pathology may need to be accounted for in order to maintain accurate metabolite quantification. This also suggests that a MM fitting model based on normal tissue may not be suitable for the analysis of some pathology. Elevated levels of MM have also been observed in studies of multiple sclerosis (93) and stroke (56,63). The acquisition of MM spectra using an inversion recovery sequence for each patient would prove time consuming and may preclude its use in routine clinic. Therefore, as the MM content for pathological tissue is likely to differ from normative profiles in some diseases, the more flexible Si.BL analysis method should be chosen in the absence of a patient or disease specific MM profile.

Whilst both echo time and macromolecular analysis schemes can influence the reproducibility of ^{1}H MRSI spectra; data quality parameters such as water line width and SNR also have a significant impact. Echo time is inherently linked with SNR, and therefore is an important factor to consider for protocol optimization. Loss of signal limits the amount of metabolite information that can be observed at increased echo times, as lower level signals get closer to and become indistinguishable from background levels decreasing fitting accuracy. Water line width is another issue that can influence the reproducibility of spectra. Table 3-5 illustrates that if a rejection criterion is not set, the available reproducibility for each metabolite can increase drastically. For example, a twofold change in reproducibility can be observed in the

case of tNAA compared to water line width <0.1 ppm. Water line width is also dependent on imaging location, meaning voxel placement may become an issue in protocol design. In this study, poorer water line widths were observed for spectra collected with a slice going through the Basal Ganglia, particularly in the frontal region, due a closer proximity to susceptibility inducing air-tissue boundaries e.g. sinuses. This proved particularly problematic for short-echo spectra, resulting in the rejection of over a third of voxels due to water line width (>0.1ppm). This loss of information would prove particularly disadvantageous if the voxels discarded are in an area of pathological interest.

This study demonstrates several factors are needed to be taken into consideration in MRSI protocol optimization including: echo time, macromolecular analysis schemes, metabolite of interest, location and data quality, all which are not necessarily independent from each other. This study mainly focuses on the intra-subject reproducibility within the same session rather than accuracy. Metabolite concentrations were calculated for each echo time and MM analysis scheme and were found to be consistent with those previously published in literature for parietal white matter (70,80). A slight underestimation was found for a TE=144ms suggesting accuracy is decreased at longer TE which could be due to T2 bias on the metabolite estimates. True measures of accuracy are difficult to establish in volunteers and patients due to a lack of alternative methods for measuring NMR visible metabolite concentrations. For this reason, partial volume corrections for white matter, grey matter and cerebrospinal fluid were not required for this study - as COV measured were only performed between voxels with identical tissue constituents. Further work is needed to develop methods for establishing combined reproducibility and accuracy.

3.5 Conclusion

In this study, echo time, macromolecular baseline analysis and data quality parameters were all found to impact the reproducibility of ^{1}H MRSI data. These results highlight the importance of careful selection of echo time and analysis methodology where optimal reproducibility is sought for a primary metabolite of interest. Overall, this study found that a TE=80ms produced the most reproducible metabolite values for tNAA, tCho, tCr and Glth in healthy volunteers. However, the combined use of a short TE sequence and the MM analysis scheme Ex.BL may be preferred as a compromise between good accuracy, good SNR and T2 bias on metabolite estimates.

4. Sensitivity Encoding for fast 1H MRSI Water Reference Acquisition

4.1 Introduction

Absolute quantification of metabolite concentrations is important. However, the requirement for an internal standard water reference acquisition poses a challenge, as it increases acquisition time considerably for MRSI acquisitions. This can preclude its use in routine clinic. Absolute quantification has significant advantages over more commonly used ratios; firstly, ratios can become unstable particularly if the denominator metabolite is present in low concentrations. Secondly as all metabolites may be equally affected due to an overall increase or decrease in denominator, the determination of the cause/impact of a change can prove difficult.

Fast-MRSI methods have been developed which reduce the scan time required to acquire both the metabolite and water reference data. As discussed previously in chapter 2, sensitivity encoding (SENSE) and reduced resolution (current Philips default MRSI protocol) are two techniques that can be used to speed up scan time; by either reducing the number of phase encoding steps or sampling fewer points in k-space respectively. The reduced resolution technique may primarily be used to assist in post processing steps; for example, phase correction and line shape correction but for this study we have focused on its use for absolute metabolite quantitation.

An alternative to acquiring a water reference scan is to determine the absolute concentrations using an external reference system; Bonekamp et al (14) investigated the use of SENSE in conjunction with an external reference “phantom replacement” technique. This method is advantageous as no additional patient scan time is required. It also doesn’t rely on water content and relaxation time estimations as it uses a

standard with known concentration. It does however suffer from B1 inhomogeneity effects, further enhanced by the need for a larger Field of View (FOV), which also results in an increase in scan time.

For SENSE spatial resolution is theoretically preserved, however increasing SNR loss is associated with higher reduction factors (94). As water reference data inherently has high SNR, we hypothesis that SENSE will be the superior in the collection of fast water reference data collection in comparison to the reduced resolution method.

Therefore, as the SNR is extremely high for water reference data, we propose that in order to maintain accurate measurements of lower concentration metabolites, SENSE R=1 (no-under sampling) should be used for the collection of metabolite data and SENSE R=3 for water reference data collection. In this study, we compare the accuracy of the two fast methods – SENSE with reduction factor 3 in both directions and reduced resolution in their ability to reconstruct an equivalent fully sampled MRSI water reference acquisition. In order to do this a comparison between water amplitudes was made. The fast method which provided water amplitudes closest to the fully sampled method was regarded as most accurate. In order to validate the proposed methodology data was collected from three volunteers and a standard MRS (“braino”) phantom. This study has also been peer reviewed and published in Magnetic Resonance in Medicine journal (95).

4.2 Methods

4.2.1 MRSI Data Collection

All MR scanning was performed on a 3T Philips Achieva TX MR System using a 32-channel head coil at Birmingham Children's Hospital, UK. This study had full ethical approval and informed consent was obtained for all subjects.

Data was collected from three healthy volunteers (aged between 20 and 25) and a "braino" MRS phantom containing the following constituents:10mM creatine hydrate, 2mM choline chloride, 5mM dl-lactic acid, 1mL/L Gd-DPTA (Magnevist), 12.5mM 1-glutamic acid, 7.5mM myo-inositol, 12.5mM N-acetyl-1aspartic acid (NAA), 0.1% sodium azide, 56mM sodium hydroxide (NaOH) and 50mM potassium phosphate monobasic (KH2PO4) (96).

For MRSI grid positioning, an initial T1 weighted 3D Fast Low Angle Shot (FLASH) MRI 1mm isotropic reference scan was obtained. All MRSI grids were manually positioned above the corpus callosum (Figure 4-2a) with the following acquisition parameters: Field of View (FOV) matrix size 15x13; voxel size 13mm x 13mm x 13mm; TE=35ms; TR=2s; half echo acquisition mode. In each case PRESS localisation was applied to excite a 6x6 voxel region (78mm x 78mm x 13mm) centrally within the FOV. This corresponds to a fully excited 5x5 region with a ½ voxel margin outside the PRESS excitation region. Since NMR visible water concentrations are fairly constant throughout the head (~40M), we intentionally included these partially excited voxels (equating to a 7x7 region) in the analysis in order to ensure the fast MRSI methods could be used to accurately reconstruct non-uniform water distributions. In all MRSI examinations, in order to reduce acquisition time, the points of k-space outside the

elliptical boundary were not sampled (97). In post processing, a k-space hamming filter was applied to reduce ringing artefacts. No additional averaging was performed during k-space acquisition.

Preliminary studies (Section 4.3.1) comparing the SENSE method with the fully sampled MRSI acquisition highlighted a systematic difference in scaling between SENSE and no SENSE acquisitions. This was due to a rescaling step required in the SENSE reconstruction. Therefore, to allow a true comparison between the SENSE R=3 and reduced resolution method, SENSE reconstruction was also enabled for both the reduced resolution and full acquisition scans with speed up factor R=1 (no under sampling) in both directions. Resultant scans therefore have a consistent scaling factor between the full acquisition, reduced resolution and SENSE methods. For the remainder of this study the following terminology will be used to describe each type of MRSI acquisition used: “full acquisition no-SENSE” will refer to the fully sampled MRSI grid no SENSE scaling, 153 phase encoding steps, scan time= 5 minutes 6 s; “full acquisition” will refer to the fully sampled MRSI grid with SENSE R=1 scaling, 153 phase encoding steps, scan time= 5 minutes 6s; “reduced resolution acquisition” will refer to a 2x reduction in k-space sampling for both dimensions with SENSE scaling (R=1), 32 phase encoding steps, scan time= 1minute 4 s; and “SENSE acquisition” will refer to the standard SENSE reconstruction with a x3 reduction k-space sampling (R=3) for both dimensions, 28 phase encoding steps, scan time= 56s.

Patient and phantom MRSI scans were performed in succession with identical FOV and PRESS geometries within each session. Each of the following scans were collected for both patient and phantom data: full acquisition no-SENSE; full acquisition (R=1); SENSE R=3 acquisition; and reduced resolution acquisition.

4.2.2 Data Analysis

All MRSI spectra were exported into DICOM format from the scanner work station and imported into TARQUIN MRS quantitation software (24) for analysis. Water amplitude measurements were made in time domain by back extrapolating the initial part of the FID to time=0 (methodology provided in (24)). The calculated water amplitudes for each voxel within the FOV were imported into MATLAB R2012a software for statistical analysis. Water amplitude maps of the grid were generated for each acquisition; full acquisition no-SENSE, full acquisition (R=1); SENSE R=3 acquisition; and reduced resolution acquisition. Subsequent analysis was performed on all voxels within the PRESS excitation (Volume of Interest (VOI)) and the partially excited region (7x7 grid). Bland Altman plots and associated statistics (64) as detailed in chapter 2 were used to measure the agreement between the different MRSI acquisition protocols, in order to establish the most accurate fast-MRSI technique.

This studies analysis also focused on the average across voxels in order to ease the ability to make direct comparisons between subjects and literature values. Although an advantage of MRSI is the increase in spatial specificity for individual cases, when comparing multiple subjects' due to the large amount of data acquired an average comparison is more suitable.

4.3 Results

4.3.1 Scaling of sensitivity encoded MRSI data in comparison with the full acquisition (no-SENSE).

In order to validate the use of full acquisition (R=1) as a valid comparator data set for the fast-MRSI techniques, quantitative analysis was performed between the full

acquisition and full acquisition (no-SENSE) data. Figure 1 shows a Bland Altman plot between the full acquisition methods for a phantom and volunteer data set. The mean difference and standard deviations in amplitude between the no-SENSE and SENSE R=1 full acquisitions were -0.13 ± 3.62% for a phantom and was slightly increased for volunteers with a mean difference of -0.48 ± 5.51% (Figure 4-1).

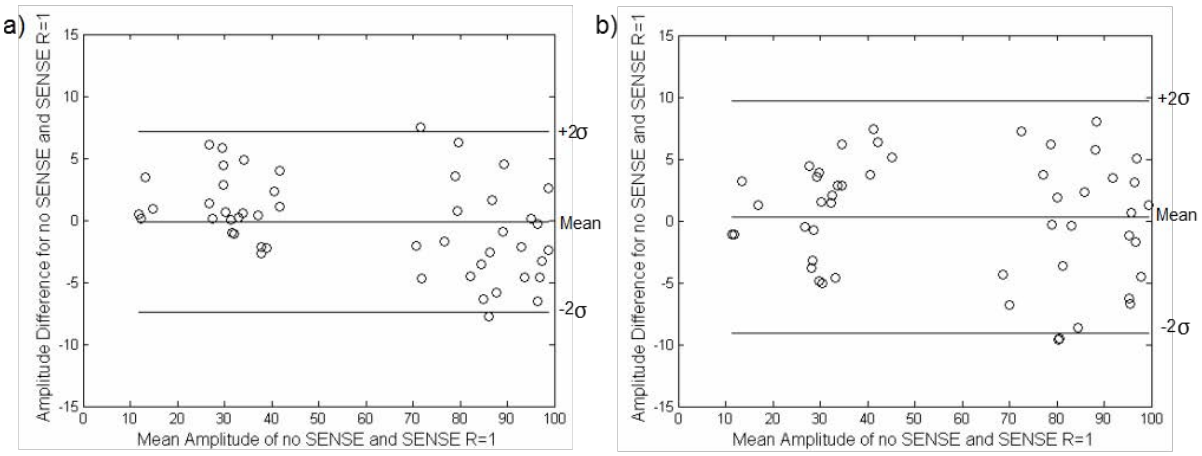

Figure 4-1 Water amplitude Bland-Altman plots to assess variance between full acquisition (SENSE R=1) and full acquisition no-SENSE for a) phantom and b) volunteer data.

4.3.2 Comparison between full acquisition and fast-MRSI techniques

Water amplitude maps (Figure 4-2b) were produced for the 6x6 PRESS excitation VOI (Figure 4-2a) for the full acquisition and fast-MRSI methods for both volunteer (shown in Figure 4-2b) and phantom data. An initial visual inspection of the water amplitude intensity maps (Figure 4-2b) clearly shows that SENSE R=3 has proven to be superior in producing a more accurate reconstruction of the full acquisition data when compared to the reduced resolution method.

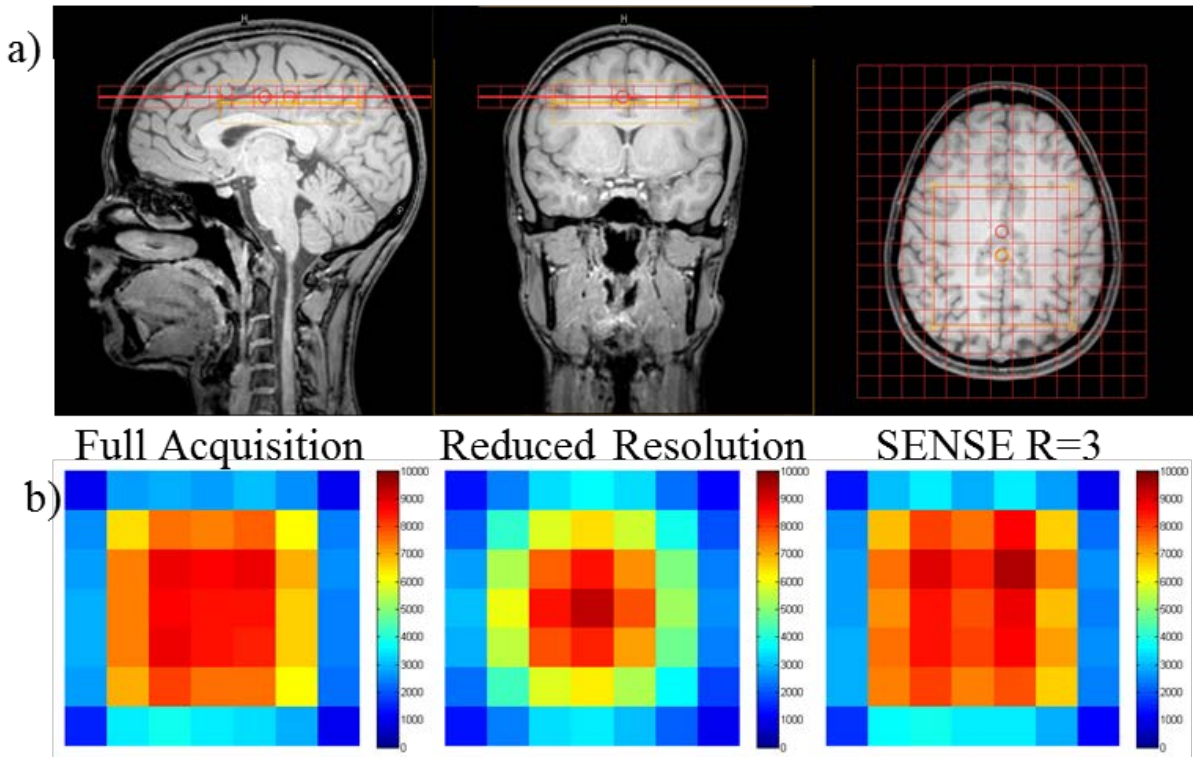

Figure 4-2 (a) MRSI geometry for volunteer 2 including 6x6 voxel PRESS volume which is collocated with the shim box shown in orange; (b) water amplitude maps extracted from volunteer 2 for full acquisition; reduced resolution acquisition; and SENSE acquisition (R=3)

The mean differences and standard deviations between full acquisition compared to SENSE and versus the reduced resolution acquisitions are shown in Table 4-1 for both the phantom and volunteers. These were calculated in order to determine any systematic or random distributed differences between the full acquisition and the fast-MRSI techniques. For SENSE acquisition within the “braino” phantom a mean difference in water amplitude of 2.31 ± 2.09% with low variability observed about the mean. Increased variability in the phantom study was observed with the reduced resolution technique with mean difference and standard deviation of 11.1 ± 11.1%.

Table 4-1 Comparison of mean differences between reduced resolution x2 and SENSE R=3 Vs full acquisition MRSI.

Water Amplitude/ Max amplitude (%)			
		Mean difference	**Standard Deviation**
SENSE R=3 Vs Full Acquisition	**Braino Phantom**	2.31	2.09
	Volunteer 1	0.75	2.95
	Volunteer 2	2.49	3.40
	Volunteer 3	3.17	3.21
Reduced Resolution x2 Vs Full Acquisition	**Braino Phantom**	11.11	11.09
	Volunteer 1	9.87	10.16
	Volunteer 2	11.19	11.12
	Volunteer 3	9.95	10.96

Results between volunteers were generally consistent with similar errors found between the phantom and volunteer studies for both fast-MRSI methods. The average mean and standard deviation was 2.1 ± 3.2% and 10.3 ± 10.7% for the SENSE acquisition and reduced resolution techniques respectively. The use of SENSE provided approximately three times more accuracy than the reduced resolution method, both in terms of systematic bias and randomly distributed differences. These statistics are also consistent with the visual differences observed in the intensity maps shown in Figure 4-2b.

4.3.3 Water amplitude MRSI reproducibility

Duplicate full acquisition (R=1) and SENSE (R=3) water reference scans were acquired for both volunteer and phantom data sets in order to assess the reproducibility

of these techniques. The mean water amplitude difference and its standard deviation was determined between repeats. A mean difference of -0.02 ± 0.26% and -0.45 ± 0.8% for the full acquisition (R=1) phantom and volunteer scans was observed respectively. An increase in SENSE factor to R=3 resulted in a mean amplitude difference between repeated scans for the phantom of 0.26 ± 0.34% and -0.94 ± 1.1% for the volunteer. Better reproducibility was observed within the phantom for both cases, suggesting that subject motion introduces an additional random error of less than 1%.

4.3.4 Phantom metabolite concentration using SENSE and reduced resolution water reference data

The water reference data from SENSE (R=3) and the reduced resolution technique were used to estimate the absolute metabolite concentrations found within the “braino” phantom. The same fully sampled (R=1) water suppressed data was used for both analyses to ensure any differences could be attributed to the water reference data. The following metabolites with known concentrations were present within the phantom: 12.5mM total N-acetyl-laspartic acid (tNAA), 10mM Creatine (tCr), 2mM total Choline (tCho) and 12.5mM Glutamate (Glu). Mean metabolite concentrations were extracted from the central fully excited 5x5 voxel region. Metabolite estimations were found to be more accurate with the use of SENSE R=3 compared to the reduced resolution technique in the collection of water data (Table 4-2).

Table 4-2 Braino phantom absolute mean concentration across the VOI for SENSE R=1 metabolite data calibrated with SENSE R=3 and reduced resolution water reference data

	SENSE R=3		Reduced Resolution	
Metabolite	Mean Concentration (mM)	Standard Deviation (mM)	Mean Concentration (mM)	Standard Deviation (mM)
tNAA	11.98	1.14	16.01	2.71
tCr	9.75	1.49	12.92	2.29
tCho	2.72	0.47	3.61	0.72
Glu	13.70	1.07	18.39	3.43

A consistent over estimation in metabolite concentrations was found for the reduced resolution technique due to an incorrect increased water amplitude estimation at the PRESS box edges (Figure 4-3). It can also be seen that SENSE provides a more uniform metabolite distribution as would be expected within a phantom.

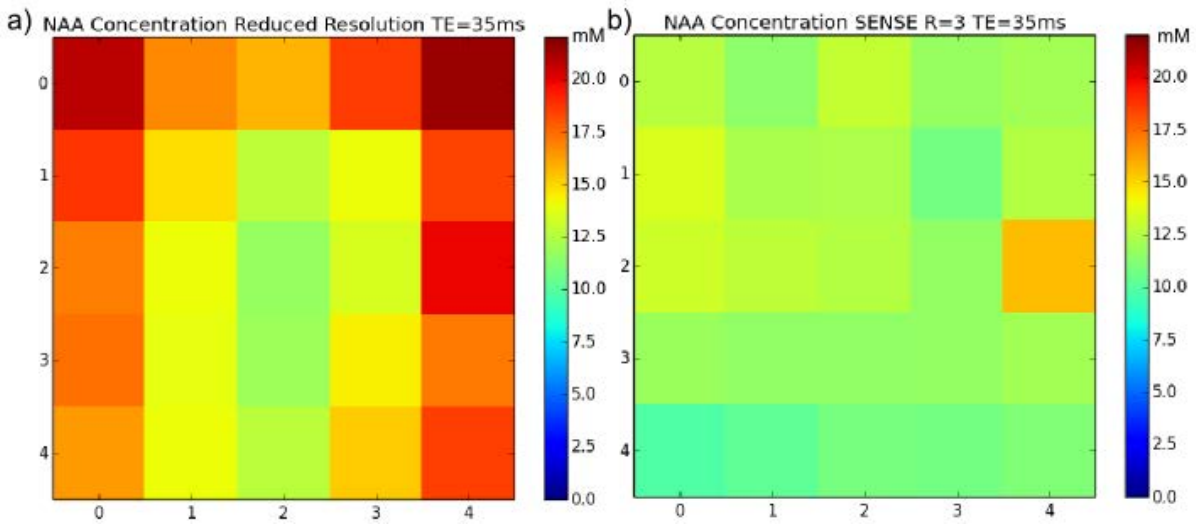

Figure 4-3 NAA concentration map from a) reduced resolution water reference data and b) SENSE (R=3) water reference data for the central 5x5 region.

4.3.5 Parietal white matter metabolite concentrations using SENSE and reduced resolution water reference data

Volunteer absolute concentrations were extracted using the TARQUIN algorithm in order to demonstrate the feasibility of combining fully sampled water suppressed data with fast-MRSI water reference data. Left and right parietal white matter voxels (six in total) were taken for each of the three volunteers. Table 4-3 shows the average volunteer metabolite concentrations using SENSE (R=3) and reduced resolution water reference data across the six voxels for tNAA, tCr, tCho and Glu.

Table 4-3 Average metabolite concentrations, using SENSE R=3 and reduced resolution water data, across three volunteers, the mean is taken from 6 parietal white matter voxels (two from each volunteer).

	Parietal White matter SENSE R=3		Parietal White Matter Reduced Resolution	
Metabolite	Mean Concentration (mM)	Standard deviation (mM)	Mean Concentration (mM)	Standard deviation (mM)
tNAA	8.53	0.30	10.62	0.34
tCr	5.56	0.16	6.89	0.15
tCho	1.14	0.14	1.41	0.19
Glu	5.45	0.21	6.77	0.18

Metabolite concentrations determined using SENSE (R=3) water reference data were found to be more consistent with those found within the literature for healthy volunteers (70,80) whereas the reduced resolution technique also overestimated these values.

4.4 Discussion

The purpose of this study was to validate the use of SENSE for the collection of fast-MRSI water reference data within the brain for the absolute quantification of metabolites. A comparison was made between SENSE and reduced resolution acquisitions in their ability to (i) reconstruct fully sampled volunteer and phantom data; (ii) reproduce known metabolite concentrations from phantom data, and (iii) produce metabolite concentrations from healthy volunteers. SENSE proved superior and offered significant improvement in accuracy over the reduced resolution method. To

the best of the author's knowledge this is the first study to have validated the use of SENSE for the purpose of water reference data collection.

Improvement in accuracy with the use of SENSE particularly at the edges of the PRESS excitation region (Figure 4-2) was expected; as the reduced resolution technique involves zero-filling in k-space, effectively applying an interpolation. SENSE instead is based on k-space reconstruction rather than an interpolation. For the reduced resolution method, with a given spatial dimension, the point spread function is inversely proportional to the number of acquired phase encoding points (for a fixed FOV) – rather than the number of zero-filled points. Therefore, SENSE can provide improved resolution over a time-equivalent reduced resolution acquisition.

Whilst this study has not directly tested the accuracy of the methods on water concentration distributions in highly heterogeneous tissue, the heterogeneity caused by the PRESS excitation boundary (1/2 voxel margin) is a valid model for testing accuracy. We therefore expect that a similar investigation into heterogeneous tissue water distributions, for example in pathology, would yield comparable results. Furthermore, accurate measures of water amplitudes for use in metabolite quantitation close to the boundary of the PRESS excitation region are desirable, and it is clear from this study that SENSE outperforms the reduced resolution method in these regions.

Absolute metabolite quantitation is generally desired over metabolite ratios, because in the case of ratios, the source of variation for a given ratio cannot be determined as to whether it is due to a relative increase in one metabolite or a decrease in the other (31). Whilst the collection of fast accurate water reference data for metabolite quantitation in MRSI was the primary objective for this study; the collection of water

reference data could also prove useful for the measurement of the “proton resonance frequency shift” for use of non-invasive thermometry (98). Therefore, this type of acquisition could be used in the generation of temperature maps across the brain.

An alternative approach to absolute quantitation is to perform pattern recognition directly on the acquired spectral data. These methods can prove advantageous as they are relatively straightforward to implement as the required statistical methodology e.g. independent component analysis are readily available. There is also no additional scan time required which can prove appealing due to clinical scan time constraints. However, as seen in the previous chapter MRS data can have issues which these methods are not optimised to deal with, e.g. variable line widths, unstable baselines and residual water. Therefore, the best approach would be to apply pattern recognition to the absolute quantitative data, this has been previously demonstrated in both paediatric and adult brain tumour studies (99,100).

MR protocol development presents a compromise between scan-time, spatial resolution (voxel size) and the effect of unwanted T1 and T2 weighting. The protocol we have presented in this study addresses the issue of scan time and provides the option of absolute concentrations for a minimal increase (<1 min) in scan time. MRSI resolution is comparatively poor compared to other MR techniques. However, the additional spectral dimension allows a non-invasive insight into tissue metabolism. Meaning MRSI is ideal for the investigation of certain pathologies such as cancer. The MRSI parameters used for this study were chosen to represent typical values for clinical MRSI acquisitions where short scan times are particularly important. Despite partial volume effects and incomplete relaxation, useful clinical information can be obtained from the voxel sizes and repetition times used within this study.

Data quality is an important factor to consider. The use of sensitivity encoding produces an inherent reduction in SNR. The quality of metabolite information acquired using SENSE has previously been assessed by several groups concluding no significant losses were found in comparison with full acquisition data (14,101,102). A study by Bonekamp et al (14) used a sense factor R=2 and observed excellent spectral quality. Excellent agreement was found for the ability of SENSE to reconstruct the full acquisition (no under sampling) data. However, high SNR losses were found by Van Cauter et al for low concentration metabolites such as myo-inositol for a SENSE factor of R=3.6 (73). To preserve these lower concentration metabolites, we propose the use of SENSE R=1 for the collection of metabolite data and SENSE R=3 for water reference data collection. This allows a reduction in scan time for both metabolite and water reference data from 10 min 16s to 6min 6s.

Two other methods that have proven promising for the acceleration of MRSI data collection are (1) EPI methods such as PEPSI (16,17) and (2) compressed sensing (103). In this study, we decided to focus on SENSE due to its wider commercial availability and therefore greater clinical relevance. The strategy of sacrificing SNR rather than resolution is an effective one for the collection of water reference data as, unlike metabolite data, you can afford a decrease in SNR as the water signal is extremely high. We propose that other fast-MRSI methods that follow this example will be similarly successful. Particularly the use of compressed sensing, in isolation or in combination with SENSE may offer a further reduction in scan time and therefore would make an interesting extension to this work.

4.5 Conclusion

SENSE has been shown to be approximately three more times more accurate than the “gold standard” reduced resolution technique for acquiring fast MRSI water reference maps. When compared to the fully sampled acquisition water amplitude differences were found to be less than 4% with the use of SENSE. Healthy volunteer parietal white matter concentrations were found to be comparable with literature when using the SENSE method. Whereas, the reduced resolution technique overestimated these values. These findings validate the use of SENSE MRSI for the accurate collection of water reference data in a feasible time frame for the purposes of absolute metabolite quantitation in a clinical setting.

5. Sensitivity Encoding for fast 1H MRSI Water Reference Acquisition: A Clinical Implementation

5.1 Introduction

In Chapter 4, the use of sensitivity encoding (SENSE) for fast ^{1}H MRSI water reference acquisition was validated. White matter metabolite concentrations were extracted for healthy volunteers by collecting a fast-water reference acquisition in conjunction with a fully sampled (SENSE R=1) water suppressed acquisitions. Values obtained were found to be comparable to those within the literature (95). In this chapter, the clinical implementation of this protocol is assessed with respect to data quality and its success in differentiating between patients with known diseases and healthy volunteers.

MRSI data was acquired from two patient groups: Wolfram Syndrome and Brain Tumour Survivors. Wolfram syndrome is a rare condition which is an autosomal recessive genetic disease. It presents as a combination of insulin dependent diabetes mellitus, optic nerve atrophy, diabetes insipidus and deafness (104). It was initially believed that neurological deficit appears at the later stages of this disease (105). However, more recent studies have shown neurodegeneration is present at the early stages of the syndrome (106–108) although there are still studies that contradict this (109). Neurodegeneration in the posterior fossa and in particular the pons is increasingly well recognized but degeneration in the supratentorial region is less well established.

Approximately two out of every three paediatric patients diagnosed with brain tumours will become long term survivors. Brain Tumour Survivors (BTS) commonly suffer late effects to their overall neurological function including neuro-cognition. This can be

attributed to: direct neurological damage to the developing brain due to; brain tumour removal, long-term chemotherapy toxicity effects and the effects of radiotherapy to the central nervous system (110). These are particularly prominent when tumours are diagnosed and treated at a young age but the deficits can evolve slowly over a long period of time. Conventional MRI appearances commonly correlate poorly with current and in particular future neurocognitive deficits. A number of studies have looked at the use of MRI in the study of Paediatric Brain Tumour Survivors (111–114) using a variety of structural and functional imaging techniques including fMRI, Diffusional Tensor Imaging (DTI) and SVS. Previous MR Spectroscopy studies (111,112) have looked at metabolite ratios to assess brain tissue damage and neuronal function recovery. Reduction in tNAA levels along with elevated tCho are indicative of neurodegeneration (5). The identification of metabolite biomarkers using MRSI in the study of long term brain tumour survivors (BTS) could provide more insight into post-treatment effects and neurodegeneration.

This study aimed to assess the clinical implementation of the fast 2D MRSI protocol developed in Chapter 4 (95). Data quality, along with the ability to distinguish between “normals”, patients with Wolfram syndrome and Brain Tumour Survivors (BTS) was assessed to see if any metabolite biomarkers of neurological dysfunction could be identified.

5.2 Methods

All MR scanning was performed on a 3 Tesla Philips Achieva TX MR system with a 32-channel head coil at Birmingham Children’s Hospital, UK. All patients and

volunteers who participated in the study gave their informed consent under full ethical approval.

5.2.1 MRSI data collection

Data was collected from 16 subjects: 8 Brain Tumor Survivors (BTS) whose primary brain tumour was located in the posterior fossa, 7 Wolfram patients and 3 healthy volunteers. One patient from both the BTS and Wolfram patient groups was excluded due to incorrect grid positioning resulting in a final study cohort of 7 BTS (Table 5-1), 6 Wolfram patients (Table 5-2) and 3 healthy volunteers (Table 5-2).

Table 5-1 Brain Tumour Survival Group Cases: Age, Tumour Type and Treatment Details

Case	Age	Group	Treatment
1	14.1	BTS - Pilocytic Astrocytoma	Surgery
2	10.3	BTS - Ependymoma	Surgery + Chemotherapy + Focal RT to PF
3	13.8	BTS - Ependymoma	Surgery + Chemotherapy + Shunt (Right)
4	10.3	BTS - Pilocytic Astrocytoma	Surgery
5	16.2	BTS- Pilocytic Astrocytoma	Surgery
6	11.5	BTS - Medulloblastoma	Surgery + Chemotherapy + Cranio-spinal RT 23.4 Gy
7	13.8	BTS - Pilocytic Astrocytoma	Surgery + Chemotherapy

RT = Radiotherapy and PF= Posterior Fosser

Table 5-2 Wolfram and Healthy Volunteer Case Ages

Case	Age	Group
8	13.0	Wolfram
9	18.5	Wolfram
10	14.9	Wolfram
11	14.8	Wolfram
12	13.3	Wolfram
13	9.4	Wolfram
14	23.0	Healthy Volunteer
15	23.2	Healthy Volunteer
16	23.0	Healthy Volunteer

For MRSI grid positioning, a 3D T1 axial MRI already acquired within the scanning session was selected in order to plan on the standard axial plane. For cases 1 to 13 all MRSI grid positions were placed manually so that the bottom of the slice was just touching the inferior aspect of the corpus callosum (Figure 5-1a-c). Data collected from healthy volunteer cases (14 to 16) were taken from the study detailed in Chapter 4 with the MRSI grid manually placed above the corpus callosum. Water suppressed with sensitivity encoding (SENSE) Factor R=1 and unsuppressed with SENSE Factor R=3 acquisitions were acquired separately with the following acquisition parameters: Field of View (FOV) matrix size 15x13; voxel size 13mm x 13mm x 13mm; TE=35ms; TR=2s; half echo acquisition mode. In each case PRESS localization was applied to excite a 6x6 voxel region (78mm x 78mm x 13mm) centrally within the FOV. In order to remove the effect of outer volume excitation only voxels from the central 5x5 region were analyzed. In all MRSI acquisitions, in order to further reduce acquisition time, the points

of k-space outside the elliptical boundary were not sampled (97). In post processing, a k-space hamming filter was applied to reduce ringing artefacts. No additional averaging was performed during k-space acquisition.

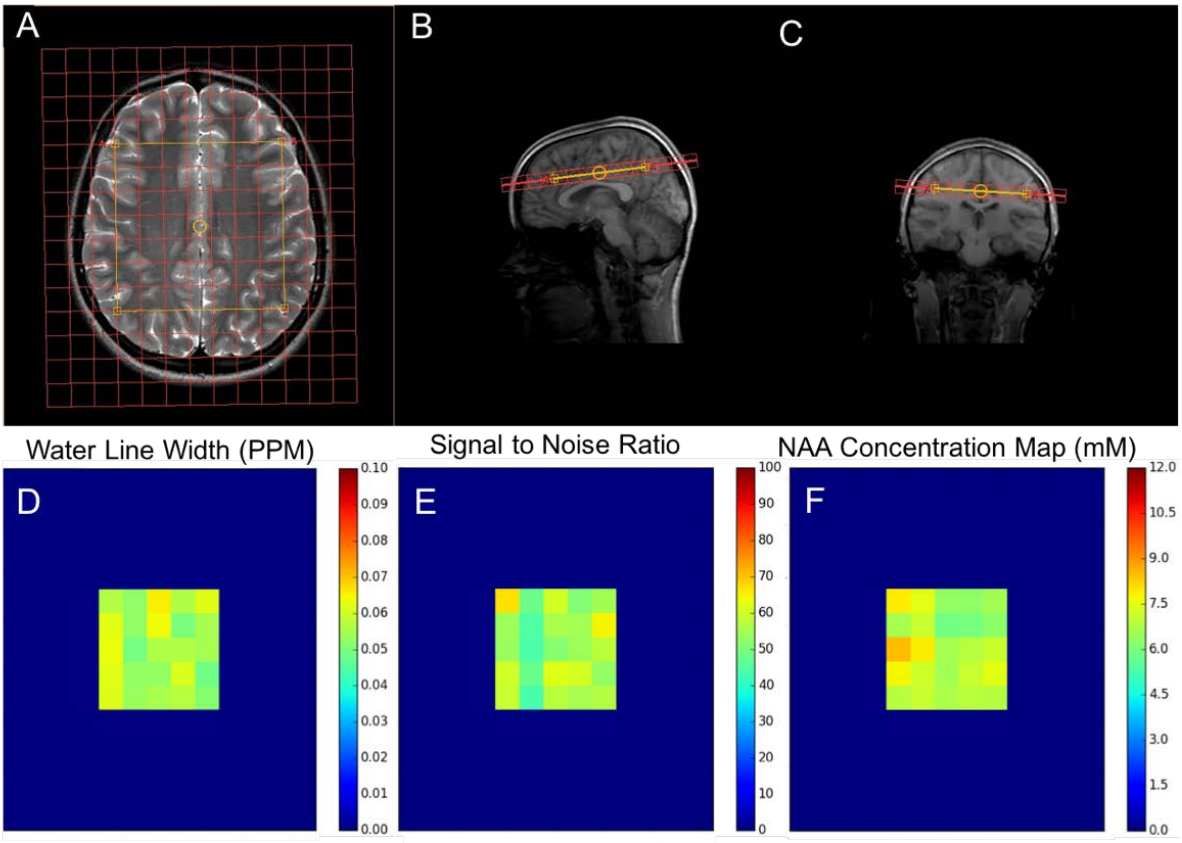

Figure 5-1 Example subject MRSI Grid Planning Screen Shot (A-C), Water Line Width (D), Signal to Noise Ratio (E) and NAA Concentration Map (F)

5.2.2 Spectral Fitting

All spectral analysis was performed using the TARQUIN software package (23). Spectra were fitted using the Experimental Baseline (Ex.BL) basis set optimized in Chapter 3. An average healthy volunteer macromolecule (MM) spectrum was compiled and narrow metabolite signals for NAA, NAAG, TCho, TCr and TCrCH2 included in the basis set.

5.2.3 Data analysis

MRSI spectra exported from the scanner workstation in DICOM format were imported into TARQUIN. Subsequent data analysis was performed using Python programming language. Spectra were assessed with respect to data quality parameters Signal-to-Noise Ratio (SNR max) and Water Line Width (FWHM). Spectra were subject to a Water Line Width rejection criterion >0.1ppm. The number of voxels excluded due to this was calculated for each subject to assess the robustness of this protocol in a clinical setting. Mean white matter metabolite concentrations were calculated for each patient group and compared to healthy volunteers and values within the literature. Mean parietal white matter concentrations were taken from four voxels for each patient case and healthy volunteer. Grey matter concentrations were not calculated as the central voxels contained multiple tissue types making its separation difficult. The ability of the technique to separate between patient groups and healthy volunteers using the calculated mean white metabolite concentration and metabolite ratios for each subject was also assessed using a one-way ANOVA test using Microsoft excel. The degrees of freedom within groups for this test across the three subject groups is 13 and 2 between groups. Mean metabolite concentrations were calculated from 4 white matter voxels for each case. Two sample T-tests were then used to assess the significance of any separation between groups, the P Value as consistent with the literature has been used as a measure of statistical significance. This analysis focused on the average across voxels in order to ease the ability to make direct comparisons between subjects and “normal” values. Although an advantage of MRSI is the increase in spatial specificity for individual cases, when comparing multiple subjects due to the large amount of data acquired an average comparison is more suitable.

5.3 Results

5.3.1 The Effect of Sensitivity Encoding on the Quality of Clinical Data

Mean SNR, Water FWHM and respective standard deviations across the PRESS excitation Volume of Interest (VOI) was calculated for each case. Acceptable mean SNR across the VOI was found with a value >15 found across all patients. Lower SNR was observed for Case 3, 5 and 12. For Case 3 a right shunt has been placed which may explain the loss in the signal for this region. Higher variability across the VOI in SNR was also observed for these cases.

Table 5-3 Mean SNR and Water FWHM and their respective standard deviations for each patient case VOI

Group	Case	SNR max	Standard Deviation	Water FWHM (PPM)	Standard Deviation
BTS	**1**	56.31	6.84	0.06	0.00
	2	48.10	3.80	0.05	0.01
	3	29.01	15.58	0.06	0.03
	4	38.10	4.37	0.06	0.01
	5	20.33	24.90	0.04	0.05
	6	40.47	1.43	0.06	0.00
	7	54.34	4.55	0.05	0.00
Wolfram	**8**	47.71	1.84	0.08	0.01
	9	34.50	17.31	0.06	0.03
	10	45.52	8.81	0.08	0.01
	11	41.27	20.74	0.06	0.03
	12	18.65	22.91	0.04	0.05
	13	65.41	3.64	0.06	0.01

Overall, acceptable water line width was found across all subjects. Increased variability in water line width across the VOI was also observed for the cases 3, 5 and 12.

5.3.2 The Effect of Water Line Width on Voxel Loss

The number of voxels lost due to a rejection criterion of 0.1ppm was calculated for each case (Table 5-4). For 8 out of 13 patient cases no voxels were excluded due to this criterion. The maximum percentage of voxels lost across all volunteers was 20%. Thus, the minimum number of voxels remaining was 20. This demonstrates the robustness of this protocol which would allow more metabolite information to be obtained accurately compared to a single voxel acquisition. Figure 5-2 shows an example of the voxel loss locations for Case 3. Close proximity to the right shunt could be the cause of poorer quality spectra within this region. Inhomogeneity effects due to ineffective shimming across this region, due to the shunt, may have resulted in the exclusion of voxels due to our rejection criterion. Increased line width can be observed for the remaining voxels located near this physiological feature. Voxel loss is also observed in the frontal region which could be attributed to closer proximity to air-tissue interfaces i.e. the sinuses resulting in broadened line widths.

Table 5-4 Subject voxel loss due to rejection line width criterion >0.1ppm

Group	Case	Group	Voxels lost	Voxels lost %
BTS	1	BTS	0	0
	2	BTS	0	0
	3	BTS	4	16
	4	BTS	0	0
	5	BTS	4	16
	6	BTS	0	0
	7	BTS	0	0
Wolfram	8	Wolfram	0	0
	9	Wolfram	3	12
	10	Wolfram	0	0
	11	Wolfram	5	20
	12	Wolfram	5	20
	13	Wolfram	0	0
		Total	**21**	**6**

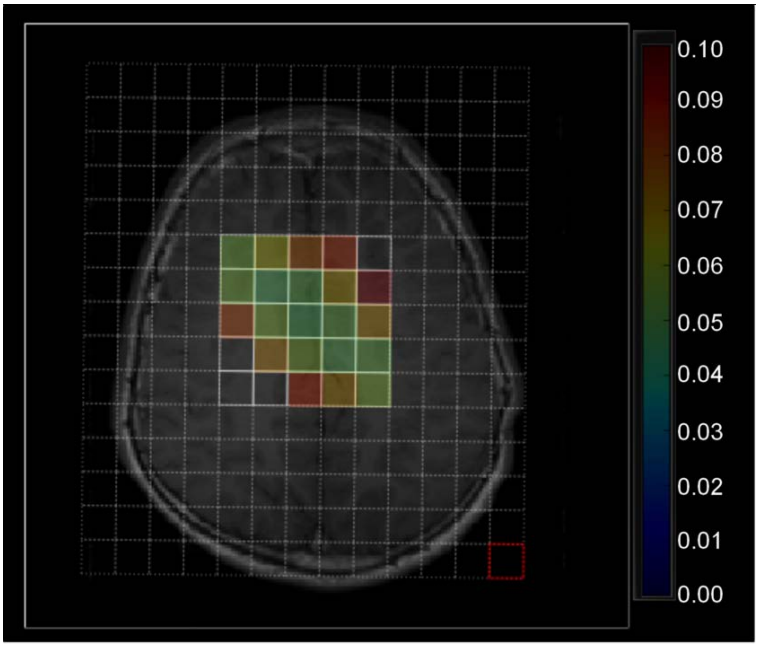

Figure 5-2 Water Line Width Map for Case 3 showing voxels lost due to Water Line Width Rejection Criterion

5.3.3 Mean White Matter Concentrations: A Comparison between Patient Groups and Healthy Volunteers

Mean white matter metabolite concentrations for tNAA, tCr and tCho were obtained for each patient case by taking the average of 4 manually selected voxels within this region for each subject (Table 5-5). White matter concentrations were also obtained from three healthy volunteers to act as a comparator group (Table 5-6). Figure 5-3A and B show the mean tNAA and tCho concentration for each subject case. It is unclear from these plots as to whether there is separation between the groups. Therefore, an ANOVA test was performed to assess whether the white matter concentrations for tNAA and tCho were significantly different between these three groups. For tNAA they were found to be significantly different ($P<0.05$, $F = 5.7$ and F Critical=3.8). However, no significance was found for tCho ($P=0.13$, $F= 2.4$ and F Critical = 3.8). Subsequent t tests were performed between groups to see what this difference for tNAA was

attributed to. Brain tumour survivors were compared to the Wolfram patient group; no significant difference was found (P=0.08, degrees of freedom=11 and Cohens d=1.72). A t-test between Wolfram and the healthy volunteer group was found to be significantly different (P<0.05 P=0.03, degrees of freedom=4 and Cohens d=3.74), this is further illustrated in Figure 5-3C and 3D. However, the difference between the Healthy Volunteer group and Brain Tumour Survivor patients for tNAA was not found to be significant (P=0.11, degrees of freedom=8 and Cohens d= 1.88). However, when the Wolfram and Brain Tumour Survivor patients are grouped and a t-test performed against the "Normal" group a significant difference is found (P=0.01, degrees of freedom=14 and Cohens d=2.9). Overall, we conclude that our protocol has the ability to be successful in distinguishing between these two subject groups with the caveat that the number of healthy volunteers is very small.

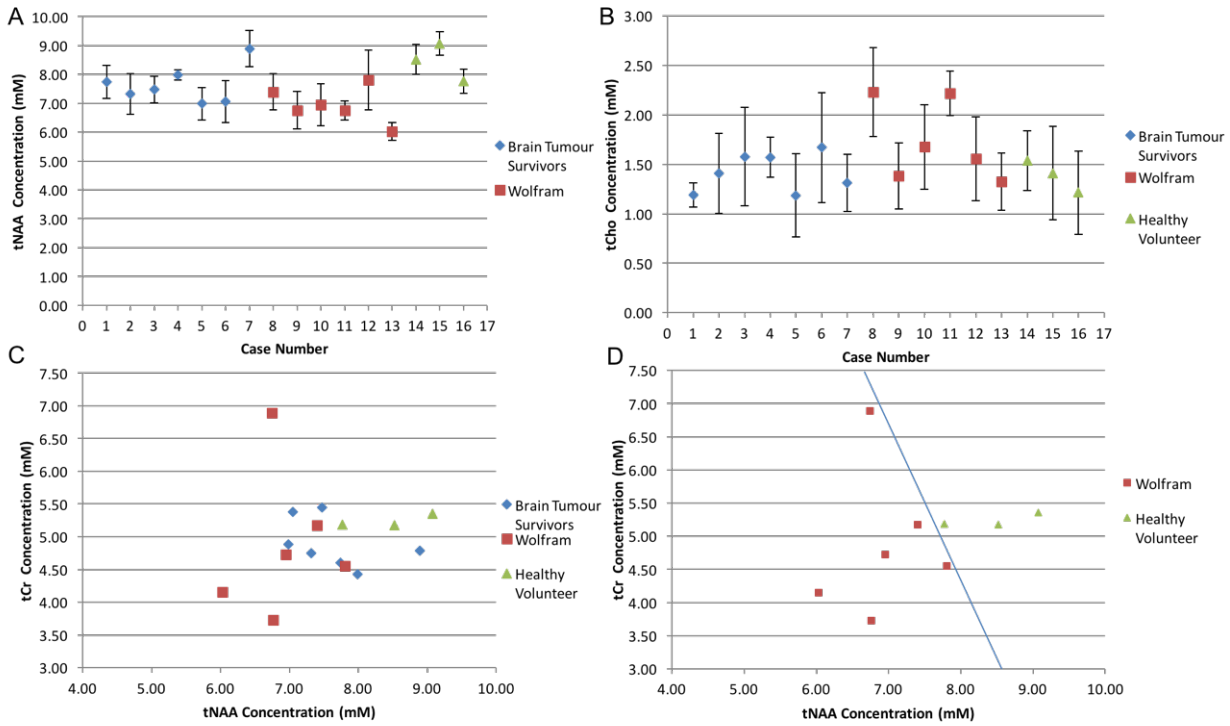

Figure 5-3 (A) Mean tNAA Concentration for each subject (B) Mean tCho Concentration for each subject (C) Plot of tCr versus tNAA for each patient group to show separation (D) tCr versus tNAA plot to show separation between Wolfram and Healthy Volunteers

Table 5-5 Mean White Matter Metabolite Concentrations and their standard deviation for Brain Tumour Survivors (BTS) and Wolfram Patients

Group	NAA Concentration mM		Cr Concentration mM		Cho Concentration mM	
BTS	**Mean**	**Std**	**Mean**	**Std**	**Mean**	**Std**
1	7.74	0.57	4.60	0.69	1.19	0.12
2	7.32	0.70	4.75	1.69	1.41	0.40
3	7.48	0.46	5.44	1.55	1.58	0.50
4	7.99	0.18	4.43	0.80	1.57	0.20
5	6.99	0.57	4.88	1.54	1.19	0.42
6	7.05	0.72	5.38	1.95	1.67	0.55
7	8.89	0.62	4.79	0.84	1.31	0.29
Wolfram	**Mean**	**Std**	**Mean**	**Std**	**Mean**	**Std**
8	7.40	0.63	5.18	1.56	2.23	0.45
9	6.76	0.66	3.73	1.16	1.38	0.33
10	6.95	0.72	4.73	1.54	1.68	0.43
11	6.74	0.33	6.89	0.86	2.22	0.23
12	7.81	1.04	4.55	1.58	1.56	0.43
13	6.03	0.30	4.15	0.66	1.32	0.29

Table 5-6 Mean White Matter Metabolite Concentrations and their Standard Deviations for Healthy Volunteers

Group	NAA Concentration mM		Cr Concentration mM		Cho Concentration mM	
Healthy Volunteer	Mean	Std	Mean	Std	Mean	Std
14	8.52	0.52	5.17	1.71	1.54	0.30
15	9.07	0.41	5.35	1.31	1.41	0.47
16	7.77	0.42	5.19	1.69	1.21	0.42

5.4.4 Metabolite Ratios: A Comparison between Patient Groups and Healthy Volunteers

Metabolite ratios were also calculated in order to assess whether our protocol could distinguish between patient groups and healthy volunteers ("Normals") using metabolite ratios. Mean metabolite ratios were calculated (Table 5-7) and plots for tNAA/tCr (Figure 5-4A), tNAA/tCho (Figure 5-4B) and tCho/tCr (Figure 5-5) were created. Clear separation cannot be observed from the plots alone. An ANOVA test was performed for each of these metabolite ratios. A significant difference between subject cases was found for tNAA/tCho ($F = 6.7$ and F Critical=3.8) and tCho/tCr ($F = 7.7$ and F Critical=3.8) only with $P<0.01$. For tNAA/tCho a significant difference was observed between Brain Tumour Survivors and Wolfram patients ($P<0.05$, degrees of freedom=11 and Cohens d=1.69) and Wolfram and "Normal" Subjects ($P<0.01$ degrees of freedom=7 and Cohens d=3.85). A significant difference was also observed for these groupings for tCho/tCr with a $P<0.05$ for both (degrees of freedom, Cohens d = 10, 44.27 and 7, 56.92 for BTS and Wolfram and Wolfram and "Normal" subjects respectively). For both the absolute concentrations and metabolite ratios a significant difference was observed between Wolfram and Normal subjects suggesting this patient group has a greater difference from "normal" metabolite values. The use of metabolite ratios also found a significant difference between the two patient groups: Wolfram and Brain Tumour Survivors. The complimentary use of metabolite ratios and absolute concentrations together could provide further assistance in the separation of "diseased" and "non-diseased" brain tissue.

Table 5-7 Mean Metabolite Ratios NAA/Cr, NAA/Cho and Cho/Cr and their Standard Deviations for Brain Tumour Survivors (BTS), Wolfram Patients and Healthy Volunteers

Group	NAA/Cr		NAA/Cho		Cho/Cr	
BTS	**Mean**	**Std**	**Mean**	**std**	**Mean**	**std**
1	1.68	0.28	6.51	0.82	0.26	0.05
2	1.54	0.57	5.19	1.57	0.30	0.14
3	1.37	0.40	4.74	1.53	0.29	0.12
4	1.80	0.33	5.09	0.67	0.35	0.08
5	1.43	0.47	5.89	2.14	0.24	0.12
6	1.31	0.49	4.23	1.47	0.31	0.15
7	1.86	0.35	6.78	1.56	0.27	0.08
Wolfram	**Mean**	**Std**	**Mean**	**Std**	**Mean**	**Std**
8	1.43	0.45	3.31	0.72	0.43	0.16
9	1.81	0.59	4.89	1.27	0.37	0.15
10	1.47	0.50	4.15	1.14	0.35	0.15
11	0.98	0.13	3.04	0.34	0.32	0.05
12	1.72	0.64	5.02	1.52	0.34	0.15
13	1.45	0.24	4.56	1.02	0.32	0.09
Healthy Volunteers	**Mean**	**Std**	**Mean**	**Std**	**Mean**	**Std**
14	1.65	0.55	5.55	1.15	0.30	0.11
15	1.70	0.42	6.43	2.17	0.26	0.11
16	1.50	0.49	6.40	2.24	0.23	0.11

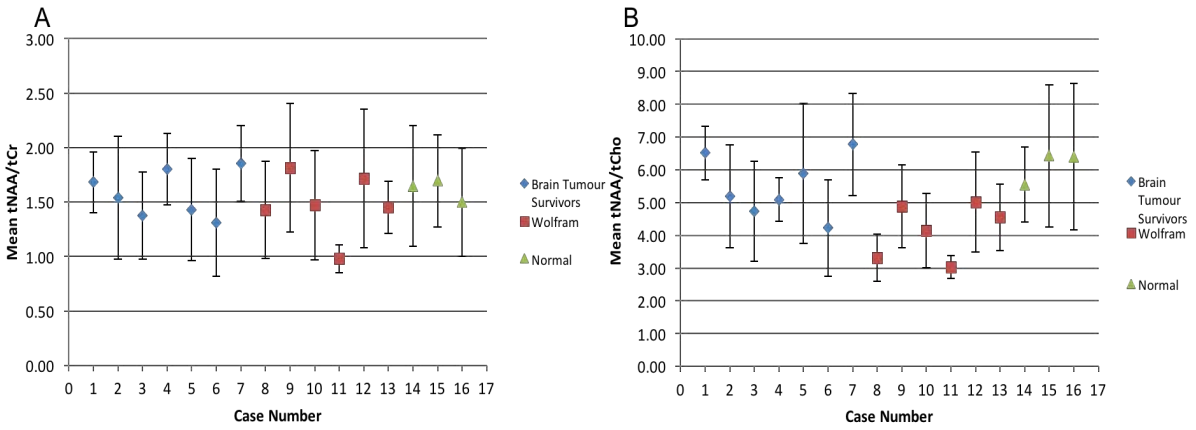

Figure 5-4 Mean metabolite ratios and their standard deviations for each subject case for (A) tNAA/tCr and (B) tNAA/tCho

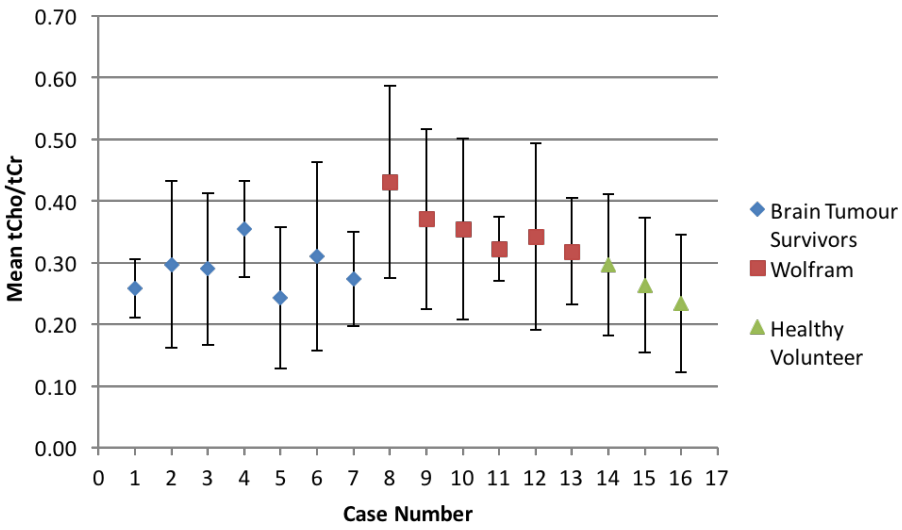

Figure 5-5 Mean metabolite ratios and their standard deviations for each subject case for tCho/tCr

5.4 Discussion

The use of sensitivity encoding for fast-MRSI water reference data collection for the absolute quantitation of metabolite information has been implemented clinically. For thirteen of the initial fifteen patient subjects correctly positioned data was acquired. Resulting in a success rate of 86% for its clinical implementation. The two patients with incorrect positioning of the MRSI grid were excluded from further analysis. These instances were early on in the study and took place without an MR Physicist present. Further assistance and training was subsequently provided to the radiographer and accurate MRSI grid positioning was achieved.

A robust protocol has been developed, with 62% of our cohort obtaining good quality data (Water Line Width <0.1ppm) for the whole PRESS excitation region. A maximum of 5 voxels out of 25 were excluded across the remaining subjects. Acceptable SNR>10 was also obtained across all subjects. Mean white matter concentrations were calculated and significant differences for tNAA were found between the Wolfram patient group and “normals”. The use of metabolite ratios tNAA/tCho and tCho/tCr in conjunction with absolute concentrations also allowed a distinction to be made between the Wolfram and “normal” data sets. These metabolite ratios were also able to distinguish between Brain Tumour Survivors and Wolfram patient groups proving metabolite ratios do have their merit within MRSI studies.

For tNAA white matter concentrations the difference between Brain Tumour Survivors and healthy volunteers was not found to be significant. However, as tNAA is a marker of neuronal integrity it is an important metabolite in the detection of neurocognitive deficit. All BTS subjects within this study had no history of metastatic disease present

within this imaging region. The imaging of white matter regions however is of interest as indicators of neurocognitive defects present themselves here (115,116). Reduced levels of this metabolite compared to normal would suggest an increase in brain neuronal damage. Patients undertaking this study as shown in Table 5-1 undertake a variety of treatment pathways which could affect their final prognosis. A limitation of this study is the cohort size for each treatment and tumour type. Data collection from more subjects could allow further separation between groups and treatment types and could provide information on their effect on neurocognitive function. In particular, whole brain radiotherapy particularly at a young age is the treatment which has been more closely associated with neurocognitive decline and only one of the patients received this treatment. In addition, there was no formal data available relating to neurocognitive testing and so we cannot be certain that their cognitive status was low compared with healthy volunteers.

A study by Blamek et al (111) looked at the metabolite profiles of a group of 24 patients aged 4-18 years who had received combined treatment for brain tumours. Spectra were acquired at three different time points after therapy: between 3 and 6 months, 8-12 months and approximately 18 months after treatment. Mean NAA/Cr values of 0.91, 0.91 and 0.86 were found respectively suggesting a decrease in neurological function over time. In comparison, our study found a slightly higher range of tNAA/tCr values of between 1.31-1.86. For our study, spectra were acquired for a region that had no previous history of disease. Whereas, the study by Blamek et al acquired spectra for both the tumour bed and contralateral to the tumour bed. The closer proximity to the original tumour site could explain the differences found between our studies.

A limitation of this study is that our comparator cohort of “normals” is small and are not age matched. We have not compared to literature “normals” as the area from which spectra are acquired can vary between studies. Metabolite concentrations can vary throughout the brain, therefore a more direct comparison with almost identical grid positioning was preferred. Another limitation is that these “normals” were sampled from university research students which may have higher than average tNAA. A previous study by James Davison et al (116) looked at use of single voxel spectroscopy to look at brain parieto-occipital white matter metabolite concentrations in subjects with Hunter Syndrome. These patients had various degrees of neurocognitive disability. A comparison was made with a cohort of children with normal appearing MRI but who had undergone MRS due to suspected neurodegenerative and neurocognitive conditions. White matter tNAA concentrations were found to be significantly reduced $P<0.01$ for the patients with Hunters Syndrome and to a lesser extent for Basal Ganglia grey matter ($P<0.05$). This validates the use of spectroscopy in the detection of neurocognitive dysfunction. The use of MRSI to image white matter as per our protocol would allow more information about regions of neurological deficit within the brain to be obtained for patients with suspected neurodegeneration.

A study by Lugar et al (115) found that by using MR Imaging that the Wolfram patients had lower fractional anisotropy and higher radial diffusivity in major white matter tracts and lower volume regions within the brain e.g. cerebellar white matter. These findings reflected the subjects’ neurological symptoms. As far as the authors are aware this is the first study to look at the use of MR spectroscopy for subjects with Wolfram Syndrome. Within this study, tNAA concentrations, ratios tNAA/tCho and tCho/tCr were found to be significantly different from “normals”. This would merit further investigation

with a larger cohort into the use of 2D Fast-MRSI protocols to identify metabolite biomarkers for the detection of neurodegeneration in Wolfram Syndrome patients.

5.5 Conclusion

A fast 2D-MRSI protocol with absolute metabolite quantitation has been implemented successfully for two patient groups: Wolfram and Brain Tumour Survivors. Spectra had acceptable data quality with respect to SNR and Water Line Width. Minimal voxel loss was found for the majority of patients within this study. The protocol was also able to distinguish between the Wolfram cohort and healthy volunteers demonstrating its feasibility for use in the clinical environment.

6. 3D MRSI: A Feasibility Study

6.1 Introduction

The ability to acquire accurate whole brain metabolite information has attracted great interest within both the research and clinical environment. Acquiring spectra across multiple slices would provide greater insight into metabolism throughout the brain. It would have great value for pathologies where the location of diseased tissue is not previously known, for example tumours; where the heterogeneity may not necessarily lie in the axial plane. Long acquisition times and poor-quality data e.g. due to lipid contamination from the scalp have hindered the introduction of 3D MRSI into clinic.

The use of fast-MRSI techniques such as: parallel imaging e.g. sensitivity encoding (SENSE) , Reduced Resolution (12), Compressed Sensing (103) or methods which reduce the order of phase encoding by one dimension, e.g. Echo Planar Spectroscopic Imaging (EPSI) (16,17), have all been proposed to address the long acquisition times associated with 3D MRSI acquisition. As seen in chapter four, sensitivity encoding proved to be a more accurate technique in reproducing the fully sampled data when compared to the reduced resolution technique. As EPSI and compressed sensing are not yet readily available on clinical scanners, this chapter focuses on the use of sensitivity encoding for fast-MRSI 3D acquisition with absolute quantification.

Effective lipid suppression is needed to prevent lipid signal bleed through from the scalp due to its high lipid content. A number of methods have been proposed to prevent lipid contamination. One approach is to avoid the excitation of the lipid signal itself by using a localisation sequence such as PRESS excitation. However, a disadvantage of this method is restriction in voxel placement. PRESS and its associated rectangular

VOI means it does not conform completely to the round shape of the head. An additional/ alternative method is to use outer volume suppression pulses to suppress the lipid signal by conforming to the lipid regions (117). Unfortunately, this can add complexity to the 3D MRSI planning stage meaning it takes longer to plan and is less reproducible. Another method is to apply an inversion pulse, with specific inversion time TI, to null the lipid signal and leaving the metabolite signal inverted. This takes advantage of the differences in T1 for the lipid and metabolite signals, allowing only the metabolite signal to be extracted. The latter was chosen for this study as it would allow a multi-slice brain spin-echo sequence to be acquired, making it easier to plan and would result in better sampling across the brain.

A number of studies have looked at the development of 3D MRSI protocols (71,75,118–122). These vary in methodology from the use of EPSI (75,122) or PRESS (71,121) sequences and the use of SENSE (120). Reproducibility studies (71,75,123–125) also vary in methodology e.g. pulse sequence design, field strength and quantitation. As far as the authors are aware this is the first study to look at the reproducibility of SENSE for a 3D spin echo acquisition as an alternative to less readily available techniques.

In this study, we aimed to optimise a 3D MRSI protocol that could be used clinically with an acquisition time of approximately 10 minutes. We tested the robustness of sensitivity encoding for its use in fast 3D MRSI acquisitions by comparing the use of SENSE against a fully sampled (No SENSE) acquisition. We achieved this by assessing the reproducibility of both these acquisition types across multiple healthy volunteers. We also looked at the data quality and the efficacy of the applied lipid suppression in order to assess if SENSE resulted in any degradation in data quality.

6.2 Methods

6.2.1 2D MRSI Data Collection and Optimisation

All MR Scanning was performed on a 3T Philips Achieva TX MR System using a 32-channel head coil at Birmingham University Imaging Centre (BUIC), UK. For this study, full ethical approval and informed consent was obtained for all subjects.

6.2.1.1 Lipid Suppression Optimisation

Firstly, protocol optimisation steps were carried out in 2D for echo time, lipid suppression and water suppression and then were applied to the 3D acquisition. In order to establish an optimal protocol to suppress the lipid signal; healthy volunteer 2D Spin Echo MRSI acquisitions were acquired with SPectral Attenuated Inversion Recovery (SPAIR) applied. The following parameters were used; an offset of 600Hz, PB Volume shim, inversion time TI range: 190, 200, 210, 240, 250 and 260ms. 2D MRSI grids were manually placed above the Corpus Callosum with the following acquisition parameters: half echo acquisition, TE/TR 35/2000ms, Field of View (FOV) matrix size 15x13, voxel size 13x13x13mm and sharp RF pulse set. Water suppressed and unsuppressed spectra were acquired for each inversion time. Lipid maps were generated across the whole 15x13 grid. Lipid content was calculated using the absolute sum between 1.0 and 1.9ppm divided by the mean water amplitude. The mean lipid content across this grid was then calculated for each inversion time and the data quality assessed for SNR and water line width. From these results (see section 6.3.1) an inversion time of τ=250ms was established as optimum.

6.2.1.2 Water Suppression Optimisation

To ascertain the optimal water suppression technique and echo-time a healthy volunteer 2D Spin Echo MRSI scan was acquired for three different water suppression parameters at two echo times 18 and 35ms. Spectra were acquired using the following water suppression parameters: (i) Excitation pulse with second pulse angle at 300°, (ii) Excitation pulse with second pulse angle at 550° and (iii) Multiple Optimisations Insensitive Suppression Train (MOIST). To assess the success of the water suppression techniques the mean water residual divided by the water amplitude across the whole grid was calculated for each of these scan acquisitions. The acquisition with the lowest water residual was deemed the best. From these results (see section 6.3.2) water suppression technique (ii) Excitation with second pulse angle at 550° proved to be the most successful across both echo times.

6.2.1.3 Echo Time Optimisation

In order to establish the optimum echo time a volunteer scan was acquired to assess the reproducibility and data quality for two short echo times TE=18 and 35ms. 2D Spin Echo MRSI scans were acquired in triplicate and the reproducibility was assessed using Coefficients of Variance (COV) defined as the standard deviation/mean for the following metabolites: tNaa, tCr, tCho, Glx, Ins, Glth and Tau. The voxel wise COV was calculated and a mean COV determined across the whole MRSI grid. From these results (see section 6.3.3) an echo time of 18ms was chosen for the 3D MRSI acquisition development.

6.2.3 3D MRSI Data Collection and Optimisation

The optimised parameters were then applied to the following 3D MRSI acquisition. Data was collected from four healthy volunteers (aged between 20 and 30). For MRSI grid positioning, an initial T1 weighted 3D Magnetization-Prepared Rapid Acquisition Gradient Echo (MPRAGE) reference scan was obtained. The 3D MRSI acquisition was set up in multi slice mode with a total three slices. All MRSI grid positioning were manually placed so the central slice was above with the corpus callosum (Figure 6-3) for a 3D Spin Echo sequence with the following acquisition parameters: Field of View (FOV) matrix size 15x13; voxel size 13mm x 13mm x 13mm; TE=18ms; TR=2s; half echo acquisition mode; RF Pulse normal; Pencil Beam (PB) Volume Shim; SPAIR with inversion time τ=250ms with an offset of 600Hz; Excitation water suppression with second pulse angle 550°. Water unsuppressed data was also collected for all studies for metabolite quantitation. A fully sampled (No SENSE) acquisition was acquired for one volunteer with an acquisition time of 18 minutes and 42 seconds. Three volunteer scans were acquired with SENSE factor Anterior-Posterior (AP) R=2 and Right-Left (RL)=1 with an acquisition time of 11minutes and 8 seconds. To assess the short-term reproducibility of these all 3D MRSI acquisitions were acquired in triplicate for each volunteer without grid repositioning; reshimming and water suppression frequency optimization in between scans was performed if deemed necessary.

6.2.4 3D MRSI Data Analysis

All spectral analysis was performed using the TARQUIN software package (24). MRSI spectra exported from the scanner workstation in SDAT format were imported into TARQUIN. Spectra were fitted using the Ex.BL basis set outlined and developed in

Chapter 3. A residual water filter cut off of 120Hz was set within the TARQUIN pre-processing options in order to remove any residual water signal from the analysis. Subsequent data analysis was performed using python programming language. The data was split into the individual slices: Top (Slice 3), Middle (Slice 2) and Bottom (Slice 1). The volume of interest (VOI) was extracted using a water amplitude threshold of 50%. Data quality parameters Water Line width (FWHM) and Signal to Noise (SNR) were compared across slices and volunteers. Lipid maps were generated and the mean lipid content calculated for each volunteer and slice to assess the success of the SPAIR lipid suppression technique.

Metabolite coefficients of variance (COV) were calculated as the voxel wise ratio of the standard deviation and mean for each volunteer and for each slice over the three MRSI acquisitions for the voxels which satisfied the quality control criteria of a water line width <0.1ppm (12.8Hz). Once again, the unsuppressed water peak FWHM was taken to be our measure of data quality due to its robustness in comparison to metabolite line width which can become unstable due to noise and artefacts. We also assume that the water line width is directly correlated with metabolite FWHM and therefore can be used as a proxy for data quality. COV's for the metabolites tNAA, tCr, tCho, Ins and Glx were calculated to assess the technical reproducibility of the SENSE 3D acquisitions compared to the fully sampled (No SENSE) acquisition. The number of voxels lost due to the water line width criteria was also evaluated for each volunteer and slice to assess the robustness of the 3D acquisition and highlight any issues due to voxel placement.

It is worth noting that this analysis focused on the average across voxels in order to ease the ability to make direct comparisons between techniques and subjects.

Although an advantage of MRSI is the increase in spatial specificity for individual cases, when comparing multiple subjects' due to the large amount of data acquired an average comparison is more suitable.

6.3 Results

6.3.1 Lipid Suppression Optimisation

To determine the optimum inversion delay for most effective lipid suppression a healthy volunteer 2D MRSI spectra was acquired using SPAIR for the following inversion delay times: 190, 200, 210, 240, 250 and 260ms. Figure 6-1 and Table 6-1 show the mean lipid values across the whole MRSI grid.

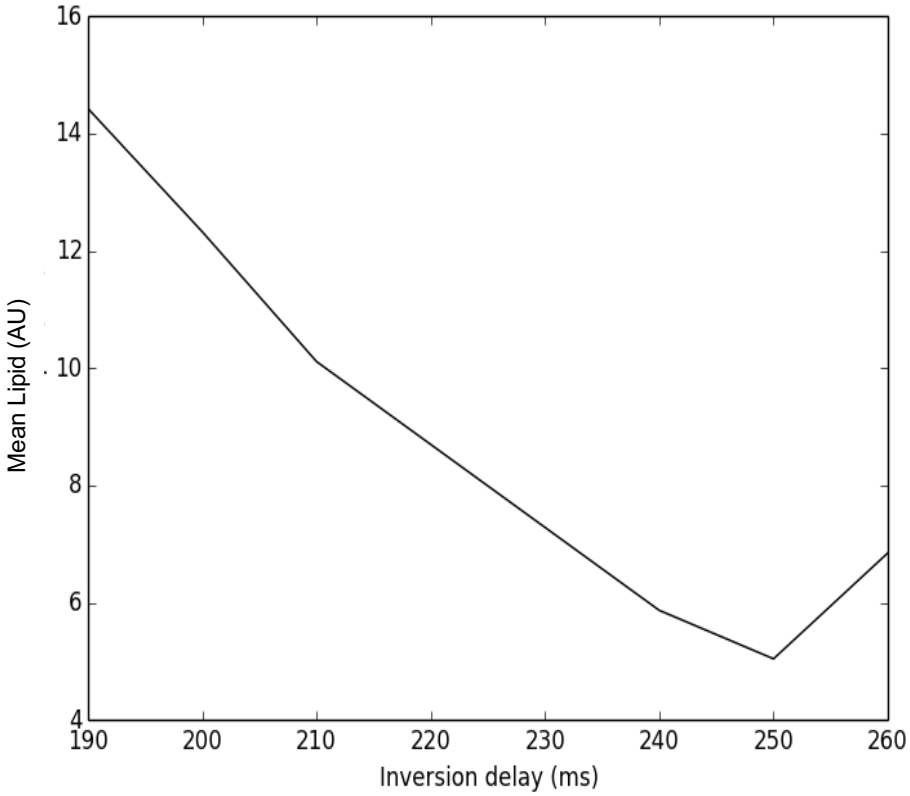

Figure 6-1 Mean Lipid across the MRSI grid for a Healthy Volunteer Spectra for multiple SPAIR Inversion Delay times

Table 6-1 Mean Lipid Values for SPAIR Pulse Inversion Delay range 190ms to 260ms

Inversion Delay (ms)	Mean Lipid (AU)	Standard Deviation
190	14.43	15.98
200	12.33	12.33
210	10.11	10.48
240	5.90	4.41
250	5.04	4.34
260	6.85	4.91

An inversion delay of 250ms proved to be superior in the reduction of lipid levels with the lowest mean lipid value of 5.04. The data quality was also assessed with the mean water FWHM and SNR max calculated across the MRSI grid (Table 6-2).

Table 6-2 Mean SNR max and Water Line Width Values for each Inversion Delay

Inversion Delay (ms)	Water FWHM (PPM)	Standard deviation (PPM)	SNR max	Standard deviation (PPM)
190	0.093	0.023	32.80	2.16
200	0.091	0.021	31.46	1.69
210	0.092	0.023	30.27	7.04
240	0.090	0.020	19.44	2.60
250	0.091	0.020	21.63	3.38
260	0.092	0.020	17.13	2.24

Low variation in water line width was observed across the above inversion delay times. All mean water line width values were found to be below the rejection criteria of

0.1ppm. Acceptable SNR of 21.63 was observed for an inversion delay of 250ms. Following on from these results an inversion delay of 250ms proved to optimal in the suppression of unwanted lipid signals and was applied in our protocol from this point forward.

6.3.2 Water Suppression Optimisation

Three techniques were assessed in their effectiveness for suppression of the water peak: Excitation pulse with a second pulse angle of 300°, Excitation with a second pulse angle of 550° and MOIST. This was done for two echo times; 18 and 35ms. Their water suppression efficacy was assessed by calculating the mean water residual, taken from the sum of the spectral components between 4 and 5ppm normalised to the mean water amplitude (Table 6-3 and Figure 6-2).

Table 6-3 Whole MRSI Grid Mean Water Residual Values normalized to the Water Amplitude for Echo times 18ms and 35ms

TE (ms)	Water Suppression Technique	Whole Grid Mean Water Residual/Water Amplitude (AU)	Standard Deviation
	Excitation 2nd PA 300°	175	144
35	Excitation 2nd PA 550°	169	121
	MOIST	366	214
	Excitation 2nd PA 300°	228	256
18	Excitation 2nd PA 550°	210	127
	MOIST	408	169

From these results, the Water Suppression Technique; Excitation with a Second Pulse Angle of 550° had the lowest water residual of 169 and 210 for echo times of 35 and 18ms respectively. MOIST had the worst performance with water residual of 366 and

406 approximately two times higher than by using an Excitation Pulse. Water suppression through Excitation with a second pulse angle of 550° was therefore deemed optimal and was chosen for the remainder of this study.

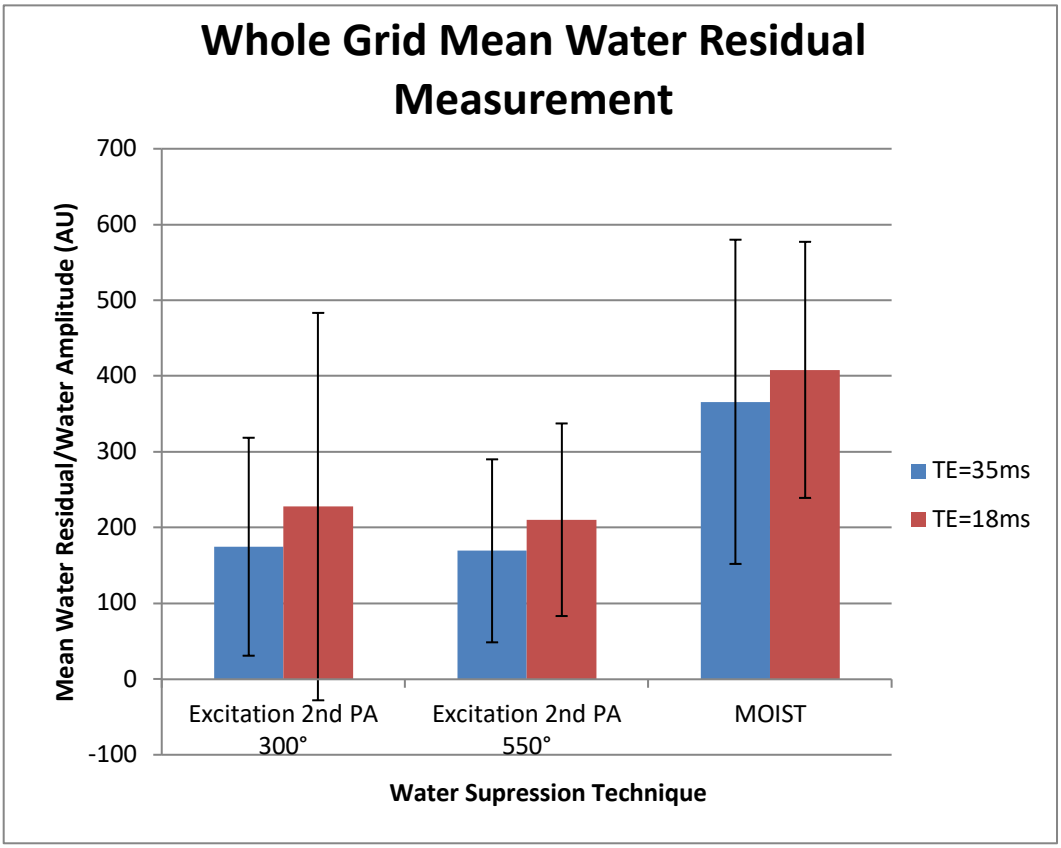

Figure 6-2 Mean Water Residual Measurement comparing Echo time and Water Suppression Techniques

6.3.3 Echo Time Optimisation

In order to establish an optimum echo time to apply to our 3D MRSI protocol, with inversion recovery based lipid suppression, the reproducibility of two echo times TE=35ms and TE=80ms was assessed. Healthy volunteer 2D MRSI scans were acquired in triplicate and the mean Coefficients of Variance calculated for the following metabolites: tNaa, tCr, tCho, Glx, Ins, Glth and Tau (Table 6-4).

Coefficients of Variance are comparable between echo times across the majority of the metabolites. However, improved reproducibility was observed for Ins. Data quality parameters Water line width and SNR were also comparable between echo times. Therefore, an echo time of 18ms was chosen to be applied to the 3D MRSI acquisitions within this chapter due its improved Ins reproducibility and acceptable data quality.

Table 6-4 Metabolite Coefficients of Variance for TE=18 and 35ms

	Coefficient of variance %						
TE (ms)	**tNAA**	**tCr**	**tCho**	**Glx**	**Ins**	**Glth**	**Tau**
18	3.35	4.30	6.80	10.87	7.78	28.29	27.19
35	2.92	4.02	5.92	11.14	13.54	26.48	22.77

Table 6-5 Mean Water Line Width and SNR Values for TE=18 and 35ms

TE (ms)	Water FWHM (ppm)	Standard Deviation	SNR max	Standard Deviation
18	0.07	0.01	20.30	3.74
35	0.07	0.01	22.69	5.25

6.3.4 Lipid suppression using Optimised 3D MRSI SPAIR acquisition.

Three-dimensional MRSI acquisitions (three slices) with SPAIR were acquired for four healthy volunteers. The MRSI grids were placed manually with the central slice aligned with the corpus callosum (Figure 6-3).

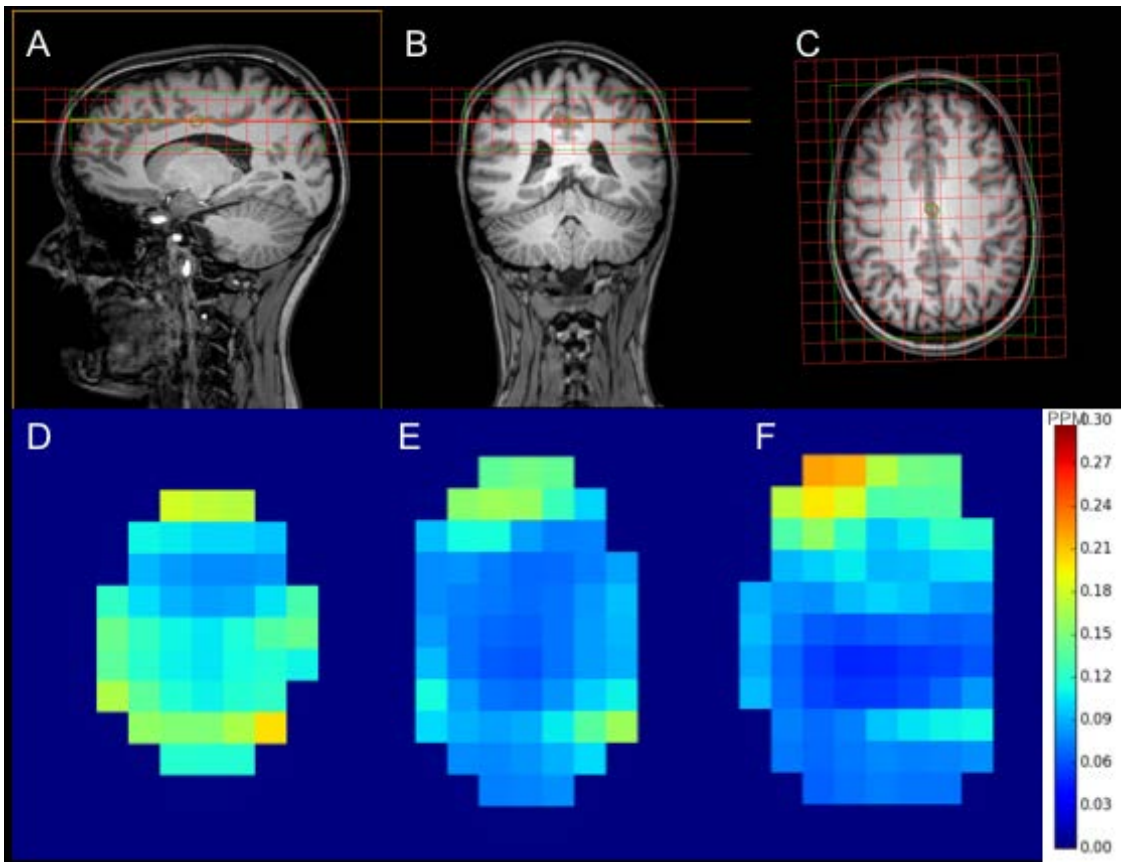

Figure 6-3 3D MRSI Planning Grid Placement for healthy volunteer 2 scan with Saggital (A), Coronal (B) and Axial (C) Views. Water Line Width (PPM) maps for the three axial slices: Top (D), Central (E) and Bottom (F) slices.

From this point forward the Top, Middle and Bottom slices will be referred to as Slice 3, 2 and 1 respectively. “No SENSE” volunteer acquisition was acquired with no SENSE factor applied. Volunteers 1, 2 and 3 were acquired with a SENSE factor of 2 in the anterior-posterior (AP) direction and 1 in the Right-Left direction (RL).

The mean lipid values for each slice were calculated for each volunteer (Table 6-6) across the whole MRSI grid.

Table 6-6 Mean Lipid Values (AU) across all slices for No SENSE and SENSE factor AP 2 and RL 1 (Volunteer 1-3)

	Slice 1		Slice 2		Slice 3	
	Mean Lipid/ mean Water Amplitude (AU)	**Standard Deviation**	**Mean Lipid/ mean Water Amplitude (AU)**	**Standard Deviation**	**Mean Lipid/ mean Water Amplitude (AU)**	**Standard Deviation**
No SENSE	6.71	5.42	6.69	5.37	7.34	6.47
Volunteer 1	7.21	5.03	9.32	6.43	8.70	7.67
Volunteer 2	8.38	5.36	9.54	6.93	9.44	8.56
Volunteer 3	6.41	4.72	7.45	5.59	7.99	6.80

Mean lipid values were lowest across all volunteers for Slice 1 (bottom) with higher lipid content observed for Slice 2 and 3 this can also be observed in Figure 6-4 which shows the distribution of the lipid across the whole MRSI grid. As expected the majority of lipid signal is located around the edge of the brain consistent with the CSF between the brain and skull. Large standard deviation is therefore observed across the grid (Table 6-6). Fully optimal lipid suppression is not fully effective for this region due to the high lipid signal contribution, however by comparison the majority of the in-brain volume lipid signal is much lower (approximately x4 in most regions). As this is the region we are interested in for quantification this validates the effectiveness of our optimised lipid suppression technique.

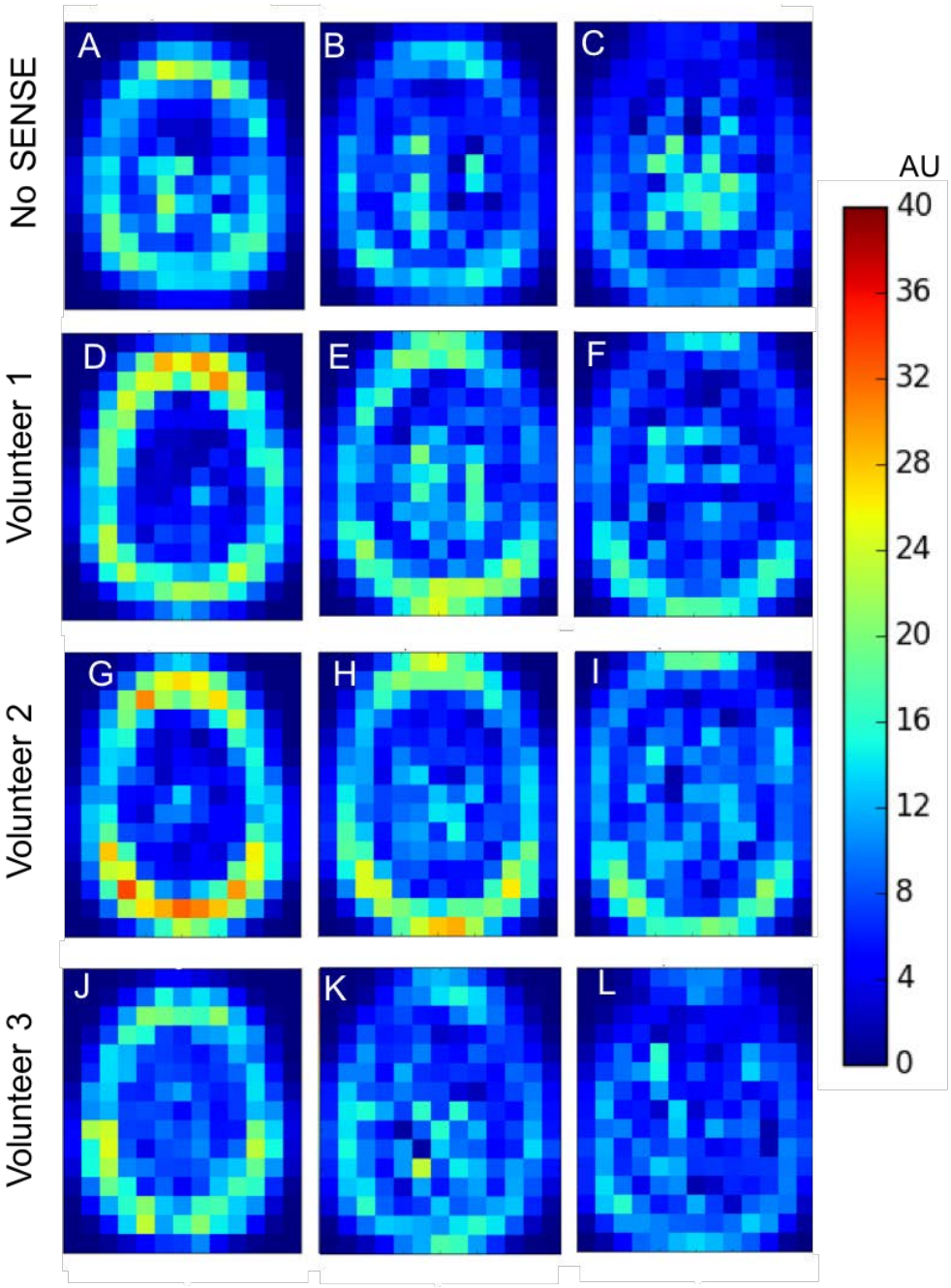

Figure 6-4 Volunteer Lipid Maps with (Volunteer 1,2 and 3) and without SENSE (No SENSE) for each image slice: Slice 3 (A, D, G and J), Slice 2 (B, E, H and K) and Slice 1 (C, F, I and L).

6.3.5 The Effect of SENSE on 3D MRSI Reproducibility

Scans were acquired in triplicate in order to test the robustness of our 3D acquisition. Reproducibility was assessed using Coefficient's of Variance (CoV) (Table 6-7 and 6-8). Water suppressed and water unsuppressed scans were acquired for metabolite quantitation.

Overall, across all slices the mean coefficients of variance are comparable between SENSE and no SENSE for all metabolites. However, variation can be observed across the three slices. For tNAA the middle slice (Slice 2) offers the most comparable coefficient of variance when comparing the no SENSE and SENSE volunteer acquisitions. For slice 1 and 3 the tNAA CoV's showed increased or even decreased variation across the volunteers with and without variation. Suggesting the addition of variation due to differing brain anatomy between volunteers may be a factor. This fluctuation of variation across slices and volunteers can also be observed for all other metabolites.

The most reproducible metabolite using this method was found to be tNAA with coefficients of variance of 10.04 with no SENSE and 12.73, 12.68 and 9.60% for volunteer 1, 2 and 3 respectively (Table 6-7). Increased variation across all volunteers was observed for tCr and tCho with a mean CoV's <25% for all slices combined. Slice 1 (lowest slice) for volunteer 2 was consistently higher for these metabolites, further suggesting inter-subject anatomical variability may influence the obtainable reproducibility from this technique.

Table 6-7 Mean metabolite Coefficients of Variance % for tNAA, tCr and tCho for No SENSE and SENSE Factor AP R=2 and RL = 1 (Volunteer 1-3).

	tNAA CoV %				tCr CoV %				tCho CoV %			
	Slice 1	**Slice 2**	**Slice 3**	**All**	**Slice 1**	**Slice 2**	**Slice 3**	**All**	**Slice 1**	**Slice 2**	**Slice 3**	**All**
No SENSE	8.37	7.32	14.44	10.04	19.22	9.09	22.73	17.01	14.45	9.64	15.13	13.07
Volunteer 1	17.01	9.84	11.34	12.73	21.74	10.59	18.76	17.03	25.31	14.48	23.12	20.97
Volunteer 2	21.62	11.03	5.40	12.68	28.49	16.67	9.71	18.29	35.13	19.79	19.20	24.71
Volunteer 3	8.43	12.01	8.37	9.60	14.51	11.57	11.45	12.51	24.25	21.23	16.15	20.54
Volunteer 1-3	15.69	10.96	8.37	11.67	21.58	12.94	13.31	15.94	28.23	18.50	19.49	22.07

Table 6-8 Mean metabolite Coefficients of Variance % for Glx and Ins for No SENSE and SENSE Factor AP R=2 and RL = 1 (Volunteer 1-3).

	Glx CoV %				Ins CoV%			
	Slice 1	Slice 2	Slice 3	All	Slice 1	Slice 2	Slice 3	All
No SENSE	32.92	22.21	23.34	26.15	20.00	30.25	22.07	24.11
Volunteer 1	34.03	39.93	23.22	32.39	42.46	30.39	23.84	32.23
Volunteer 2	50.98	50.98	27.00	42.98	37.06	24.24	20.70	27.33
Volunteer 3	25.62	22.68	30.42	26.24	30.41	27.62	27.05	28.36
Volunteer 1-3	36.88	37.86	26.88	33.87	36.64	27.42	23.86	29.31

From Table 6-8 it can be seen that as expected the highest variation can be found for the lower level metabolites Glx and Ins. An increase in variation <20% is observed for all slices with the addition of a SENSE factor of AP 2 RL 1.

Overall, increased variation is observed for slice 1 and 3 across all volunteers. Due to the close proximity of slice 1 to the sinuses (air-tissue interface) and slice 3 to the top of the skull where there may be a higher chance of lipid contamination and reduced shimming efficacy.

6.3.6 The Effect of Water Line Width and Data Quality on 3D MRSI Reproducibility

As the CoV's were calculated from the voxels that met a water line width criteria of below 0.1ppm. The number of voxels discarded due to this was also calculated (Figure 6-5 and Table 6-9) as a smaller sample voxel size could affect the overall statistics. The SNR for No SENSE and SENSE factor R: AP R=2 and RL = 1 was also investigated across the different slices.

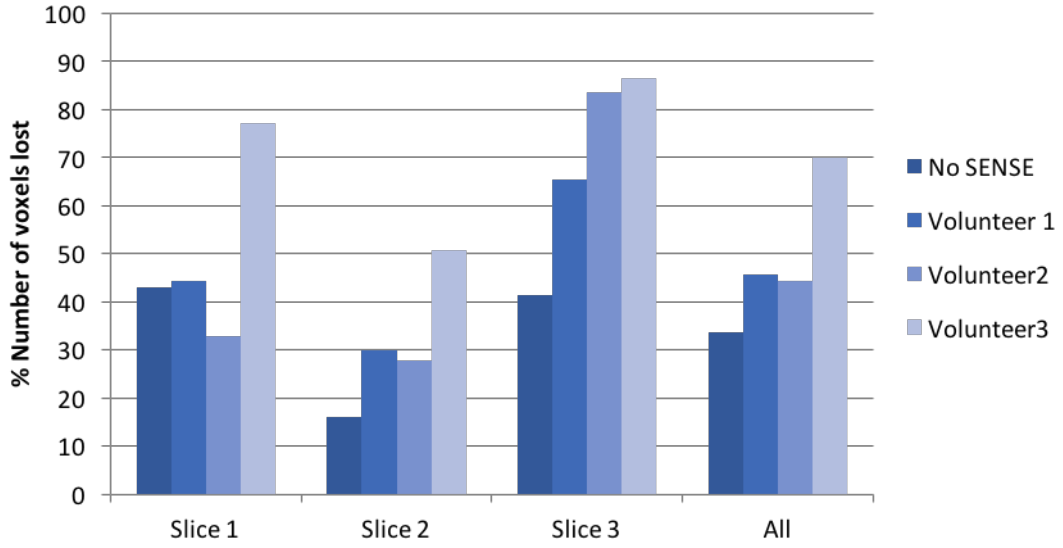

Figure 6-5 Percentage voxel loss due to Water Line Width Criteria <0.1ppm across all volunteers and slices for No SENSE and with SENSE Factor R: AP 2 and RL=1

It can be seen from Figure 6-5 that the highest percentage of voxels lost was found for slice 1 and 3 across all volunteers. No SENSE had the best performance overall with 34% of voxels lost across all slices (Table 6-9). The use of SENSE for Volunteer 1 and Volunteer 2 showed an increased % loss of approximately 10% with Volunteer 3 performing the worst with 70% of the voxels lost within the brain volume. The poorer performance for volunteer 3 could be accounted for due to anatomical differences or movement. The main contribution of voxels lost attributed to slice 1 and slice 3 suggests the effect of shimming in these more difficult to image areas has had a large impact on data loss due to the water line width criteria.

Figure 6-6 shows example tNAA coefficients of variance maps for Volunteer 2 before and after the line width criteria was applied in order to localise the regions of voxel loss. The majority of voxels for slice 1 and 2 were lost in the frontal region of the brain.

This is consistent with locality to the sinus air-tissue interface where it is known shimming can be an issue. This, consistent with data collected in chapter 3, we believe is the cause of voxel loss here for these slices. Slice 3 shows the greatest % voxel loss with only 8 voxels remaining for this slice after the Water Line Width criteria is applied. We believe this is due to the close proximity of this slice to the skull. As once again the scanner struggles to shim across bone this could have introduced further peak broadening. Thus, these voxels will be removed due to our rejection criteria.

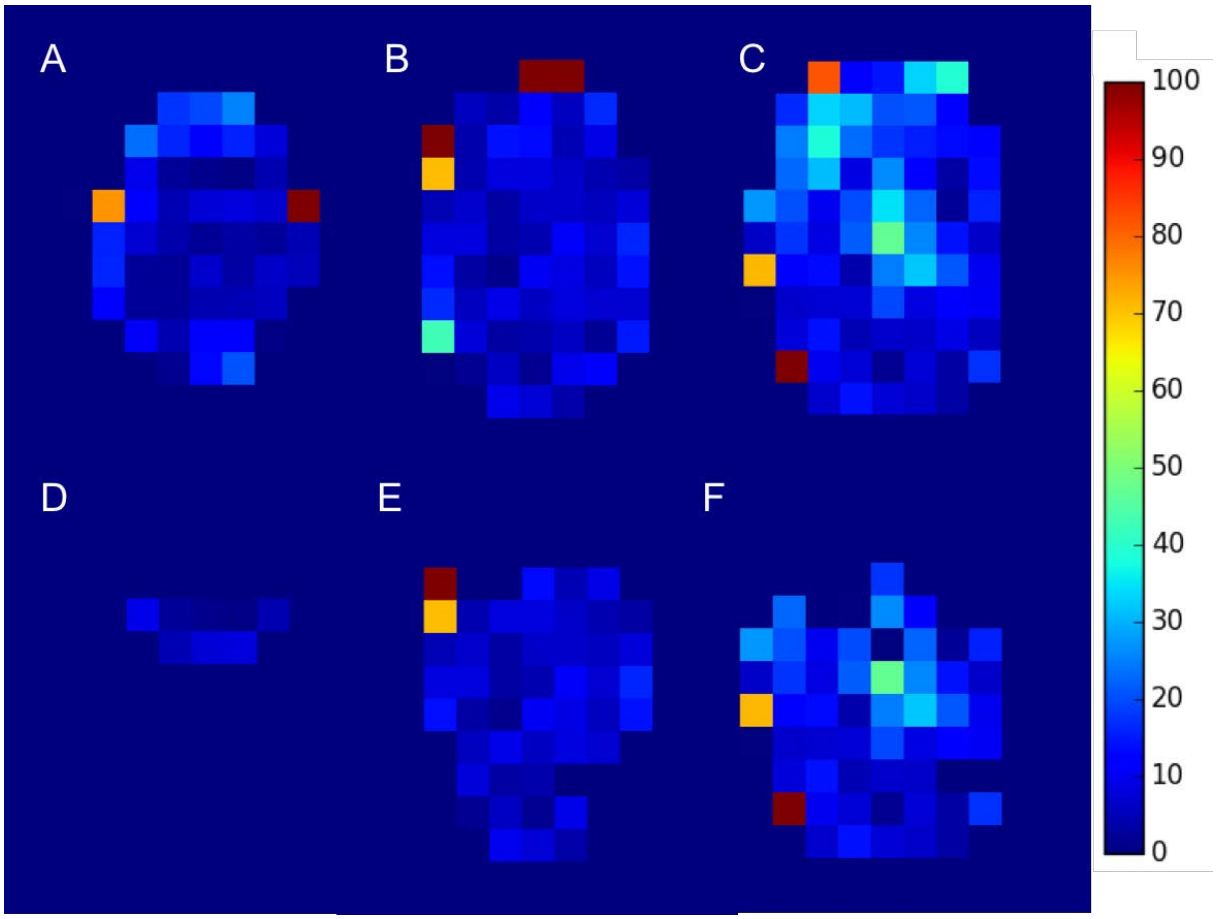

Figure 6-6 Example tNAA Coefficients of Variance maps showing voxel loss for Volunteer 2 for: Slice 3 (A and D), Slice 2 (B and E) and Slice 1 (C and F) for Before and After the Water Line Width criteria <0.1ppm was applied respectively.

Table 6-9 Number of voxels within the brain volume Before and After a Water Line Width Criteria of <0.1ppm for all slices and volunteers. A percentage of voxels lost due to this rejection criteria is also shown.

	Slice 1			Slice 2			Slice 3			All		
	Before	After	% Voxels lost	Before	After	% Voxels lost	Before	After	% Voxels lost	Before QC	After	% Voxels lost
No SENSE	70	40	43	56	47	16	46	27	41	172	114	34
Volunteer 1	79	44	44	60	42	30	52	18	65	191	104	46
Volunteer 2	76	51	33	65	47	28	49	8	84	190	106	44
Volunteer 3	70	16	77	65	32	51	44	6	86	179	54	70
Volunteer 1-3	75	37	51	63	40	36	48	11	78	187	88	53

Table 6-10 Mean SNR max and Water Line Width and corresponding Standard Deviation values calculated across all volunteers and slices for voxels with a line width criteria of <0.1ppm.

	Mean SNR max								Mean Water FWHM (PPM)							
	Slice 1	**△**	**Slice 2**	**△**	**Slice 3**	**△**	**All**	**△**	**Slice 1**	**△**	**Slice 2**	**△**	**Slice 3**	**△**	**All**	**△**
No SENSE	12.91	4.64	19.49	4.62	18.48	6.75	16.96	4.70	0.08	0.01	0.07	0.01	0.08	0.01	0.08	0.01
Volunteer 1	13.83	4.49	15.06	3.50	18.55	2.34	15.81	3.08	0.08	0.01	0.07	0.01	0.08	0.01	0.08	0.01
Volunteer 2	11.59	4.60	16.00	3.45	20.29	2.33	15.96	3.10	0.07	0.01	0.08	0.01	0.08	0.00	0.08	0.01
Volunteer 3	7.71	1.76	12.24	3.00	14.52	3.49	11.49	2.46	0.06	0.02	0.08	0.01	0.09	0.00	0.08	0.01
Volunteer 1-3	11.04	3.33	14.43	2.88	17.79	2.40	14.42	2.51	0.07	0.01	0.08	0.01	0.08	0.01	0.08	0.01

Table 6-10 shows the mean SNR and water line width values for each volunteer and slice. It can be seen that overall across all slices the use of SENSE creates a small reduction in SNR. Mean SNR values for voxels with a water line width <0.1ppm are still within acceptable limits (>5). Slice 1 (lowest slice) had the lowest SNR across all volunteers. The mean water line width across voxels meeting this criterion are unchanged through the addition of SENSE. Figure 6-7 shows SNR maps across the whole grid for all voxels within the brain volume. SNR varies across the slices for each volunteer and within the regions themselves. Voxels with high signal can be observed on the edges which could be attributed to lipid bleed through due to their close proximity to voxels with high lipid signal (Figure 6-4). Figure 6-3 D, E and F shows the Water FWHM map for volunteer without the rejection criteria. Increased line width can be observed in the frontal regions of the brain across all slices. This is consistent with previous results in chapter 3.

Overall, the data quality was acceptable across all slices with mean SNR values greater than 5 across all slices and with the addition of a SENSE factor R AP=2 and RL=1. The number of voxels lost due to the water line width criteria; 34% with no SENSE, 46, 44 and 70% for volunteers 1, 2 and 3 respectively is high. The mean percentage of voxels lost is 53% with SENSE across these volunteers. The addition of SENSE resulted in ~20% increase in voxel loss. However, a large number of voxels remained particularly for slices 2 and 3. This suggests the use of a 3D acquisition would provide more data than a single slice 2D acquisition as more metabolite information could be mapped across the brain instead of one region.

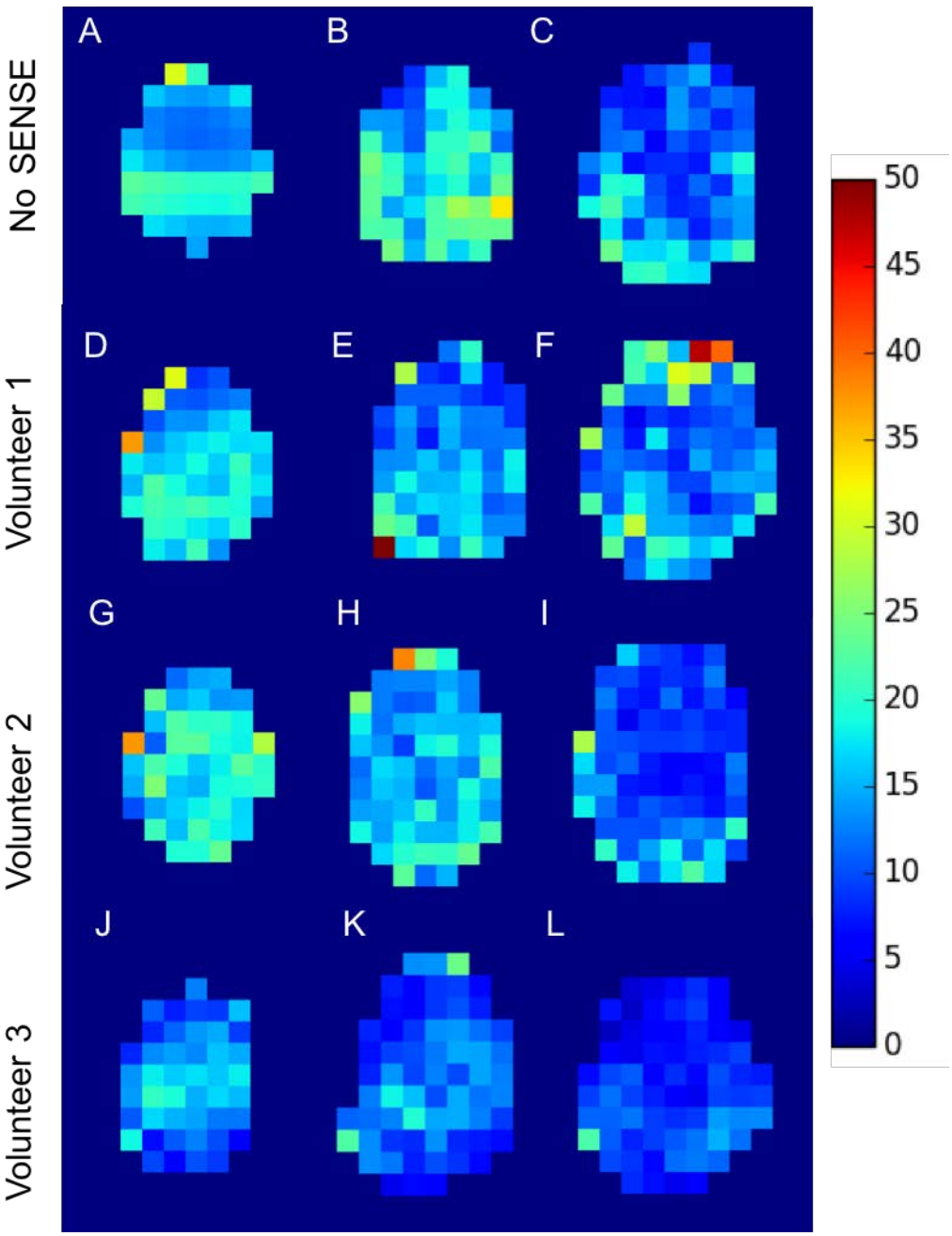

Figure 6-7 In volume SNR max maps for each volunteer for Slice 3 (A, D, G and J), Slice 2 (B, E, H and K) and Slice 1 (C, F, I and L) with no water line width threshold applied.

6.4 Discussion

The purpose of this study was to validate the use of SENSE for the collection of 3D MRSI data with absolute quantification of metabolites. A number of optimisation steps were carried out in order to design a protocol with effective lipid and water suppression. The reproducibility of healthy volunteer acquisitions with sensitivity encoding AP R=2 RL R=1 were compared to a fully sampled (No SENSE) healthy volunteer acquisition. Reproducibility was assessed using Coefficients of Variance (CoV's). Mean SNR and Water line width values were also compared and mean lipid values calculated to assess the effectiveness of lipid suppression using SPAIR. Voxel loss due to a water line width criterion was also determined for each acquisition.

Overall, data quality was found to be acceptable with the use of SENSE. Similarly, a study by Ozturk-Isik et al (120) found the use of sensitivity encoding in 3D MRSI produced acceptable SNR for Cho, Cr and NAA and also found the data was clinically interpretable. Mean coefficients of variance for all slices combined was comparable between No SENSE and SENSE. However, increased variation was observed between slices, with the middle slice 2 being the most robust. The most reproducible metabolite was found to be tNAA with higher CoV's found for tCr and tCho. Further variability was found for Glx and Ins. Mean volunteer coefficients of variance of 11.67% for tNAA, 15.94% tCr, 22.07% for tCho, 33.87% Glx and 29.31% for Ins were found for volunteers with the addition of SENSE Factor AP R=2 and RL = 1.

Ding et al (75) found comparable intra subject coefficients of variance of 14%, 15%, 20%, 31% and 31% for tNAA, tCr, tCho, Glx and Ins respectively. This study used EPSI combined with parallel imaging (acceleration factor 1.6) to collect 18 slices for a 50 x

50 FOV in an acquisition time of 16 minutes. A comparable line width threshold of 11Hz was also used as a rejection criterion for voxels containing poor quality spectra. However, the number of voxels discarded due to this criterion is not stated. Our study acquired 3 slices in 11 minutes 8 seconds which although fewer slices were acquired throughout the brain this acquisition would fit within a clinical scanning session more easily. This acquisition time could be reduced further if a higher SENSE factor was applied to the water unsuppressed acquisition as discussed in chapter 4. The addition of compressed sensing (126) although not readily available could also provide a further reduction in scan time and would make an interesting extension to this study. Further slices could therefore be acquired in order to obtain a whole brain MRSI acquisition.

Li et al (123) also assessed the intra-subject reproducibility of a 3D MRSI protocol using PRESS finding comparable COVs of 13.8%, 18.5% and 20.1% for tNAA, tCr and tCho respectively for a long TE = 135ms. This acquisition however took 54 minutes which would not be feasible in a clinical setting. Langer et al (71) also used PRESS and found comparable coefficients of variance of 13.5%, 21.7%, 18.3%, 24% and 21% for tNAA, tCr, tCho, Glx and Ins respectively for an echo time of 30ms. Our study found slightly higher COV's for tCho, Glx and Ins. Langer et al used a Gill-Thomas- Cosman (GTC) stereotactic head frame which may have reduced variability due to patient motion. The limitation of the excitation to the PRESS box would also reduce variation due to lipid contamination. Four 5x5 voxel slices (100 voxels) were acquired with an acquisition time 12minutes 54 seconds. By comparison our study provided a similar number of acceptable quality voxels even after the line width criterion was applied.

The introduction of sensitivity encoding resulted in increased percentage voxel loss; <15% for Volunteer 1 and 2 and 36% increase for Volunteer 3. However, a comparable

number of voxels remained ~100 for No SENSE, Volunteer 1 and Volunteer 2. The largest number of voxels were lost for Volunteer 3. Suggesting inter-subject variability could be a factor in the implementation of this 3D MRSI protocol. Ding et al (75) found inter-subject COV's were up to 6% higher than those for intra-subject variability. Further investigation involving more subjects with our proposed 3D MRSI protocol would be needed to assess this further.

Lipid interference appears to be higher in the SENSE acquisitions compared to the acquisition with No SENSE factor applied. Kirchner et al (127) found that the SENSE reconstruction algorithm can cause the voxels to be susceptible to the effects of lipid signal bleed through, which could explain the higher lipid content observed within this study. As the SPAIR lipid suppression pulse does not have the ability to fully suppress the lipid signal, this method maybe limited in its effectiveness particularly in regions close to the scalp. The use of saturation bands placed over the scalp, although adding extra complexity to the MRSI planning stages, may offer assistance in the suppression of these outer volume lipid signals.

6.5 Conclusion

Overall, we have developed a 3D MRSI spin echo protocol that would allow metabolite information to be mapped through the brain for three slices as an alternative to less readily available techniques. Metabolite CoV's were calculated in order to test the robustness of this protocol with good results. We were able to obtain metabolite information with good SNR and water line width across more regions than would be attainable with a 2D acquisition. This protocol has been optimised to minimise the

effects of lipid contamination and inefficient water suppression which would allow more robust metabolite information to be mapped throughout the brain.

7. Conclusions and Further work

7.1 Objective 1- Investigation into the effect of both acquisition parameters and fitting methods on 1H MRSI Reproducibility

The first objective was to look at the effect of both acquisition parameters i.e. short or long echo time and fitting methods i.e. fitting models on the reproducibility of ^{1}H MRSI data. This was achieved through the assessment of both echo time (TE=35, 80 and 144ms) and two macromolecular (MM) baseline analysis schemes simulated (Si.BL) and experimentally derived (Ex.BL) and their influence on reproducibility. Both the choice of MM analysis scheme and echo time were found to have an impact on the reproducibility of 1H MRSI data. These results highlighted the importance of careful echo time selection and analysis methodology. For optimal reproducibility, the primary metabolite of interest should be taken into consideration. Overall, this study found that an intermediate echo time of 80ms produced the most reproducible metabolite values for tNAA, tCho, tCr and Glth in healthy volunteers. However, the combined use of a short TE sequence and the MM analysis scheme Ex.BL could be recommended as a result of this study as a compromise between good accuracy, good SNR and T2 bias on metabolite estimates.

7.1.1 Future Work

It has been established in a number of studies (52,56,63,92,93) that the MM content within the brain varies between different pathologies. Therefore, an interesting extension to this project would be to investigate the development of disease specific experimental macromolecular analysis schemes to assess if any improvement in fitting accuracy could be made compared to a healthy volunteer model.

The introduction of fast-MRSI methods e.g. SENSE and their effect on the reproducibility of 2D MRSI protocols using Ex.BL could also be evaluated. Due to their associated SNR losses, investigation into their effect on longer echo time acquisitions could also help establish optimal protocols for clinical MRSI studies. Particularly, where a reduction in scan time is important.

Finally, future work could also include the assessment of techniques with respect to both reproducibility and accuracy by comparing to normative values. This would involve the use of segmentation for white matter, grey matter and cerebral spinal fluid (CSF) in order to perform partial volume corrections.

7.2 Objective 2- Investigation into the effect of fast-MRSI techniques on accuracy for water reference data acquisition.

The second objective was to assess the ability of fast-MRSI techniques to accurately reproduce fully sampled water reference data. The use of SENSE for the collection of fast-MRSI water reference data within the brain for absolute quantification of metabolites was validated through a comparison with a “gold standard” reduced resolution technique. Accuracy was assessed by ability to (i) reconstruct fully sampled volunteer and phantom data; (ii) reproduce known metabolite concentrations from phantom data, and (iii) produce metabolite concentrations from healthy volunteers. SENSE proved to be approximately three times more effective and offered significant improvement in accuracy over the reduced resolution method. These findings validated the use of SENSE MRSI for the accurate measurement of absolute metabolite concentrations in a feasible time frame (~6minutes) for use within a clinical setting.

7.2.1 Future Work

The use of compressed sensing, although currently not widely available, in conjunction with SENSE would allow a further reduction in scan time. A further study investigating the combination of these two techniques and their ability to reconstruct fully sampled data, if successful, would further ease the introduction of MRSI into the clinical setting. Another extension to this project would be the assessment of increasing SENSE factors on the accuracy of metabolite data collection.

7.3 Objective 3- The use of fast-MRSI techniques in clinical practice.

The third objective was to implement fast-MRSI techniques into clinical practice. Spectra were acquired successfully for two patient groups using the protocol developed in Chapter 4. The use of SENSE for fast-MRSI water reference data for absolute quantitation of metabolite information in clinic was assessed. Data quality and the protocols ability to separate between patient groups Brain Tumor Survivors (BTS), Wolfram Patients and “healthy volunteers”. Spectra had acceptable data quality with respect to SNR and Water Line Width. Minimal voxel loss was found for the majority of patients within this study. The protocol was also able to distinguish between the Wolfram cohort and healthy volunteers validating its use in the clinical environment.

7.3.1 Future Work

A limitation of this study is the small comparator “normal” cohort, although significant differences between “normal” and the Wolfram patient group was observed even with this sample size. If further data could be acquired across all groups the use of this protocol clinically could be validated further. This would provide more information into

the investigation of neuronal dysfunction within different pathologies. The use of an age matched “normal” comparator would also help assess the effectiveness of our protocol.

7.4 Objective 4- Development and optimisation of 3D-MRSI protocol

The final and fourth objective of this study was to develop and optimise a 3D-MRSI protocol. A 3D MRSI spin echo protocol was developed that successfully mapped robust metabolite information through the brain for three slices. Spectra were acquired throughout the brain in a clinically feasible acquisition time of 11 minutes and 8 seconds using the lipid inversion technique SPAIR. Metabolite CoV’s were calculated in order to test the robustness of this protocol with good results. Good SNR and water line width across more regions compared to a 2D MRSI acquisition was obtained. This protocol had also been optimised to minimise the effects of lipid contamination and inefficient water suppression which allows robust metabolite information to be mapped throughout the brain.

7.4.1 Future Work

Investigation into inter-subject variability would further test the robustness of this 3D-MRSI protocol. Moderate inter-subject variability was observed within our study for this technique. Further Data collection would provide useful information into the success of our protocol for a wider subject group.

The use of a higher SENSE factors on the water reference data would provide a further reduction in scan time. Therefore, investigation into different SENSE factors or the combined use of compressed sensing once again would further compliment this study.

8. References

1. Wilson M, Cummins CL, Macpherson L, Sun Y. Magnetic resonance spectroscopy metabolite profiles predict survival in paediatric brain tumours. Eur. J. Cancer [Internet] 2013;49:457–464.

2. Pruel M, Caramanos Z, Collins D, Villemure J, Leblanc R, Olivier A, Pokrupa R, Arnold D. Accurate, noninvasive diagnosis of human brain tumors by using proton magnetic resonance spectroscopy. Nat. Med. 1996;2:323–325.

3. Astrakas LG, Zurakowski D, Tzika AA, Zarifi MK, Anthony DC, Girolami U De, Tarbell NJ, Black PM. Noninvasive Magnetic Resonance Spectroscopic Imaging Biomarkers to Predict the Clinical Grade of Pediatric Brain Tumors to Predict the Clinical Grade of Pediatric Brain Tumors. Clin. Cancer Res. 2004;10:8220–8228.

4. Colla M, Ende G, Bohrer M, Deuschle M, Kronenberg G, Henn F, Heuser I. MR spectroscopy in Alzheimer's disease: gender differences in probabilistic learning capacity. Neurobiol. Aging [Internet] 2003;24:545–552.

5. Oz G, Alger JR, Barker PB, et al. Clinical proton MR spectroscopy in central nervous system disorders. Radiology [Internet] 2014;270:658–679.

6. Davison JE, Davies NP, Wilson M, Sun Y, Chakrapani A, McKiernan PJ, Walter JH, Gissen P, Peet AC. MR spectroscopy-based brain metabolite profiling in propionic acidaemia: metabolic changes in the basal ganglia during acute decompensation and effect of liver transplantation. Orphanet J. Rare Dis. [Internet] 2011;6:19.

7. Birch R, Peet AC, Dehghani H, Wilson M. Influence of macromolecule baseline on (1) H MR spectroscopic imaging reproducibility. Magn. Reson. Med. [Internet] 2017;77:34–43.

8. Wansapura JP, Holland SK, Dunn RS, Ball WS. NMR relaxation times in the human brain at 3.0 tesla. J. Magn. Reson. Imaging [Internet] 1999;9:531–538.

9. van Zijl PCM, Moonen C, Alger JR, Cohen J, Chesnick S. High field localized proton spectroscopy in small volumes: greatly improved localization and shimming using shielded strong gradients. Magn. Reson. Med. 1989;10:256–265.

10. Barker PB, Lin DDM. In vivo proton MR spectroscopy of the human brain. Prog. Nucl. Magn. Reson. Spectrosc. 2006;49:99–128.

11. Haase A, Frahm J, Hänicke W, Matthaei D. 1H NMR chemical shift selective (CHESS) imaging. Phys. Med. Biol. [Internet] 1985;30:341–344.

12. Skoch A, Jiru F, Bunke J. Spectroscopic imaging: basic principles. Eur. J. Radiol. [Internet] 2008;67:230–239.

13. Lustig M, Donoho D, M. Pauly J. Sparse MRI: The Application of Compressed Sensing for Rapid MR Imaging. Magn. Reson. Med. 2007;58:1182–1195.

14. Bonekamp D, Smith MA, Zhu H, Barker PB. Quantitative SENSE-MRSI of the human brain. Magn. Reson. Imaging [Internet] 2010;28:305–313.

15. Pruessmann KP, Weiger M, Sheidegger MB, Boesiger P. SENSE: Sensitivity Encoding for Fast-MRI. Magn. Reson. Med. 1999;42:952–962.

16. Mansfield P. Spatial mapping of the chemical shift in NMR. Magn. Reson. Med. [Internet] 1984;1:370–386.

17. Posse S, Tedeschi G, Risinger R, Ogg R, Le Bihan D. High speed 1H spectroscopic imaging in human brain by echo planar spatial-spectral encoding. Magn. Reson. Med. [Internet] 1995;33:34–40.

18. Ebel A, Maudsley AA, Weiner MW, Schuff N. Achieving sufficient spectral bandwidth for volumetric 1H echo-planar spectroscopic imaging at 4 Tesla. Magn. Reson. Med. 2005;54:697–701.

19. Barkhuijsen H, de Beer R, Bovée WMM., van Ormondt D. Retrieval of frequencies, amplitudes, damping factors, and phases from time-domain signals using a linear least-squares procedure. J. Magn. Reson. [Internet] 1985;61:465–481.

20. Barkhuijsen H, Beer De R, van Ormondt D. Improved algorithm for noniterative time-domain model fitting to exponentially damped magnetic resonance signals. J. Magn. Reson. 1987;73:553–557.

21. Vanhamme L, van den Boogaart A, Van Huffel S. Improved method for accurate and efficient quantification of MRS data with use of prior knowledge. J. Magn. Reson. 1997;129:35–43.

22. Provencher S. Estimation of metabolite concentrations from localized in vivo proton NMR spectra. Magn. Reson. Med. 1993;30:672–679.

23. Wilson M, Reynolds G, Kauppinen RA, Arvanitis TN, Peet AC. A constrained least-squares approach to the automated quantitation of in vivo ^{1}H magnetic resonance spectroscopy data. Magn. Reson. Med. [Internet] 2011;65:1–12.

24. Wilson M, Reynolds G, Kauppinen RA, Arvanitis TN, Peet AC. A constrained least-squares approach to the automated quantitation of in vivo ^{1}H magnetic resonance spectroscopy data. Magn. Reson. Med. [Internet] 2011;65:1–12.

25. Govindaraju V, Young K, Maudsley AA. Proton NMR chemical shifts and coupling constants for brain metabolites. NMR Biomed. [Internet] 2000;13:129–153.

26. de Graaf R. In Vivo NMR Spectroscopy Principles and Techniques. Second Edi. Chichester: John Wiley and Sons Ltd; 2007.

27. Behar KL, Rothman DL, Spencer DD, Petroff OA. Analysis of macromolecule resonances in 1H NMR spectra of human brain. Magn. Reson. Med. [Internet] 1994;32:294–302.

28. Cudalbu C, Mlynárik V, Gruetter R. Handling macromolecule signals in the quantification of the neurochemical profile. J. Alzheimers. Dis. [Internet] 2012;31 Suppl 3:S101-115.

29. Seeger U, Klose U, Mader I, Grodd W, Nägele T. Parameterized evaluation of macromolecules and lipids in proton MR spectroscopy of brain diseases. Magn. Reson. Med. [Internet] 2003;49:19–28.

30. Kreis R. Issues of spectral quality in clinical 1H-magnetic resonance spectroscopy and a gallery of artifacts. NMR Biomed. [Internet] 2004;17:361–381.

31. Tong Z, Yamaki T, Harada K, Houkin K. In vivo quantification of the metabolites in normal brain and brain tumors by proton MR spectroscopy using water as an internal standard. Magn. Reson. Imaging [Internet] 2004;22:735–742.

32. Ernst T, Kreis R, Ross B. Absolute quantitation of water and metabolites in the human brain. I. Compartments and water. J. Magn. Reson. Ser. B [Internet] 1993;102:1–8.

33. Keevil SF, Barbiroli B, Brooks JC. Absolute Metabolite Quantification By In Vivo MR Spectroscopy: II. A Multicentre Trial Of Protocols For In Vivo Localised Proton Studies of Human Brain. Magn. Reson. Imaging 1998;16:1093–1106.

34. Govindaraju V, Young K, Maudsley AA. Proton NMR chemical shifts and coupling constants for brain metabolites. NMR Biomed. [Internet] 2000;13:129–153.

35. Frahm J, Bruhn H, Gyngell ML, Merboldt KD, Hänicke W, Sauter R. Localized proton NMR spectroscopy in different regions of the human brain in vivo. Relaxation times and concentrations of cerebral metabolites. Magn. Reson. Med. 1989;11:47–63.

36. Wang Y, Li SJ. Differentiation of metabolic concentrations between gray matter and white matter of human brain by in vivo 1H magnetic resonance spectroscopy. Magn. Reson. Med. 1998;39:28–33.

37. Miller BL, Moats RA, Shonk T, Ernst T, Woolley S, Ross BD. Alzheimer disease: depiction of increased cerebral myo-inositol with proton MR spectroscopy. Radiology 1993;187:433–437.

38. Shonk TK, Moats RA, Gifford P, Michaelis T, Mandigo JC, Izumi J, Ross BD. Probable Alzheimer disease: diagnosis with proton MR spectroscopy. Radiology 1995;195:65–72.

39. Voevodskaya O, Sundgren PC, Strandberg O, Zetterberg H, Minthon L, Blennow K, Wahlund L-O, Westman E, Hansson O. Myo-inositol changes precede amyloid pathology and relate to APOE genotype in Alzheimer disease. Neurology 2016;86:1754–1761.

40. Croall I, Smith FE, Blamire AM. Magnetic Resonance Spectroscopy for Traumatic Brain Injury. Top. Magn. Reson. Imaging 2015;24:267–274.

41. Kierans AS, Kirov II, Gonen O, Haemer G, Nisenbaum E, Babb JS, Grossman RI, Lui YW. Myoinositol and glutamate complex neurometabolite abnormality after mild traumatic brain injury. Neurology 2014;82:521–528.

42. Ross BD, Ernst T, Kreis R, et al. 1H MRS in acute traumatic brain injury. J. Magn. Reson. Imaging 8:829–840.

43. Trabesinger AH, Weber OM, Duc CO, Boesiger P. Detection of glutathione in the human brain in vivo by means of double quantum coherence filtering. Magn. Reson. Med. 1999;42:283–289.

44. Terpstra M, Vaughan TJ, Ugurbil K, Lim KO, Schulz SC, Gruetter R. Validation of glutathione quantitation from STEAM spectra against edited 1H NMR spectroscopy at 4T: application to schizophrenia. MAGMA 2005;18:276–282.

45. Cooper AJ, Kristal BS. Multiple roles of glutathione in the central nervous system. Biol. Chem. 1997;378:793–802.

46. Aasly JO, Sæther O, Johansen KK, Bathen TF, Giskeødegård GF, White LR. Changes to Intermediary Metabolites in Sporadic and LRRK2 Parkinson's Disease Demonstrated by Proton Magnetic Resonance Spectroscopy. Parkinsons. Dis.

2015;2015:264896.

47. Sian J, Dexter DT, Lees AJ, Daniel S, Agid Y, Javoy-Agid F, Jenner P, Marsden CD. Alterations in glutathione levels in Parkinson's disease and other neurodegenerative disorders affecting basal ganglia. Ann. Neurol. 1994;36:348–355.

48. Veech RL. The metabolism of lactate. NMR Biomed. 1991;4:53–58.

49. Bruhn H, Frahm J, Gyngell ML, Merboldt KD, Hänicke W, Sauter R. Cerebral metabolism in man after acute stroke: new observations using localized proton NMR spectroscopy. Magn. Reson. Med. 1989;9:126–131.

50. Lin A-Q, Shou J-X, Li X-Y, Ma L, Zhu X-H. Metabolic changes in acute cerebral infarction: Findings from proton magnetic resonance spectroscopic imaging. Exp. Ther. Med. 2014;7:451–455.

51. Zhang M, Sun X, Zhang Z, Meng Q, Wang Y, Chen J, Ma X, Geng H, Sun L. Brain metabolite changes in patients with type 2 diabetes and cerebral infarction using proton magnetic resonance spectroscopy. Int. J. Neurosci. 2014;124:37–41.

52. Howe FA, Barton SJ, Cudlip SA, et al. Metabolic profiles of human brain tumors using quantitative in vivo 1H magnetic resonance spectroscopy. Magn. Reson. Med. [Internet] 2003;49:223–232.

53. Madan A, Ganji SK, An Z, Choe KS, Pinho MC, Bachoo RM, Maher EM, Choi C. Proton T2 measurement and quantification of lactate in brain tumors by MRS at 3 Tesla in vivo. Magn. Reson. Med. 2015;73:2094–2099.

54. Gotsis ED, Fountas K, Kapsalaki E, Toulas P, Peristeris G, Papadakis N. In vivo proton MR spectroscopy: the diagnostic possibilities of lipid resonances in brain tumors. Anticancer Res. 16:1565–1567.

55. Bulik M, Jancalek R, Vanicek J, Skoch A, Mechl M. Potential of MR spectroscopy for assessment of glioma grading. Clin. Neurol. Neurosurg. 2013;115:146–153.

56. Saunders DE, Howe FA, van den Boogaart A, Griffiths JR, Brown MM. Discrimination of metabolite from lipid and macromolecule resonances in cerebral infarction in humans using short echo proton spectroscopy. J. Magn. Reson. Imaging [Internet] 7:1116–1121.

57. Narayana PA, Wolinsky JS, Jackson EF, McCarthy M. Proton MR spectroscopy of gadolinium-enhanced multiple sclerosis plaques. J. Magn. Reson. Imaging 2:263–270.

58. Tourbah A, Stievenart JL, Abanou A, Iba-Zizen MT, Hamard H, Lyon-Caen O, Cabanis EA. Normal-appearing white matter in optic neuritis and multiple sclerosis: a comparative proton spectroscopy study. Neuroradiology 1999;41:738–743.

59. Davie CA, Hawkins CP, Barker GJ, Brennan A, Tofts PS, Miller DH, McDonald WI. Serial proton magnetic resonance spectroscopy in acute multiple sclerosis lesions. Brain 1994;117 (Pt 1:49–58.

60. Behar KL, Ogino T. Characterization of macromolecule resonances in the 1H NMR spectrum of rat brain. Magn. Reson. Med. 1993;30:38–44.

61. Vold R, Waugh J, Klein M, Phelps D. Measurement of spin relaxation in complex systems. J. Chem. Phys. 1968;48:3831–3832.

62. Hwang JH, Graham GD, Behar KL, Alger JR, Prichard JW, Rothman DL. Short echo time proton magnetic resonance spectroscopic imaging of macromolecule and metabolite signal intensities in the human brain. Magn. Reson. Med. 1996;35:633–639.

63. Graham GD, Hwang JH, Rothman DL, Prichard JW. Spectroscopic assessment of alterations in macromolecule and small-molecule metabolites in human brain after stroke. Stroke. [Internet] 2001;32:2797–2802.

64. Bland JM, Altman DG. Statistical methods for assessing agreement between two methods of clinical measurement. Lancet [Internet] 1986;1:307–310.

65. Scheenen TWJ, Klomp DWJ, Wijnen JP, Heerschap A. Short echo time 1H-MRSI of the human brain at 3T with minimal chemical shift displacement errors using adiabatic refocusing pulses. Magn. Reson. Med. [Internet] 2008;59:1–6.

66. Felblinger J, Kreis R, Boesch C. Effects of physiologic motion of the human brain upon quantitative 1H-MRS: analysis and correction by retro-gating. NMR Biomed. 1998;11:107–114.

67. Haupt C, Kiefer A, Maudsley AA. In-plane motion correction for MR Spectroscopic Imaging. Magn. Reson. Med. 1998;39:749–753.

68. Snoussi K, Gillen JS, Horska A, Puts NAJ, Pradhan S, Edden RAE, Barker PB. Comparison of brain gray and white matter macromolecule resonances at 3 and 7 Tesla. Magn. Reson. Med. [Internet] 2015;74:607–13.

69. Maudsley AA, Domenig C, Sheriff S. Reproducibility of serial whole-brain MR spectroscopic imaging. NMR Biomed. [Internet] 2010;23:251–256.

70. Wiebenga OT, Klauser AM, Nagtegaal GJA, Schoonheim MM, Barkhof F, Geurts JJG, Pouwels PJW. Longitudinal absolute metabolite quantification of white and gray matter regions in healthy controls using proton MR spectroscopic imaging. NMR Biomed. [Internet] 2014;27:304–311.

71. Langer DL, Rakaric P, Kirilova A, Jaffray DA, Damyanovich AZ. Assessment of metabolite quantitation reproducibility in serial 3D-(1)H-MR spectroscopic imaging of human brain using stereotactic repositioning. Magn. Reson. Med. [Internet] 2007;58:666–673.

72. Tsai S-Y, Lin Y-R, Wang W-C, Niddam DM. Short- and long-term quantitation reproducibility of brain metabolites in the medial wall using proton echo planar spectroscopic imaging. Neuroimage [Internet] 2012;63:1020–1029.

73. Van Cauter S, Sima DM, Luts J, et al. Reproducibility of rapid short echo time CSI at 3 tesla for clinical applications. J. Magn. Reson. Imaging [Internet] 2013;37:445–456.

74. Deelchand DK, Adanyeguh IM, Emir UE, Nguyen T-M, Valabregue R, Henry P-G, Mochel F, Öz G. Two-site reproducibility of cerebellar and brainstem neurochemical profiles with short-echo, single-voxel MRS at 3T. Magn. Reson. Med. [Internet] 2015;73:1718–1725.

75. Ding X-Q, Maudsley AA, Sabati M, Sheriff S, Dellani PR, Lanfermann H. Reproducibility and reliability of short-TE whole-brain MR spectroscopic imaging of human brain at 3T. Magn. Reson. Med. [Internet] 2015;73:921–928.

76. Gottschalk M, Lamalle L, Segebarth C. Short-TE localised 1H MRS of the human brain at 3 T: quantification of the metabolite signals using two approaches to account for macromolecular signal contributions. NMR Biomed. [Internet] 2008;21:507–517.

77. Cudalbu C, Bucur A, Graveron-Demilly D, Beuf O, Cavassila S. Comparison of two strategies of background-accommodation: influence on the metabolite concentration estimation from in vivo Magnetic Resonance Spectroscopy data. Conf. Proc. ... Annu. Int. Conf. IEEE Eng. Med. Biol. Soc. IEEE Eng. Med. Biol. Soc. Annu. Conf. [Internet] 2007;2007:2077–2080.

78. Schaller B, Xin L, Cudalbu C, Gruetter R. Quantification of the neurochemical profile using simulated macromolecule resonances at 3 T. NMR Biomed. [Internet] 2013;26:593–599.

79. Posse S, Ricardo O, Dager SR, Alger J. MR spectroscopic imaging: Principles and recent advances. J. Magn. Reson. Imaging 2013;37:1301–1325.

80. Natt O, Bezkorovaynyy V, Michaelis T, Frahm J. Use of phased array coils for a determination of absolute metabolite concentrations. Magn. Reson. Med. [Internet] 2005;53:3–8.

81. Veenith T V, Mada M, Carter E, et al. Comparison of inter subject variability and reproducibility of whole brain proton spectroscopy. PLoS One [Internet] 2014;9:e115304.

82. Gasparovic C, Bedrick EJ, Mayer AR, Yeo RA, Chen H, Damaraju E, Calhoun VD, Jung RE. Test-retest reliability and reproducibility of short-echo-time spectroscopic imaging of human brain at 3T. Magn. Reson. Med. [Internet] 2011;66:324–332.

83. Jang D-P, Lee J-M, Lee E, Park S, Kim J-J, Namkoong K, Yoon K-J, Kim I-Y, Kim SI. Interindividual reproducibility of glutamate quantification using 1.5-T proton magnetic resonance spectroscopy. Magn. Reson. Med. [Internet] 2005;53:708–712.

84. Poels EMP, Kegeles LS, Kantrowitz JT, Javitt DC, Lieberman JA, Abi-Dargham A, Girgis RR. Glutamatergic abnormalities in schizophrenia: a review of proton MRS findings. Schizophr. Res. [Internet] 2014;152:325–332.

85. Wilson M, Gill SK, MacPherson L, English M, Arvanitis TN, Peet AC. Noninvasive detection of glutamate predicts survival in pediatric medulloblastoma. Clin. Cancer Res. [Internet] 2014;20:4532–4539.

86. Lally N, Mullins PG, Roberts M V, Price D, Gruber T, Haenschel C. Glutamatergic correlates of gamma-band oscillatory activity during cognition: a concurrent ER-MRS and EEG study. Neuroimage [Internet] 2014;85 Pt 2:823–833.

87. Hancu I. Optimized glutamate detection at 3T. J. Magn. Reson. Imaging [Internet] 2009;30:1155–1162.

88. Mullins PG, Chen H, Xu J, Caprihan A, Gasparovic C. Comparative reliability of proton spectroscopy techniques designed to improve detection of J-coupled metabolites. Magn. Reson. Med. [Internet] 2008;60:964–969.

89. Schubert F, Gallinat J, Seifert F, Rinneberg H. Glutamate concentrations in human brain using single voxel proton magnetic resonance spectroscopy at 3 Tesla. Neuroimage [Internet] 2004;21:1762–1771.

90. Hancu I, Port J. The case of the missing glutamine. NMR Biomed. [Internet] 2011;24:529–535.

91. Kelley DA, Wald LL, Star-Lack JM. Lactate detection at 3T: compensating J coupling effects with BASING. J. Magn. Reson. Imaging [Internet] 1999;9:732–737.

92. Craveiro M, Clément-Schatlo V, Marino D, Gruetter R, Cudalbu C. In vivo brain macromolecule signals in healthy and glioblastoma mouse models: 1H magnetic resonance spectroscopy, post-processing and metabolite quantification at 14.1 T. J. Neurochem. [Internet] 2014;129:806–815.

93. Mader I, Seeger U, Weissert R, Klose U, Naegele T, Melms A, Grodd W. Proton MR spectroscopy with metabolite-nulling reveals elevated macromolecules in acute multiple sclerosis. Brain [Internet] 2001;124:953–961.

94. Pruessmann KP, Weiger M, Scheidegger MB, Boesiger P. SENSE: sensitivity encoding for fast MRI. Magn. Reson. Med. [Internet] 1999;42:952–62.

95. Birch R, Peet AC, Arvanitis TN, Wilson M. Sensitivity encoding for fast (1) H MR spectroscopic imaging water reference acquisition. Magn. Reson. Med. [Internet] 2015;73:2081–6.

96. Soreni N, Noseworthy MD, Cormier T, Oakden WK, Bells S, Schachar R. Intraindividual variability of striatal (1)H-MRS brain metabolite measurements at 3 T. Magn. Reson. Imaging [Internet] 2006;24:187–94.

97. Maudsley AA, Matson GB, Hugg JW, Weiner MW. Reduced phase encoding in spectroscopic imaging. Magn. Reson. Med. [Internet] 1994;31:645–651.

98. Bainbridge A, Kendall GS, Vita E De, Hagmann C, Kapetanakis A, Cady EB, Robertson NJ. Regional neonatal brain absolute thermometry by (1) H MRS. NMR Biomed. [Internet] 2012;26:416–423.

99. Opstad KS, Ladroue C, Bell BA, Griffiths JR, Howe FA. Linear discriminant analysis of brain tumour (1)H MR spectra: a comparison of classification using whole spectra versus metabolite quantification. NMR Biomed. [Internet] 2007;20:763–770.

100. Davies NP, Wilson M, Harris LM, Natarajan K, Lateef S, Macpherson L, Sgouros S, Grundy RG, Arvanitis TN, Peet AC. Identification and characterisation of childhood cerebellar tumours by in vivo proton MRS. NMR Biomed. [Internet] 2008;21:908–918.

101. Dydak U, Weiger M, Pruessmann KP, Meier D, Boesiger P. Sensitivity-encoded spectroscopic imaging. Magn. Reson. Med. [Internet] 2001;46:713–722.

102. Dydak U, Meier D, Lamerichs R, Boesiger P. TECHNICAL NOTE Trading Spectral Separation at 3T for Acquisition Speed in Multi Spin-Echo Spectroscopic Imaging. Neuroradiology 2006;27:1441–1446.

103. Geethanath S, Baek H-M, Ganji SK, Ding Y, Maher EA, Sims RD, Choi C, Lewis MA, Kodibagkar VD. Compressive sensing could accelerate 1H MR metabolic imaging in the clinic. Radiology [Internet] 2012;262:985–994.

104. Minton JAL, Rainbow LA, Ricketts C, Barrett TG. Wolfram syndrome. Rev. Endocr. Metab. Disord. [Internet] 2003;4:53–59.

105. Barrett TG, Bundey SE, Macleod AF. Neurodegeneration and diabetes: UK nationwide study of Wolfram (DIDMOAD) syndrome. Lancet (London, England) [Internet] 1995;346:1458–1463.

106. Pickett KA, Duncan RP, Hoekel J, Marshall B, Hershey T, Earhart GM, Washington University Wolfram Study Group. Early presentation of gait impairment in Wolfram Syndrome. Orphanet J. Rare Dis. [Internet] 2012;7:92.

107. Pickett KA, Duncan RP, Paciorkowski AR, Permutt MA, Marshall B, Hershey T, Earhart GM, Washington University Wolfram Study Group. Balance impairment in individuals with Wolfram syndrome. Gait Posture [Internet] 2012;36:619–624.

108. Hershey T, Lugar HM, Shimony JS, Rutlin J, Koller JM, Perantie DC, Paciorkowski AR, Eisenstein SA, Permutt MA, Washington University Wolfram Study Group. Early brain vulnerability in Wolfram syndrome. PLoS One [Internet] 2012;7:e40604.

109. Bischoff AN, Reiersen AM, Buttlaire A, Al-Lozi A, Doty T, Marshall BA, Hershey T, Washington University Wolfram Syndrome Research Group. Selective cognitive and psychiatric manifestations in Wolfram Syndrome. Orphanet J. Rare Dis. [Internet] 2015;10:66.

110. Turner CD, Rey-Casserly C, Liptak CC, Chordas C. Late effects of therapy for pediatric brain tumor survivors. J. Child Neurol. [Internet] 2009;24:1455–1463.

111. Blamek S, Larysz D, Ficek K, Sokół M, Miszczyk L, Tarnawski R. MR spectroscopic evaluation of brain tissue damage after treatment for pediatric brain tumors. Acta Neurochir. Suppl. [Internet] 2010;106:183–186.

112. Blamek S, Wydmański J, Sokół M, Matulewicz L, Boguszewicz L. Magnetic resonance spectroscopic evaluation of brain tissue metabolism after irradiation for pediatric brain tumors in long-term survivors: a report of two cases. Acta Neurochir. Suppl. [Internet] 2010;106:191–194.

113. King TZ, Wang L, Mao H. Disruption of White Matter Integrity in Adult Survivors of Childhood Brain Tumors: Correlates with Long-Term Intellectual Outcomes. PLoS One [Internet] 2015;10:e0131744.

114. Robinson KE, Pearson MM, Cannistraci CJ, Anderson AW, Kuttesch JF, Wymer K, Smith SE, Compas BE. Neuroimaging of executive function in survivors of pediatric brain tumors and healthy controls. Neuropsychology [Internet] 2014;28:791–800.

115. Lugar HM, Koller JM, Rutlin J, Marshall BA, Kanekura K, Urano F, Bischoff AN, Shimony JS, Hershey T, Washington University Wolfram Syndrome Research Study Group. Neuroimaging evidence of deficient axon myelination in Wolfram syndrome. Sci. Rep. [Internet] 2016;6:21167.

116. Davison JE, Hendriksz CJ, Sun Y, Davies NP, Gissen P, Peet AC. Quantitative in vivo brain magnetic resonance spectroscopic monitoring of neurological involvement in mucopolysaccharidosis type II (Hunter Syndrome). J. Inherit. Metab. Dis. [Internet] 2010;33 Suppl 3:S395-399.

117. Duyn JH, Gillen J, Sobering G, van Zijl PC, Moonen CT. Multisection proton MR spectroscopic imaging of the brain. Radiology [Internet] 1993;188:277–282.

118. Lin F-H, Tsai S-Y, Otazo R, Caprihan A, Wald LL, Belliveau JW, Posse S. Sensitivity-encoded (SENSE) proton echo-planar spectroscopic imaging (PEPSI) in the human brain. Magn. Reson. Med. [Internet] 2007;57:249–57.

119. Lecocq A, Le Fur Y, Maudsley AA, et al. Whole-brain quantitative mapping of metabolites using short echo three-dimensional proton MRSI. J. Magn. Reson. Imaging [Internet] 2015;42:280–289.

120. Ozturk-Isik E, Chen AP, Crane JC, Bian W, Xu D, Han ET, Chang SM, Vigneron DB, Nelson SJ. 3D sensitivity encoded ellipsoidal MR spectroscopic imaging of gliomas at 3T. Magn. Reson. Imaging [Internet] 2009;27:1249–57.

121. Ozhinsky E, Vigneron DB, Nelson SJ. Improved spatial coverage for brain 3D PRESS MRSI by automatic placement of outer-volume suppression saturation bands. J. Magn. Reson. Imaging [Internet] 2011;33:792–802.

122. Sabati M, Zhan J, Govind V, Arheart KL, Maudsley AA. Impact of reduced k-space acquisition on pathologic detectability for volumetric MR spectroscopic imaging. J. Magn. Reson. Imaging [Internet] 2014;39:224–34.

123. Li BSY, Babb JS, Soher BJ, Maudsley AA, Gonen O. Reproducibility of 3D proton spectroscopy in the human brain. Magn. Reson. Med. [Internet] 2002;47:439–446.

124. Chard DT, McLean MA, Parker GJM, MacManus DG, Miller DH. Reproducibility of in vivo metabolite quantification with proton magnetic resonance spectroscopic imaging. J. Magn. Reson. Imaging [Internet] 2002;15:219–225.

125. Tedeschi G, Bertolino A, Campbell G, Barnett AS, Duyn JH, Jacob PK, Moonen CT, Alger JR, Di Chiro G. Reproducibility of proton MR spectroscopic imaging findings. AJNR. Am. J. Neuroradiol. [Internet] 17:1871–1879.

126. Geethanath S, Baek H-M, Ganji SK, Ding Y, Maher EA, Sims RD, Choi C, Lewis M a, Kodibagkar VD. Compressive sensing could accelerate 1H MR metabolic imaging in the clinic. Radiology [Internet] 2012;262:985–994.

127. Kirchner T, Fillmer A, Tsao J, Pruessmann KP, Henning A. Reduction of voxel bleeding in highly accelerated parallel (1) H MRSI by direct control of the spatial response function. Magn. Reson. Med. [Internet] 2015;73:469–480.